

Contract Program or
Project Title: Heavy-Section Steel Technology (HSST) Program

Subject of this Document: Experimental Program for Investigating the Influence
of Cladding Defects on Burst Pressure

Type of Document: Letter Report

Authors: B. R. Bass
W. J. McAfee
P. T. Williams
S. Yin
R. K. Nanstad
M. Sokolov

Date of Document: September 2004

Responsible NRC Individual
and NRC Office or Division M. T. Kirk
Division of Engineering Technology
Office of Nuclear Regulatory Research

Prepared for the
U. S. Nuclear Regulatory Commission
Washington, D.C. 20555-0001
Under Interagency Agreement DOE 1886-N653-3Y
NRC JCN No. Y6533

OAK RIDGE NATIONAL LABORATORY
Oak Ridge, Tennessee 37831-8056
managed by
UT-BATTELLE, LLC
for the
U. S. DEPARTMENT OF ENERGY
under contract DE-AC05-00OR22725

Experimental Program for Investigating the Influence of Cladding Defects on Burst Pressure

B. R. Bass
W. J. McAfee
P. T. Williams
S. Yin
R. K. Nanstad
M. Sokolov

Oak Ridge National Laboratory
Oak Ridge, Tennessee

Manuscript Completed—May 2004
Date Published— September 2004

Prepared for the
U.S. Nuclear Regulatory Commission
Office of Nuclear Regulatory Research
Under Interagency Agreement DOE 1886-N653-3Y

NRC JCN No. Y6533

OAK RIDGE NATIONAL LABORATORY
Oak Ridge, Tennessee 37831-8063
managed by
UT-BATTELLE, LLC
for the
U. S. DEPARTMENT OF ENERGY
under contract DE-AC05-00OR22725

CAUTION

This document has not been given final patent clearance and is for internal use only. If this document is to be given public release, it must be cleared through the site Technical Information Office, which will see that the proper patent and technical information reviews are completed in accordance with the policies of Oak Ridge National Laboratory and UT-Battelle, LLC.

This report was prepared as an account of work sponsored by an agency of the United States government. Neither the United States government nor any agency thereof, nor any of their employees, makes any warranty, express or implied, or assumes any legal liability or responsibility for the accuracy, completeness, or usefulness of any information, apparatus, product, or process disclosed, or represents that its use would not infringe privately owned rights. Reference herein to any specific commercial product, process, or service by trade name, trademark, manufacturer, or otherwise, does not necessarily constitute or imply its endorsement, recommendation, or favoring by the United States government or any agency thereof. The views and opinions of authors expressed herein do not necessarily state or reflect those of the United States government or any agency thereof.

Experimental Program for Investigating the Influence of Cladding Defects on Burst Pressure

B. R. Bass, W. J. McAfee, P. T. Williams, S. Yin, R. K. Nanstad, and M. Sokolov
Oak Ridge National Laboratory
P. O. Box 2009
Oak Ridge, TN, 37831-8056

Abstract

An experimental program was conducted by the Heavy-Section Steel Technology Program at the Oak Ridge National Laboratory (ORNL) to evaluate the structural significance of defects found in the unbacked cladding of the Davis-Besse vessel head. Experiments performed within that program were not intended to represent the “as found” condition of the Davis-Besse wastage cavity, but were designed to provide a technical basis for understanding failure characteristics of the flawed cladding. The initial task focused on design and construction of a test facility at ORNL that included a temperature control chamber, safety containment vessel, pressure loading system, and data acquisition system. In a parallel activity, clad burst specimens were designed and fabricated for testing in the experimental facility; source material for those specimens was taken from beltline sections of a reactor pressure vessel (RPV) that was never put into service. The facility/specimen design provided capability for testing to failure of unbacked RPV cladding [dimensions: 6 in. diameter, 0.24 in. thickness (nominally)] under pressure loading at a stable temperature of 600 °F.

Two shake-down tests (CB 1-2) were performed to verify the performance of the test facility and specimen design. Upon completion of the shake-down tests, ORNL conducted a full test matrix in two phases, the first of which (Phase I) consisted of one unflawed and five flawed specimens (CB 3-8). A follow-on Phase 2 matrix consisted of one unflawed and four flawed specimens (CB 9-13); additional instrumentation for recording crack-mouth opening displacement (CMOD) was employed on three of the flawed specimens tested in Phase 2. Failure pressure data from those tests, normalized by clad layer thickness, indicated a high degree of repeatability for the tests performed in both phases of the clad burst program. Unflawed clad burst specimens failed around the full perimeter of the disk from plastic instability; an analytical model for plastic collapse was shown to adequately predict those results. The flawed specimens tested in the program failed by ductile tearing of the notch defect through the clad layer.

Analytical interpretations that utilized three-dimensional (3-D) finite element models of the clad burst specimens were performed for both Phases 1 and 2. To support those analyses, material characterization of the RPV cladding was carried out at 600 °F, including tensile testing and J-R testing in the T-S and T-L orientations. Fractographic studies were performed on failed defects in the flawed burst specimens to verify the ductile mode of failure. Comparisons of computed results from 3-D finite element models with measured gage displacement data (i.e., center-point deflection and CMOD) indicated reasonably good agreement up to the region of instability. For tests instrumented with the CMOD gage, good agreement between calculated and measured CMOD data up to the onset of instability implies that ductile tearing initiated near the maximum load and (with a small increase in load) rapidly progressed through the clad layer to produce failure of the specimen. Analyses of selected clad burst specimens containing flaws produced J and $CTOD$ values near failure conditions that were generally consistent with median J_Q and $CTOD$ values obtained from testing and analysis of pre-cracked Charpy specimens fabricated from the RPV cladding.

CONTENTS

<u>Section</u>	<u>Page</u>
1. Introduction	1
2. ORNL Clad Burst Test Facility	3
2.1 Test Specimen Assembly	3
2.2 Flaw Fabrication	4
2.3 Facility for Testing of Clad-Burst Specimens	4
2.3.1 Containment Vessel/Thermal Oven.....	5
2.3.2 Pressurization System.....	5
2.3.3 Data Acquisition System	5
2.4 Test Procedure	6
3. Clad-Burst Shakedown Tests	8
3.1 First Shake-down Test (CB 1).....	8
3.2 Second Shakedown Test (CB 2).....	8
4. Clad-Burst Failure Tests (Phase 1).....	11
4.1 Test Results	11
4.2 Clad Thickness Measurements	11
4.3 Analysis Results	12
5. Cladding Materials Characterization.....	13
5.1 Tensile Tests.....	13
5.2 J-R Curve Testing.....	13
6. Fractographic Studies	15
7. Clad-Burst Failure Tests (Phase 2 Matrix).....	16
7.1 Clad Thickness Measurements	16
7.2 Test Results	16
7.3 Analysis Results	17
8. Conclusions	20
References	22
Appendix A – Operating Procedure for HSST Clad Burst Test Facility.....	84
Appendix B – Machine Drawings for Fabrication of Containment Vessel Assembly	90

LIST OF TABLES

<u>Table</u>	<u>Page</u>
4.1 Failure Pressures and Post-Test Thickness Measurements for HSST Burst-Disk Tests CB 2-8*	23
5.1 Summary of All Clad-Burst Tensile Tests at 600°F—Eight Specimens from PVRUF	23
5.2. Summary of All Available Plastic-Flow Properties for SS Cladding.....	23
5.3a Summary of Pre-cracked Charpy Test Results for PVRUF Cladding at 600°F	24
5.3b Correspondence Between Ring and Clad Burst Specimen IDs	24
7.1 Summary of Failure Pressures for the Phase 2 Test Matrix	25
7.2. Notch Defect Calculations for Tests CB 11 at 2000 psig Applied Pressure (Impending Instability)	25

LIST OF FIGURES

<u>Figure</u>	<u>Page</u>
2.1. Test specimen design utilized in the HSST clad-burst testing program.....	26
2.2. Clad layer at the bottom of the machined cavity (6 in. diameter) of the test specimen	27
2.3. Cavity plate/clad specimen assembly prior to attachment of backing plate: (a) plan view and cross section; (b) cavity plate being welded to clad specimen surface	28
2.4. High-pressure connection through the cavity plate of the test specimen assembly.	29
2.5. Test specimen assembly: (a) test specimen and backing plate; (b) backing plate being attached to specimen/cavity plate assembly; and (c) assembly being moved to containment facility.	30
2.6. Schematic drawing of ORNL/HSST clad-burst test facility	31
2.7. Isometric drawing of containment vessel assembly: (a) containment vessel with upper and lower closure plates (tracked wheels are attached to lower closure plate); (b) support plate with mounted rails to move containment vessel in and out of thermal oven (only one-half of support plate extends into thermal oven).	32
2.8. Containment vessel prior to being rolled into thermal oven.	33
2.9. Digital controller unit for Thermcraft heater oven.	33
2.10. High-pressure system: (a) system overview; (b) intensifier unit and accumulator tank; (c) air-actuated control valves; and (d) cooling tank.	34
2.11. Console of data acquisition system used to control clad-burst test facility during failure test. ..	35
2.12. Photographs of thermocouple gages placed on test specimen: (a) gages interior to the specimen cavity; and (b) an exterior gage.....	36
2.13. Exploded view indicating orientation of instrumentation assembly and catcher plate relative to the test specimen assembly.	37
2.14. View of proximity transducer for measuring center point deflection of the clad layer under applied pressure loading.....	38
2.15. CMOD gage used in Phase 2 test matrix: (a) capacitance-type gage; (b) knife-edge attachment of CMOD gage to clad burst specimen CB-11.	39
2.16. Modified fixture for measuring lateral deflection of the clad disk at quarter-point locations, designed and fabricated to be compatible with simultaneous use of the capacitance-type CMOD gage.	40
2.17. Final assembly of vessel containing the test specimen assembly: (a) attachment of proximity transducer; (b) closure head lowered into position; and (c) bolting down of closure head.....	41
3.1. Views of the deformed clad layer segment resulting from the first clad-burst test: (a) surface of clad layer corresponding to clad/base metal interface prior to machining of cavity; (b) deformation of surface due to impact with proximity gage probe used to measure center point deflection of cladding under pressure loading.	42
3.2. Centerline displacement versus time as recorded during the second clad burst disk experiment, CB 2.....	43

LIST OF FIGURES (continued)

<u>Figure</u>	<u>Page</u>
3.3. Applied pressure load versus time: (a) complete loading history; and (b) loading history near time of failure for specimen CB 2.	44
3.4. Finite-element model used for ORNL analyses of clad-burst specimens (unflawed).	45
3.5. Contours of effective plastic strain computed from finite element model of clad disk specimen.	46
3.6. Contours of maximum principal stress computed from finite element model of clad disk specimen.	47
3.7. Applied pressure versus clad center-point deflection and instability pressure for the second clad burst experiment: comparison of ABAQUS finite-element predictions with measured data.	48
4.1. Clad disk removed from specimen CB 5, containing a notch of 0.050 in. initial depth; the specimen failed at a pressure of 2,641 psi.	49
4.2. Clad disk removed from specimen CB 8, containing a notch of 0.025 in. initial depth (the specimen failed at a pressure of 3,139 psi): (a) flawed surface; and (b) clad surface corresponding to inner surface of vessel.	50
4.3. Centerline displacements versus lateral pressure loading for clad-burst specimens CB 2, 3, and 4.	51
4.4. Elapsed time versus lateral pressure loading for clad-burst specimens CB 2, 3, and 4.	52
4.5. Centerline displacements versus lateral pressure loading for clad-burst specimens CB 5 and CB 6.	52
4.6. Elapsed time versus lateral pressure loading for clad-burst specimens CB 5 and CB 6.	53
4.7. Comparison of measured centerline displacements to finite-element model predictions for (a) specimens CB 2 and CB 3, (b) specimen CB 4.	54
4.7. (continued) Comparison of measured centerline displacements to finite-element model predictions for (c) specimens CB 5 and CB 6.	55
4.8. Experimentally-observed failure pressures compared to two modeled failure mechanisms: (1) plastic collapse of remaining ligament based on modified theory of Chakrabarty and Alexander (1970) for median prediction and (2) ductile tearing: (a) using J_{Ic} data from pre-cracked Charpy specimens for PVRUF cladding at 316°C (600°F).	56
4.8. (continued) (b) using J_{Ic} data from pre-cracked Charpy specimens for PVRUF cladding at 316°C (600°F)	57
5.1. Cutting plan for fabrication of tensile specimens. “R#” refers to the ring number R1 or R2 from which the tensile specimens were extracted; ring R1 was taken from clad burst specimen CB 4 and R2 from CB 5.	58
5.2. Dimensions of clad tensile specimens.	59
5.3. Plots of stress versus strain (engineering) from eight clad tensile specimens.	60
5.4. Plots of (a) true stress versus true strain data and (b) probability density functions for fitted statistical marginal distributions based on data in Table 5.2.	61

LIST OF FIGURES (continued)

<u>Figure</u>	<u>Page</u>
5.5. Cutting plan for Charpy specimens taken from clad burst specimens CB 6-8 for generation of J-R curves in the T-S and L-S orientations.	62
5.6. Cutting plan for one-half thickness Charpy specimens taken from clad burst specimen CB 3 for generation of J-R curves in the T-L orientation.....	63
5.7. Typical J-R curves obtained from the PVRUF cladding in different orientations.	64
5.8. Statistical distribution for PVRUF J_{Ic} (a) probability density with fitted Weibull density and (b) Weibull cumulative distribution function compared to cumulative probabilities of J_{Ic} data from pre-cracked Charpy specimens from PVRUF (estimated by median rank order statistic $p = (i-0.3)/(n+0.4)$).	65
5.9. Statistical distribution for J_{Ic} (a) histogram of data from NUREG/CR-5511 and 6363 extrapolated to 318.33°C (605°F) with fitted log-logistic density overplot and (b) log-logistic cumulative distribution function compared to cumulative probabilities of J_{Ic} data from NUREG/CR-5511 and 6363 estimated by median rank order statistic $p = (i-0.3)/(n+0.4)$	66
6.1. Clad-burst specimen CB 4 containing flaw with depth 0.172 in.: shear region is far from surface.	67
6.2. Clad-burst specimen CB 4 containing flaw with depth 0.172 in.: shear band reaches the surface.	67
6.3. Clad-burst specimen CB 4 containing flaw with depth 0.172 in.: transition from tearing to shear mode of fracture.	68
6.4. Clad-burst specimen CB 5 containing flaw with depth 0.050 in.....	69
6.5. Clad-burst specimen CB 5 containing flaw with depth 0.050 in.....	69
6.6. Clad-burst specimen CB 5 containing flaw with depth 0.050 in.: typical fracture surface within tearing region.	70
6.7. Clad-burst specimen CB 5 containing flaw with depth 0.050 in.: typical fracture surface within shear region.	70
7.1. Locations of pre-test clad thickness measurements made on Phase 2 clad burst specimens.	71
7.2. Pressure versus load-line displacement data for clad-burst specimen CB 9.	71
7.3. Pressure versus load-line displacement data for clad-burst specimens CB 11 and CB 12.....	72
7.4. Pressure versus load-line displacement data for clad-burst specimen CB 13.	72
7.5. Pressure versus CMOD data for clad-burst specimens CB 11 and CB 12.....	73
7.6. Pressure versus gage displacement data for clad-burst specimen CB 13.....	73
7.7. Comparisons of failure pressure versus crack depth, both normalized by clad thickness, for the Phase 1 (open symbols) and Phase 2 (filled symbols) test series consisting of CB 9 through CB 12; test CB 13 was terminated prior to failure.	74
7.8. Comparison of calculated and measured pressure versus load-line displacement for clad-burst specimen CB 9. Calculations and data represent deflections at the <u>center</u> of the clad disk. Initial root radius of FEM was 0.01 in.....	75

LIST OF FIGURES (continued)

<u>Figure</u>	<u>Page</u>
7.9. Comparison of calculated and measured pressure versus load-line displacement for clad-burst specimen CB 11. Initial root radius of FEM was 0.01 in.	76
7.10. Comparison of calculated and measured pressure versus load-line displacement for clad-burst specimen CB 12. Initial root radius of FEM was 0.001 in.	76
7.11. Comparison of calculated and measured pressure versus CMOD for clad-burst specimen CB 11.	77
7.12. Comparison of calculated and measured pressure versus CMOD for clad-burst specimen CB 12. Initial root radius of FEM was 0.001 in.	77
7.13. Comparison of calculated and measured pressure versus load-line displacement for clad-burst specimen CB 13. Initial root radius of FEM was 0.01 in.	78
7.14. Finite element model with simulated gage height above the clad surface used in analysis of test CB 13.	78
7.15. Comparison of calculated and measured pressure versus gage displacement at 0.07 in. above the clad surface for clad-burst specimen CB 13.	79
7.16. Calculated pressure versus CMOD for clad-burst specimen CB 13.	79
7.17. Applied J versus measured pressure for clad-burst specimens: (a) CB 9 (failure pressure was 3,955 psi), and (b) CB 11 and CB 12. Initial root radius of FEMs was 0.01 in.	80
7.18. J-applied versus CTOD: (a) CB 9, and (b) CB 11 and CB 12.	81
7.19. Undeformed and deformed flaw-tip of FEM model: (a) CB 9 with root radius = 0.01 in (b) CB 11 with root radius = 0.005 in, and (c) CB 11 with root radius = 0.01 in.	82
7.20. Analysis of pre-cracked Charpy specimen: (a) 3-D finite element model of PCVN specimen; (b) applied J versus CTOD curve generated from analysis.	83

1. Introduction

In support of the Nuclear Regulatory Commission (NRC), the Heavy-Section Steel Technology (HSST) Program at the Oak Ridge National Laboratory (ORNL) has investigated the influence of cladding defects on burst pressure of the damaged Davis-Besse (D-B) reactor pressure vessel (RPV) upper head. Previous analyses of the D-B head performed by ORNL (Williams et al. 2003) included both deterministic and probabilistic assessments of the pressure retained by the cladding in the corrosion wastage region of the RPV head in the absence of cladding defects. Results of those analyses supported the conclusion that rupture of the cladding at pressures up to the relief-valve set-point pressure (2,500 psi) is an unlikely event. However, those previous analyses did not consider the impact of significant defects in the cladding on this conclusion; information regarding actual defects found in wastage area cladding of D-B became available only after completion of those analyses.

Subsequently, the HSST program was commissioned by the NRC to develop and fabricate a test facility for performing large-scale clad-burst experiments to support NRC/RES efforts to evaluate the structural significance of cladding defects found in the wastage cavity of D-B. This report describes the test specimen, test facility, and experimental effort that constituted the clad burst test program conducted at ORNL in response to the NRC request. The experiments described herein were not intended to represent the “as found” condition of the Davis-Besse wastage cavity, but were designed to provide a technical basis for understanding failure characteristics of the flawed cladding.

Tasks accomplished within the HSST clad-burst testing program at ORNL include the following:

- Based on specifications defined by the NRC, ORNL designed a test specimen and test facility; the test facility was constructed at the Y-12 site in Oak Ridge and included a temperature control chamber, safety containment vessel, pressure loading system, and data acquisition system.
- An ORNL document was prepared for operation of the facility (*Operating Procedure for HSST Clad Burst Test Facility*, Specification No. MET-EMP-SOG81 Rev. 0, January 2003) and approved by cognizant ORNL management, safety officers and quality assurance specialists; that document is included as Appendix A of this report;
- Two shakedown failure tests (CB 1 and CB 2) were conducted in the facility using test specimens fabricated from the wall of the Pressure Vessel Research Users’ Facility (PVRUF) vessel [Pennell and Pugh (1989)]; conditions in the second test (CB 2) satisfied

the criteria that were defined in specifications for the facility as drafted by the NRC (NRC Facility Specifications, 2003);

- Based on evaluation of test results, the facility was declared to be operational by ORNL;
- A test matrix was defined to quantify the influence of cladding defects on the burst pressure and on the mode of failure for the ORNL-designed test specimens. The original test matrix, consisting of 12 specimens, was divided into two phases (i.e., Phases 1 and 2) of six specimens each; only five specimens were actually tested in Phase 2.
- The Phase 1 test matrix, consisting of one unflawed and five flawed specimens (nos. CB 3-8), was completed during FY 2003.
- A second Phase 2 matrix was executed in FY 2004, including one unflawed and 4 flawed specimens tested to failure (i.e., CB 9-13), as well as additional instrumentation for recording crack-mouth opening displacement (CMOD) on selected flawed specimens.
- Material characterization of the PVRUF cladding was carried out at 600°F, including tensile testing, J-R testing in the T-S and T-L orientations, as well as fractographic studies of failed defects in the flawed burst specimens.
- Analytical interpretations were performed for clad-burst specimens tested in the Phase 1 and 2 programs to confirm failure models developed and described in a companion report [Williams, Yin, and Bass (2004)]. Those failure models were used to assess the structural integrity of the unbacked cladding in Davis Besse.

Detailed descriptions of the tasks conducted within the clad-burst testing program at ORNL are given in the following sections.

2. ORNL Clad Burst Test Facility

The clad burst test specimen and facility designed and fabricated at ORNL to satisfy the NRC specifications are described in this section.

2.1 Test Specimen Assembly

The test specimen (shown in Fig. 2.1) is machined from a 22 in. diameter blank extracted from the beltline region of the PVRUF shell (the vessel head and bottom were no longer available). The inner surface of the cladding in the test section is left in the “as found” condition, i.e., no machining is performed on that surface. (Here, the inner surface of the test specimen cladding corresponds to the inner surface of the parent RPV). The ferritic material in the test specimen consists of PVRUF plate exclusively, i.e., no weld metal was utilized.

A cavity is machined beneath the cladding having a circular diameter of 6 in. (see Figs. 2.1 and 2.2). This configuration provides an exposed clad surface that is larger in cross sectional area than the “foot print” measured from the dental mold taken from the D-B cavity (28.3 in.² for the test specimen versus approximately 18 in.² for the D-B cavity [Hyres (2003)]). The fabrication drawings prepared by ORNL called for a nominal clad thickness of 0.24 in. over the exposed section of cladding, which approximates that of the D-B cavity. However, the actual specimens received from the machine shop exhibited lower clad thicknesses, the mean values of which varied in the range 0.14-0.23 in. The discrepancy between target and measured values can be traced, in part, to the requirement that the circular cavity of the specimen be machined down to the clad/ferritic “interface.” In practice, that interface was found to be an irregular surface, the definition of which proved to be somewhat subjective for those machinists responsible for fabricating the specimens. A tendency to remove all but small traces of ferritic material from the bottom of the cavity resulted in relatively thinner clad layers in several specimens.

A 2 in.-thick cavity plate is welded to the clad specimen to produce a thin, sealed cavity over the inner clad surface (see Fig. 2.3). A high-pressure connection through the center of the cavity plate (see Fig. 2.4) allows for pressure loading of this cavity bounded on one side by the inner surface of the clad layer. During a typical test, pressure over the clad inner surface is increased until structural failure of the clad layer is detected. Structural failure of the specimen is indicated by a

sudden (plastic instability/complete rupture) or slower (ductile tearing) pressure drop as measured by the in-line pressure transducers.

A backing plate [see Fig. 2.5(a)] is bolted to the test specimen/cavity plate unit to produce an assembly ready for testing (except for instrumentation described below). Tension in the 12 hold-down bolts [2 in. diameter, SA540, or equivalent, spaced at equal intervals around the circumference of the specimen, shown in Fig. 2.5(b)] is increased sufficiently such that the weld used to attach the cavity plate to the test specimen will not experience tensile stress at any time during the loading transient. This configuration is intended to prevent failure of the seal weld during the high-pressure loading transient. In Fig. 2.5(c), the test specimen assembly is ready for placement into the containment vessel of the test facility (described below).

2.2 Flaw Fabrication

The flaws in the clad burst specimens were machined using the electro-discharge machining (EDM) process. A graphite shim, 0.010-0.012 in. thick, was cut with the leading edge in the shape of the final flaw. All flaws were flat-bottomed with radii at each end equal to the flaw depth, i.e., a 0.050 in. deep flaw would have 0.050 in. radii at each end. The flaws were all 2 in. long at the free surface. Since the curvature of the specimen surface being flawed was convex, the flaw was the prescribed thickness at the midpoint only; each end was approximately 0.006 in. shallower than the midpoint. The flaw was machined using a plunge-cut, perpendicular to the backside clad surface. Successive shims were used as each shim wore down due to erosion that is typically associated with the process. The final cut was made with a fresh shim to assure that the flaw profile was as specified (within ± 0.002 in.). Due to the thickness of the shim material and the manner in which the graphite electrode erodes, the radius of the machined flaw tip was estimated to be in the range of 0.005 in. to 0.01 in. No further alteration of these finite root-radius defects was made prior to testing; in particular, no effort was made to fatigue-sharpen the notches.

2.3 Facility for Testing of Clad-Burst Specimens

Major components of the clad-burst test facility are depicted in the schematic drawing of Fig. 2.6. Those components include (a) a containment vessel, (b) a thermal oven, and (c) a high-pressure system for loading of the clad layer in the specimen. Not shown is a data acquisition system for controlling test parameters and recording test results. Each of the elements is describe in more detail in the following sections.

2.3.1 Containment Vessel/Thermal Oven

A two-part cylindrical vessel is used to contain the test specimen assembly during a test intended to produce failure of the specimen cladding; the overall dimensions of the vessel are 25 in. inner diameter, 8 in. wall thickness, and 48 in. height. The containment vessel is designed to capture any elements that could be ejected from the test assembly following failure of the cladding. Four inch thick plates provide upper and lower closure of the vessel. Castors are attached to the lower plate to allow the vessel to be rolled in and out of the thermal oven on steel tracks. Isometric drawings of the vessel and rail track assembly are shown in Fig. 2.7; machine drawings of the vessel are include as Appendix B.

Control of test temperature is achieved by placing the containment vessel and test specimen assembly into a Thermcraft floor-model heat-treatment oven; a photograph in Fig. 2.8 shows the containment vessel in front of the oven. Maximum operating temperature for the Thermcraft is 750°F. The digital controller shown in Fig. 2.9 maintains the oven environmental temperature to within ± 2 °F of the controller set point.

2.3.2 Pressurization System

Major components of the high-pressure loading system are illustrated schematically in the diagram of Fig. 2.6. Photographs of those components as they appear in the actual test facility are provided in Fig. 2.10, including the intensifier unit and accumulator tank, air-actuated control valves, and cooling tank for the pressure line exiting the oven.

2.3.3 Data Acquisition System

The computer-controlled data acquisition system is used to perform the following functions: (a) monitor transducer output from thermocouples, pressure gages, proximity displacement gage, and CMOD gage; (b) write transducer data to disk at a sampling rate controlled by the user; (c) control all valves and gas supply and display their configuration; and (d) control operation of the intensifier unit. A photograph of the computer console and signal-conditioning unit is included in Fig. 2.11.

During all phases of a burst test, temperatures are monitored using thermocouples located at various positions, including (1) the oven environment, (2) the upper, mid, and lower sections of the containment vessel, (3) exterior points on the test specimen, and (4) four points within the specimen cavity. Photographs of thermocouple gages attached to the test specimen assembly are

shown in Fig. 2.12. System pressure is monitored from the console at the locations shown in Fig. 2.6.

In Fig. 2.13, an exploded view is shown of (a) the capacitance-type proximity transducer used for measuring center-point deflection of the clad disk during the Phase 1 test matrix and (b) the catcher plate, relative to the test specimen assembly. The catcher plate is designed to protect the base of the proximity transducer from cladding fragments that could break free during a high-pressure test. A close-up view of the proximity displacement transducer used for the Phase 1 test matrix is shown in the photograph of Fig. 2.14.

A capacitance-type CMOD gage [Fig. 2.15(a)] was used in testing of three flawed specimens (i.e., CB 11-13) as part of the Phase 2 matrix. The gage is positioned on knife-edge attachments that were tack-welded to the cladding on each side of the flaw [see Fig. 2.15(b)]. Installation of the CMOD gage precluded use of the center-point proximity gage (Fig. 2.14). Thus, a new fixture for measuring lateral deflection of the clad disk at quarter-point locations (measured along the diameter of the disk that contained the plane of the flaw) was designed and fabricated to be compatible with simultaneous use of the CMOD gage (see Fig. 2.16). The maximum range for the new lateral deflection transducer is 0.30 in.

Final preparations for a test include attachment of the displacement transducer to the test specimen, which is followed by lowering of the upper closure head over the transducer/test specimen assembly, and bolting down of that closure head (see Fig. 2.17).

2.4 Test Procedure

A brief outline of the test procedure is given as follows:

1. Apply instrumentation at the appropriate points of the assembly and bolt the fabricated test specimen to the pressure backing plate.
2. Place the test specimen assembly into the containment unit and close the upper head of the unit.
3. Connect all instrumentation cables from the specimen assembly to the appropriate inputs of the data acquisition system.
4. Place the containment unit into the Thermcraft heater oven and bring the oven to test temperature.

5. Activate the computer-controlled data acquisition system and test the specimen to failure of the cladding.
6. Secure the data recorded on the data acquisition system.

A detailed description of the test procedure is provided in the document included as Appendix A.

3. Clad-Burst Shakedown Tests

3.1 First Shake-down Test (CB 1)

Heating of the thermal oven was initiated on a schedule that allowed 24 hours to bring the test specimen to a target temperature of approximately 600°F. After that target temperature was achieved, the operating procedure for the pressure-loading sequence was initiated by the project manager. A pressure of 10 ksi applied to the clad layer of the specimen was achieved after approximately one minute of loading. Subsequently, five additional cycles of the high-pressure pump were required to maintain pressure on the clad layer in the range 9-11 ksi over a 10 min period. During that period, the center point deflection of the clad layer increased monotonically, with complete failure of the cladding occurring at a measured deflection of approximately 1.1 in. Following loss-of-pressure, all data were secured and the cool-down cycle was initiated for the oven.

Following complete cool-down to room temperature, the containment vessel was disassembled to provide access to the test specimen assembly. Inspection of the assembly revealed that the clad layer failed by tearing completely around the circumference of the cavity (see Fig. 3.1). Impact of the unrestrained clad disk with the displacement transducer probe resulted in severe tearing/deformation of a portion of the disk as well as some damage to the instrumentation since this first test did not have the catcher plate shown in Fig. 2.13.

3.2 Second Shakedown Test (CB 2)

Emphasis in the second test (i.e., CB 2) was placed on achieving a substantially lower rate of specimen pressurization to minimize dependence of the clad deformation on loading rate.

The following parameters were employed in the test:

- The loading rate for the test was approximately 100 psi/min;
- Three hold periods (approx. five min. each) were conducted at 2,200, 4,000, and 6,000 psi;
- The disk temperature was 602°F.

The unflawed disk went unstable at a pressure of 6,153 psi and failed. The total loading cycle occurred over a period of approximately 75 min. Failure occurred around the perimeter of the 6 in. diameter clad disk. The failed clad disk was launched into the catcher plate attached to the specimen.

Figures 3.2–3.7 depict some of the measured data from the second test, as well as analytical interpretations derived from elastic-plastic finite element analyses. In Fig. 3.2, the measured centerline displacement is plotted as a function of time; the three pressure hold intervals are shown in the plot. The applied pressure versus time is depicted in Fig. 3.3; the complete loading history is shown in Fig. 3.3(a), while the loading history near failure is given in Fig. 3.3(b).

Analytical interpretations of the experiment are summarized in Figs. 3.4–3.7. It should be noted that those analysis results are based on generic clad tensile properties - material characterization of the clad material utilized in the test was not available at the time those analyses were performed. Also, the finite element model of the test specimen incorporated a nominal clad thickness of 0.25 in., whereas the mean thickness of the cladding in the specimen (measured post-test) was 0.227 in. Figure 3.4 depicts a three-dimensional (3-D) finite-element model of the clad disk used in the ABAQUS analyses; the inset figure shows the stress-strain curves used in the model. Figures 3.5–3.6 illustrate contours of effective plastic strain and maximum principal stress, respectively, computed from the finite-element model at 7,290 psi; the latter value corresponds to a point of numerical (plastic) instability for the finite model and is taken as the computed failure pressure. Those results predict that failure of the unflawed disk should occur at the perimeter of the disk from plastic instability; the latter prediction was confirmed by the outcome of the experiment.

In Fig. 3.7, the measured pressure versus clad center-point deflection is compared with the prediction from ABAQUS finite-element calculations. Also shown in Fig. 3.7 is the failure condition predicted by a model based on the work of Chakrabarty and Alexander (1970), using a clad thickness of 0.25 in. Chakrabarty and Alexander (1970) applied Tresca's yield criterion and associated flow rule in the development of a theoretical model for plastic bulging of circular diaphragms under a lateral pressure loading. The resulting strain distributions (which included the effects of strain hardening) in the neighborhood of the deformed hemispherical pole provided a theoretical estimate for the polar strain at instability. The specific failure mechanism addressed by this model was *incipient tensile plastic instability* (i.e., plastic collapse) of the diaphragm which was the expected failure mode for the unflawed clad disk tests. The measured and computed

failure pressures can be rendered more comparable if they are normalized by the appropriate clad thickness: measured data, 6.15 ksi/0.227 in. = 27.1 ksi/in.; 3-D finite element model, 7.29 ksi/0.25 in. = 29.2 ksi/in.; C & A, 6.9 ksi/ 0.25 in. = 27.6 ksi/in. There was reasonable agreement between measured data and the analytical predictions, especially considering that generic stress-strain properties were used in the calculations.

Based on evaluations of the second shakedown test and analyses of that test, within the context of the NRC requirements (NRC Facility Specifications, 2003), ORNL declared the test facility to be operational and suitable for conducting the testing program requested by the NRC.

4. Clad-Burst Failure Tests (Phase 1)

4.1 Test Results

Table 4.1 summarizes the failure pressure results for the second shakedown test and the six clad-burst failure tests conducted within the Phase I matrix. Two of those test specimens (i.e., CB 2-3) were unflawed and five contained surface flaws of length 2 in. and depths ranging from 0.025 in. to 0.172 in. As discussed previously, failure of the unflawed specimens was due to plastic instability around the perimeter of the 6 in. diameter clad disk, as predicted by the analyses. Failure of the flawed specimens was due to through-clad cracking that initiated from the fabricated defects; there was no evidence of plastic instability around the perimeter of the disk such as that exhibited by the unflawed specimens. Fracture surfaces for all five of the flawed specimens exhibited clear indications of a ductile tearing mode of fracture (discussed further in Section 6 of this report). Figures 4.1 and 4.2 show photographs of clad disks removed (post-test) from specimen CB 5 (containing a notch of 0.050 in. initial depth) and specimen CB 8 (tested with a notch of 0.025 in. initial depth), respectively. A comparison of the specimen surfaces shown in Figs. 4.1(a) and 4.2(a) indicates that more ferritic material was left on the clad layer of specimen CB 5 (Fig. 4.1) during machining of the circular cavity than on CB 8 (Fig. 4.2). The latter observation is consistent with the greater mean thickness recorded for specimen CB 5 in Table 4.1.

Figure 4.3 provides plots of centerline displacement versus pressure loading measured in tests CB 2, CB 3, and CB 4; specimens CB 2 and 3 were nominally identical unflawed specimens. Plots of elapsed time versus applied pressure loading from the same three tests are shown in Fig. 4.4. During the loading transient, specimen CB 3 was subjected to full unload-reload cycles at 1,000 psi intervals to provide data on permanent deformation of the clad layer as a function of applied pressure. Analogous plots for clad-burst tests 5 and 6 are given in Figs. 4.5 and 4.6. The latter two tests were fabricated with nominally identical notches having a depth of 0.050 in.

4.2 Clad Thickness Measurements

Posttest measurements of the clad layer thickness were made on seven of the test specimens at 24 points distributed over the circular clad disk; a digital micrometer was employed for those measurements. Mean values of the thickness measurements are given in Table 4.1; flaw depth normalized by the mean thickness is also given for the flawed specimens in Table 4.1. Those

mean values range from 0.164 in. to 0.227 in. and for reasons previously discussed, are significantly lower than the target value of 0.24 in.

4.3 Analysis Results

Post-test interpretations of the clad-burst tests were carried out using three-dimensional finite-element analyses and measured data from the tests. Figures 4.7(a)–4.7(c) provides comparisons between the measured center-point deflections for tests CB 2–6 and the displacements predicted by finite-element models of the test specimens. Unflawed specimens CB 2 and CB 3 represent nominally the same geometry and are compared in Fig. 4.7(a). Likewise, specimens CB5 and CB 6, representing the same flaw geometry (0.05 in. depth, 2 in. length), are compared in Fig. 4.7(c). In Fig. 4.7(b), addition of a constant offset value (i.e., -0.14 in.) to the measured deflection values improves agreement with computed values for the flawed test specimen CB 4. (It should be noted that these analyses provide no information concerning the pressure level that corresponds to initiation of ductile tearing in the flawed test specimens.)

In Fig. 4.8, experimentally-observed failure pressures, normalized by mean clad thickness, from the clad burst tests of Phase 1 (see Table 4.1) are compared to two modeled failure mechanisms: (1) plastic collapse of the remaining ligament based on a modified theory of Chakrabarty and Alexander (1970) for median prediction and (2) ductile tearing. Figure 4.8(a) uses J_{Ic} data from pre-cracked Charpy specimens for PVRUF cladding at 316°C (600°F), described herein in Section 5. The 99% confidence interval for the plastic-collapse mode is based on combined model and material uncertainties. The 99% confidence interval on ductile tearing initiation is based on a Weibull distribution fitted to the PVRUF J_{Ic} data only (see Fig. 5.8). Figure 4.8(b) also uses J_{Ic} data from pre-cracked Charpy specimens for PVRUF cladding at 316°C (600°F). The 99% confidence interval for the plastic-collapse mode is based on material uncertainty only and is derived from a bivariate lognormal distribution that includes correlated uncertainties in the yield and ultimate true stresses. The 99% confidence interval on ductile tearing initiation is unchanged from that of Fig. 4.8(a). The plots given in Fig. 4.8 are consistent with the observed dominance of ductile tearing as the failure mode for the flawed specimens.

5. Cladding Materials Characterization

Characterization of the PVRUF cladding was carried out at 600°F, including tensile testing and J-R testing in the T-S and T-L orientations. Those data play an important role in interpretations of the experimental results and in evaluations of the cladding failure models.

5.1 Tensile Tests

A set of cladding stress-strain curves was generated at 600 °F using tensile specimens fabricated post-test from the clad layer of the flawed specimens CB 4 and CB 5. Tensile specimens were cut from the clad layer of each specimen according to the diagram given in Fig. 5.1; two specimens were cut parallel to the flaw plane in the central test section, while the remaining two were in the transverse orientation. All specimens were taken from the annular ring surrounding the clad disk that was pressurized to failure in the burst tests. The test section of each specimen (see Fig. 5.2) had a cross section with dimensions of 0.25 in. x 0.1875 in. Plots of stress versus strain (engineering) obtained from the eight clad tensile specimens are compared in Fig. 5.3. Results for the eight tensile tests are summarized in Table 5.1. Yield and ultimate stress values from the PVRUF tensile data¹ are compared in Table 5.2 with other clad data, including archival data (NUREG/CR-3927, NUREG/CR-5511, and NUREG/CR-6363), as well as data generated from cladding removed from the Davis-Besse cavity (Hyres, 2003). In Fig. 5.4, plots are provided for (a) true stress versus true strain data and (b) probability density functions for fitted statistical distributions based on data in Table 5.2.

5.2. J-R Curve Testing

Sets of *J-R* curves were generated for the clad layer of the PVRUF material² in the T-L, T-S and L-S orientations at 600 °F using pre-cracked Charpy-type specimens taken from clad-burst specimens CB 3 and CB 6-8. Figure 5.5 depicts the cutting plan for Charpy specimens taken from clad burst specimens CB 6-8 and used for generation of *J-R* curves in the T-S and L-S orientations. Through-thickness composition of these specimens consisted of (approximately) equal parts base metal and cladding. The specimens were side-grooved and then pre-cracked completely through the base metal and slightly into the cladding layer. The cutting plan for one-

¹ Previously unpublished PVRUF cladding tensile data.

² Previously unpublished PVRUF cladding ductile-tearing data.

half thickness Charpy specimens taken strictly from the clad layer of clad burst specimen CB 3 is shown in Fig. 5.6. The latter Charpy specimens were used for generation of clad layer J-R curves at 600°F in the T-L orientation. Results obtained from the J-R testing program are summarized in Table 5.3. Typical J-R curves obtained from the PVRUF cladding in different orientations are shown in Fig. 5.7.

A statistical distribution for PVRUF J_{Ic} data is shown in Fig. 5.8 in the form of (a) probability density with fitted Weibull density and (b) Weibull cumulative distribution function compared to cumulative probabilities of J_{Ic} data from pre-cracked Charpy specimens from PVRUF (estimated by median rank order statistic $p = (i-0.3)/(n+0.4)$). The PVRUF data in Fig. 5.8 can be compared with archival data given in Fig. 5.9. Figure 5.9(a) provides a histogram of data from NUREG/CR-5511 and NUREG/CR-6363 extrapolated to 318°C (605°F) with fitted log-logistic density overplot. In Fig. 5.9(b), a log-logistic cumulative distribution function is compared to cumulative probabilities of J_{Ic} data from NUREG/CR-5511 (Haggag et al. 1990) and NUREG/CR-6363 (Haggag et al. 1997) estimated by median rank order statistic $p = (i-0.3)/(n+0.4)$.

6. Fractographic Studies

The Metals and Ceramics Division at ORNL conducted fractographic studies of flaws in specimens CB 4-7 to determine the extent of failure of each defect due to ductile failure and tensile (necking) instability. Fracture surfaces from the four specimens were examined by scanning electron microscope. Although the initial notch depth was variable, all fracture surfaces exhibited similar features. In all cases, the majority of the fracture surface was represented by ductile dimples that are clear indications of a tearing mode of fracture. Cracks grow from the bottom of the notch through the thickness. Practically, there was no crack growth on the edges of the notch, regardless of the notch depth. On all specimens, an area of ductile dimples was surrounded by a very narrow band of “glide”-like or “shear”-like appearance. On all specimens, the width of the band varied slightly around an average value of about 0.25 mm. The flat appearance of the fracture surface in these bands indicates lower fracture toughness values associated with this mode of fracture compared to the tearing fracture. Results obtained from clad-burst specimens CB 4 and CB 5 are shown in Figs. 6.1-6.3 and Figs. 6.4-6.7, respectively.

7. Clad-Burst Failure Tests (Phase 2 Matrix)

In response to NRC requests, ORNL performed four additional clad burst failure tests to (1) evaluate repeatability of test results, and (2) record CMOD data (in two tests) that potentially could be used to infer initiation of ductile tearing. Flaws were fabricated in three of the four specimens tested as part of this Phase 2 matrix. Those flaw dimensions were given as follows: specimen CB 9, 0.025 in. x 2 in. flaw; specimens CB 11 and CB 12 both contained a 0.050 in. x 2 in. flaw; the fourth specimen, CB 10, was tested as an unflawed specimen. A fifth flawed specimen (flaw depth 0.025 in. and length 2.0 in.), CB 13, was tested up to an applied pressure of 1,700 psi and then subjected to a planned termination of the test prior to reaching failure. Objectives of test CB 13 were to perform unloading compliance measurements (at approximately 100 psi intervals) and to determine the extent of stable ductile tearing (if any) of the flaw prior to reaching onset of instability.

7.1 Clad Thickness Measurements

Pretest clad thickness measurements were made at 48 locations on the exposed clad surface of each specimen, the mean values of which are given in Table 7.1; locations for those measurements are marked by open white circles on the clad surface in Fig. 7.1. The thickness measurements were incorporated into post-test analytical interpretations of the experiments.

For specimen CB 13, both surfaces of the clad layer were machined (EDM) to remove as many imperfections as possible and to provide a test section of uniform cylindrical contour and thickness. This resulted in a smaller mean thickness (0.14 in) compared to the other specimens.

7.2 Test Results

In Phase 2, failure modes for the unflawed and flawed specimens were the same as those described for the Phase 1 matrix. The failure pressures recorded in each of the four failure experiments are given in Table 7.1. In Figs. 7.2-7.4, measured data describing pressure versus deflection of the clad surface are compared for test specimens CB 9, CB 11, CB 12 and CB 13. Data for specimen CB 9 are center-point deflections recorded using the original proximity transducer depicted in Fig. 2.14; CMOD measurements were not attempted for the latter test. The quarter-point deflections plotted for specimens CB 11, CB 12, and CB 13 were recorded using the redesigned proximity transducer (see Fig. 2.16) that is compatible with the CMOD transducer

(see Fig. 2.15) employed in the latter tests. The quarter-point deflection plots terminate at 0.30 in., which is the maximum range of the capacitance-type transducers used in the tests. In Fig. 7.4, unloading compliance cycles are evident in the measured data for CB 13.

Plots of measured pressure versus CMOD for specimens CB 11 and CB 12 are given in Fig. 7.5; in those plots, the recorded gage data have been corrected to account for the elevation of the capacitance gage above the clad surface (approximately 0.07 in). Instability of the defect near the failure pressures is reflected in the rapid increase of measured values for CMOD. The uncorrected gage displacement data for CB 13 are shown in Fig. 7.6.

Failure pressures versus crack depth (with both parameters normalized by estimated or measured mean clad thicknesses) for the Phase 2 test series are compared with those from Phase 1 in Fig. 7.7. Also shown are plots of median predictions with 99% confidence intervals for ductile tearing-initiation and for plastic collapse of the test specimens (see Section 4). For ductile-tearing initiation, the 99% confidence interval was developed from a Weibull statistical distribution fitted to PVRUF J_{Ic} pre-cracked Charpy V-notch data (sample size = 14 data points) taken at 600 °F. The median plastic collapse curve is based on a modified theoretical treatment of plastic collapse of the remaining ligament of a flaw, centered in a circular burst disk. The original theory (without the flaw) is due to Chakrabarty and Alexander (1970). The 99% confidence interval for the remaining-ligament plastic-collapse curves were derived from statistical distributions that characterize the uncertainty in the predictive accuracy of plastic instability solutions (a log-Laplace distribution) and the uncertainty in the PVRUF plastic-flow properties, specifically bivariate inverted-Weibull distributions fitted to PVRUF yield and ultimate (tensile) stress data (sample size = 8 data points) taken at 600 °F. The comparisons shown in Fig. 7.7 indicate a high degree of repeatability for the tests performed in the two phases of the clad burst program. For test CB 2, CB 3, and CB 10 with no flaw, comparison with the theoretical prediction confirms the previously observed bias of the theory to predict burst pressures slightly (conservatively) higher than the experimental data.

7.3 Analysis Results

In Figs. 7.8-7.12, 3-D finite-element model solutions for tests CB 9, CB 11 and CB 12 are compared with measured data obtained from those tests. Individual 3-D models were constructed for each experiment to reflect specific flaw depths and clad thicknesses; the initial notch root radius used for each model is indicated in the appropriate figure caption. The computed results for

pressure versus cladding deflection (see Figs. 7.8–7.10) are in good agreement with the measured data up through the mid-range of loading, beyond which the finite element models stiffen somewhat relative to the data.

Corresponding finite-element model solutions of pressure versus CMOD for tests CB 11 and CB 12 are compared to measured data in Figs. 7.11 and 7.12, respectively. Plots in Fig. 7.11 illustrate the limited effect of initial notch root radius on calculated CMOD values for radii ranging from 0.0005 to 0.01 in. The 3-D finite element models allow progressive blunting of the notch defect with increasing load, but do not incorporate any mechanism for modeling of ductile initiation and tearing of the defect. The good agreement between calculated and measured CMOD data up to the onset of instability (near 2 ksi) implies that ductile tearing initiates near the maximum load and (with a small increase in load) rapidly progresses through the clad layer to produce failure of the specimen. Results from the CB 13 test are consistent with this interpretation to the extent that no evidence of ductile initiation or tearing was observed in post-test fractographic examinations of the notch defect. However, evidence from CB 13 would be more compelling had the specimen been loaded to a pressure closer to instability than that actually achieved during the test (i.e., 1700 psi).

In Fig. 7.13, calculated pressure versus load-line displacement is shown to be in good agreement with measured data for clad-burst specimen CB 13. In Fig. 7.14, a small column of elements was added to the finite element model adjacent to the crack mouth of CB 13; the height of the column (0.07 in) provides an approximate location of the knife-edge supports for the CMOD gage used in that test. Pressure versus displacement calculated at the top of the column is in good agreement with measured gage data, as shown in Fig. 7.15. A correction similar to that used for tests CB 11-12 was not applied to the CB 13 data because of the flaw depth/root diameter ratio fabricated in the latter specimen. Figure 7.16 depicts the calculated pressure versus CMOD for test CB 13.

In Fig. 7.17, applied J values versus pressure are plotted for tests CB 9, CB 11 and CB 12. Far-field J values were used in constructing the plots due to the relatively large initial root radius (i.e., 0.01 in.) used in constructing the 3-D finite element models. The J values calculated near the onset of instability for CB 9, (~ 0.9 in-kip/in.² near 3,800 psi), CB 11 (0.82 in-kip/in.² near 2,000 psi), and CB 12 (0.87 in-kip/in.² near 2,000 psi), compare well with a median $J_Q = 0.91$ in-kip/in.² determined from pre-cracked Charpy data for the PVRUF cladding at 600 °F (see Table 5.3). In comparison, the J values calculated near the onset of instability for these clad burst test specimens

did not agree well with archival data established by testing larger C(T) specimens (median $J_Q = 0.46$ in-kip/in.²). The foregoing results suggest that constraint-related factors influencing flaw behavior in the clad-burst specimens are better approximated in the pre-cracked Charpy specimens, rather than in the high-constraint C(T) specimens.

Analyses of near crack-tip deformation, described below, provide additional support for assessing failure conditions of the clad burst specimens in terms of the Charpy fracture toughness data. The relevance of pre-cracked Charpy data to the interpretation of failure conditions in the flawed clad burst specimens was explored in terms of crack-tip opening displacement (CTOD) calculations performed for the two different geometries. Plots of J -applied versus CTOD computed from 3-D finite element models of specimens CB 9, CB 11 and CB 12 are shown in Fig. 7.18. For CB 9, the CTOD for the notch near the initiation/instability region is estimated to be ~ 0.017 in. (no CMOD data are available for CB 9 to support this estimate). Values of CTOD at 2,000 psi (near the onset of initiation and then instability) for test CB 11 are given for a range of initial root radii in Table 7.2. The CTOD values vary between 0.009–0.01 in. over the initial root radii interval 0.005–0.01 in.; as indicated above in Section 2.2, the fabricated flaws were estimated to fall in the latter range. Corresponding J values are given in Table 7.2.

Figure 7.19 depicts cross sections of the deformed and undeformed notch region of 3-D finite element models used in the analyses of specimens CB 9 and CB 11. For CB 9 [see Fig. 7.19(a)], the notch has an initial root radius of 0.01 in. and is deformed to CTOD = 0.017 in. at 3,800 psi (i.e., near the failure pressure). For CB 11 [Figs. 7.19(b) and (c)], the models incorporated two initial root radii, i.e., 0.005 in. [Fig. 7.19(b)] and 0.01 in. [Fig. 7.19(c)], and represent computed deformation of the notch region at the measure failure pressure of 2,270 psi. For that condition, the computed CTOD for CB 11 is of the order 0.01 in.; results for test CB 12 are similar.

For purposes of comparison, CTOD calculations were performed for the pre-cracked Charpy specimen using 3-D finite element models. The finite element model is shown in Fig. 7.20(a) and the calculated pressure versus CTOD results are plotted in Fig. 7.20(b). At the median value of $J_Q = 0.91$ in-kip/in.², the calculated CTOD for the Charpy specimen is 0.0115 in. The latter value of CTOD is very similar to that determined from analyses of near-instability conditions in specimens CB 11 and CB 12.

8. Conclusions

A test facility for performing large-scale clad-burst experiments was designed and fabricated at ORNL to support NRC/RES efforts in evaluating the structural significance of cladding defects found in the wastage cavity of Davis-Besse vessel head. A test specimen was designed and 13 specimens were fabricated from beltline sections of the PVRUF reactor pressure vessel. Following completion of two shake-down tests (CB 1-2), ORNL tested the remaining specimens in two phases, the first of which (Phase I) consisted of one unflawed and five flawed specimens (CB 3-8). A second Phase 2 matrix was executed in FY 2004, consisting of one unflawed and four flawed specimens (CB 9-13); additional instrumentation for recording crack-mouth opening displacement (CMOD) was employed on three of the flawed specimens tested in Phase 2. Material characterization of the PVRUF cladding was carried out at 600 °F, including tensile testing and J-R testing in the T-S and T-L orientations. Fractographic studies were performed on failed defects in the flawed burst specimens. Finally, analytical interpretations were performed for the clad-burst specimens tested in both Phase 1 and 2. Specific conclusions or observations derived from that testing program include the following:

- A comparison of failure pressure data normalized by clad layer thickness indicates a high degree of repeatability for the tests performed in the two phases of the clad burst program.
- Unflawed clad burst specimens fail around the full perimeter of the disk from plastic instability; an analytical model for plastic collapse was shown to adequately predict those results.
- The flawed specimens tested in the program failed by ductile tearing of the notch defect through the clad layer. For tests instrumented with the CMOD gage, good agreement between calculated and measured CMOD data up to the onset of instability implies that ductile tearing initiates near the maximum load and (with a small increase in load) rapidly progresses through the clad layer to produce failure of the specimen. Results from the one non-failure test are consistent with this interpretation to the extent that no evidence of ductile initiation or tearing was observed in post-test fractographic examination of the notch defect.

- For the failed flaw specimens, fractographic studies revealed that a majority of the fracture surface was represented by ductile dimples, which are clear indications of a tearing mode of fracture. On all specimens, the area of ductile dimples was surrounded by a very narrow band of “glide”-like or “shear”-like appearance.
- For the failed specimens containing flaws, the failure pressures tended to fall below median predictions for ductile tearing initiation based on small specimen data, but within the 99 percent confidence limits.
- Comparisons of computed results from 3-D finite element models with measured gage displacement data (i.e., center-point deflection and CMOD) indicated reasonably good agreement up to the region of instability.
- Analyses of selected clad burst specimens containing flaws produced J and CTOD values near failure conditions that were generally consistent with median J_Q and CTOD values obtained from testing and analysis of pre-cracked Charpy specimens. This observation is derived from specimens representing two different geometries (i.e., a 6 in.-diameter by 0.25 in.-thick clad disk versus a 10 mm-thick Charpy specimen), two different loading conditions (i.e., biaxial loading of the thin plate versus uniaxial bending of the Charpy specimen) and different defect configurations (i.e., 2 in. long notch with initial root radius of 5-10 mils versus a fatigue-sharpened defect ($a/W = 0.5$) in the Charpy specimen).

References

- J. Chakrabarty and J. M. Alexander (1970), "Hydrostatic Bulging of Circular Diaphragms," *J. Strain Anal.* 5(3), 155-161.
- F. M. Haggag, W. R. Corwin, and R. K. Nanstad, (1990), *Irradiation Effects on Strength and Toughness of Three-Wire Series-Arc Stainless Steel Weld Overlay Cladding*, NUREG/CR-5511 (ORNL/TM-11439), Oak Ridge National Laboratory, February 1990.
- F. M. Haggag and R. K. Nanstad (1997), *Effects of Thermal Aging and Neutron Irradiation on the Mechanical Properties of Three-Wire Stainless Steel Weld Overlay Cladding*, NUREG/CR-6363 (ORNL/TM-13047), Oak Ridge National Laboratory, May 1997.
- J. W. Hyres (2003), *Final Report: Examination of the Reactor Vessel (RV) Head Degradation at Davis-Besse*, Report 1140-025-02-24, BWXT Services, Inc, June 2003.
- NRC Facility Specifications (2003), from NRC Form 173, SOEW 60-03-224.
- W. E. Pennell and C. E. Pugh (1989), *Mission Survey for the Pressure Vessel Research Users' Facility (PVRUF)*, NUREG/CR-5350 (ORNL/TM-11133), Oak Ridge National Laboratory, June 1989.
- P. T. Williams and B. R. Bass, (2003), "Structural Assessment of a Corrosion-Degraded Reactor Pressure Vessel Head," *Transactions of the 17th International Conference on Structural Mechanics in Reactor Technology (SMiRT 17)*, Paper No. D03-5, held in Prague, Czech Republic, on August 17–22.
- P. T. Williams, S. Yin, and B. R. Bass, (2004), "Probabilistic Structural Mechanics Analysis of the Degraded Davis-Besse RPV Head," ORNL/NRC/LTR-04/15, Oak Ridge National Laboratory, September 2004.

**Table 4.1. Failure Pressures and Post-Test Thickness Measurements
for HSST Burst-Disk Tests CB 2-8***

HSST Specimen ID	Nominal Flaw Depth, <i>a</i>	Target Thickness, <i>t₀</i>	Target <i>a/t₀</i>	Post Test Thickness, <i>t_{min}</i>	Post Test <i>a/t_{min}</i>	Failure Pressure	
	(in)	(in)	(-)	(in)	(-)	(psi)	(MPa)
2	No Flaw	0.24	0.000	0.227	0	6153	42.42
3	No Flaw	0.24	0.000	NA	0	5262	36.28
4	0.172	0.24	0.717	0.203	0.847	1438	9.91
5	0.050	0.24	0.208	0.223	0.225	2641	18.21
6	0.050	0.24	0.208	0.191	0.262	1966	13.56
7	0.100	0.24	0.417	0.164	0.610	966	6.66
8	0.025	0.24	0.104	0.193	0.130	3139	21.64

* All flaw lengths were 2 in.

**Table 5.1. Summary of All Clad-Burst Tensile Tests at 600 °F—
Eight Specimens from PVRUF**

PVRUF Specimen ID	Burst Specimen Source	Orientation*	Eng. Yield Strength (0.2%)	Eng. Ultimate Strength	Uniform Elongation	Total Elongation	True Yield Stress (0.2%)	True Ult. Stress
			(ksi)	(ksi)	(%)	(%)	(ksi)	(ksi)
1-1	4	Transverse	29.75	53.90	27.9	33.2	29.81	68.94
1-2	4	Transverse	28.79	52.63	29.3	33.2	28.85	68.05
1-3	4	Parallel	28.08	52.4	26.8	31.2	28.14	66.44
1-4	4	Parallel	29.24	52.09	26	31.2	29.30	66.44
2-1	5	Transverse	29.76	53.79	30.2	34.8	29.82	70.03
2-2	5	Transverse	29.87	53.67	29.6	33.6	29.93	69.56
2-3	5	Parallel	30.91	55.12	23.8	28.4	30.97	68.24
2-4	5	Parallel	31.16	54.95	23	26.4	31.22	67.59
PVRUF	NA	Averages	29.70	53.57	27.1	31.5	29.75	68.16

* Relative to clad deposition direction

Table 5.2. Summary of All Available Plastic-Flow Properties for SS Cladding

Source	Material	Specimen ID	Test Temp.	True Yield Stress	True Ultimate Stress	<i>K</i>	<i>n</i>
			(°F)	(ksi)	(ksi)	(ksi)	(-)
NUREG/CR-3927		CPC-79	550	29.79	73.24	102.09	0.218
NUREG/CR-3927		CPC-80	550	29.79	74.40	103.86	0.221
NUREG/CR-5511	3-wire Cladding	A20A	550	31.70	72.96	100.94	0.206
NUREG/CR-5511	3-wire Cladding	A20B	550	36.60	69.97	93.18	0.168
NUREG/CR-6363	3-wire Cladding	A18C	550	28.60	75.37	103.56	0.227
NUREG/CR-6363	3-wire Cladding	A24A	550	31.00	71.54	99.00	0.206
HSST Clad Burst Tests	PVRUF Cladding	1-1	600	29.81	68.94	95.45	0.206
HSST Clad Burst Tests	PVRUF Cladding	1-2	600	28.85	68.05	94.41	0.209
HSST Clad Burst Tests	PVRUF Cladding	1-3	600	28.14	66.44	92.16	0.209
HSST Clad Burst Tests	PVRUF Cladding	1-4	600	29.30	66.44	92.16	0.199
HSST Clad Burst Tests	PVRUF Cladding	2-1	600	29.82	70.03	97.14	0.209
HSST Clad Burst Tests	PVRUF Cladding	2-2	600	29.93	69.56	96.37	0.207
HSST Clad Burst Tests	PVRUF Cladding	2-3	600	30.97	68.24	93.98	0.197
HSST Clad Burst Tests	PVRUF Cladding	2-4	600	31.22	67.59	92.88	0.194
BWXT	DB Cladding	B2C2A1	600	30.53	70.53	97.66	0.206
BWXT	DB Cladding	B2C2A2	600	31.36	73.49	101.96	0.209
NSE Handbook	SS 308/308L	Table II	600	31.00	69.65	114.91	0.228

Table 5.3a Summary of Pre-cracked Charpy Test Results for PVRUF Cladding at 600°F

Ring 3 Full Thickness			
Charpy Specimen ID	Test Temperature	J_Q	Tearing Modulus
	(°C)	(kJ/m ²) / (in-kips/in ²)	
R3P1	315.6	166.18/0.9489	N/E
R3T1	315.6	197.18/1.126	214.71
R3T6	315.6	161.66/0.9230	172.69

Ring 4 Full Thickness			
Charpy Specimen ID	Test Temperature	J_Q	Tearing Modulus
	(°C)	(kJ/m ²) / (in-kips/in ²)	
R4P2	315.6	121.6/0.694	242.13
R4T2	315.6	185.67/1.060	160.19
R4T5	315.6	184.2/1.052	N/E

Ring 5 Full Thickness			
Charpy Specimen ID	Test Temperature	J_Q	Tearing Modulus
	(°C)	(kJ/m ²) / (in-kips/in ²)	
R5P2	315.6	143.67/0.8203	130.56
R5T1	315.6	182.15/1.040	154.60
R5T5	315.6	216.53/1.236	181.15

Half Thickness, T-L Orientation			
Charpy Specimen ID	Test Temperature	J_Q	Tearing Modulus
	(°C)	(kJ/m ²) / (in-kips/in ²)	
R0T1	315.6	139.45/0.7962	92.15
R0T2	315.6	123.71/0.7063	76.79
R0T3	315.6	112.73/0.6437	113.54
R0T5	315.6	158.33/0.9041	104.26
R0T6	315.6	103.77/0.5925	91.28

N/E = not enough data to estimate the tearing modulus

Table 5.3b Correspondence Between Ring and Clad Burst Specimen IDs

Ring Number ID	Clad Burst Specimen ID
0	CB 3
3	CB 6
4	CB 7
5	CB 8

Table 7.1. Summary of Failure Pressures for the Phase 2 Test Matrix

Clad Burst Specimen ID	Flaw Depth* (in)	Pretest Mean Clad Thickness (in)	Crack Depth / Mean Thickness, a/t (-)	Failure Pressure (psig)
CB 9	0.0250	0.196	0.128	3955
CB 10	NA	0.176	0	4353
CB 11	0.0500	0.228	0.219	2270
CB 12	0.0500	0.234	0.213	2390
CB 13	0.0250	0.140	0.179	NA*

*Planned unloading prior to failure

Table 7.2. Notch Defect Calculations for Tests CB 11 at 2000 psig Applied Pressure (Impending Instability)

Root Radius, r (in)	$CTOD$ at 2000 psig (in)	Ratio of $CTOD / 2r$ (-)	$J_{applied}$ FEM (in-kips/in ²)	$J_{applied}$ E1820 (in-kips/in ²)
0.0005	0.007058	7.0579	0.4107	0.4964
0.0010	0.006859	3.4293	0.4393	0.4824
0.0050	0.008992	0.8992	0.6940	0.6325
0.0100	0.010550	0.5276	0.8211	0.7421

$CTOD$ = crack-tip opening displacement

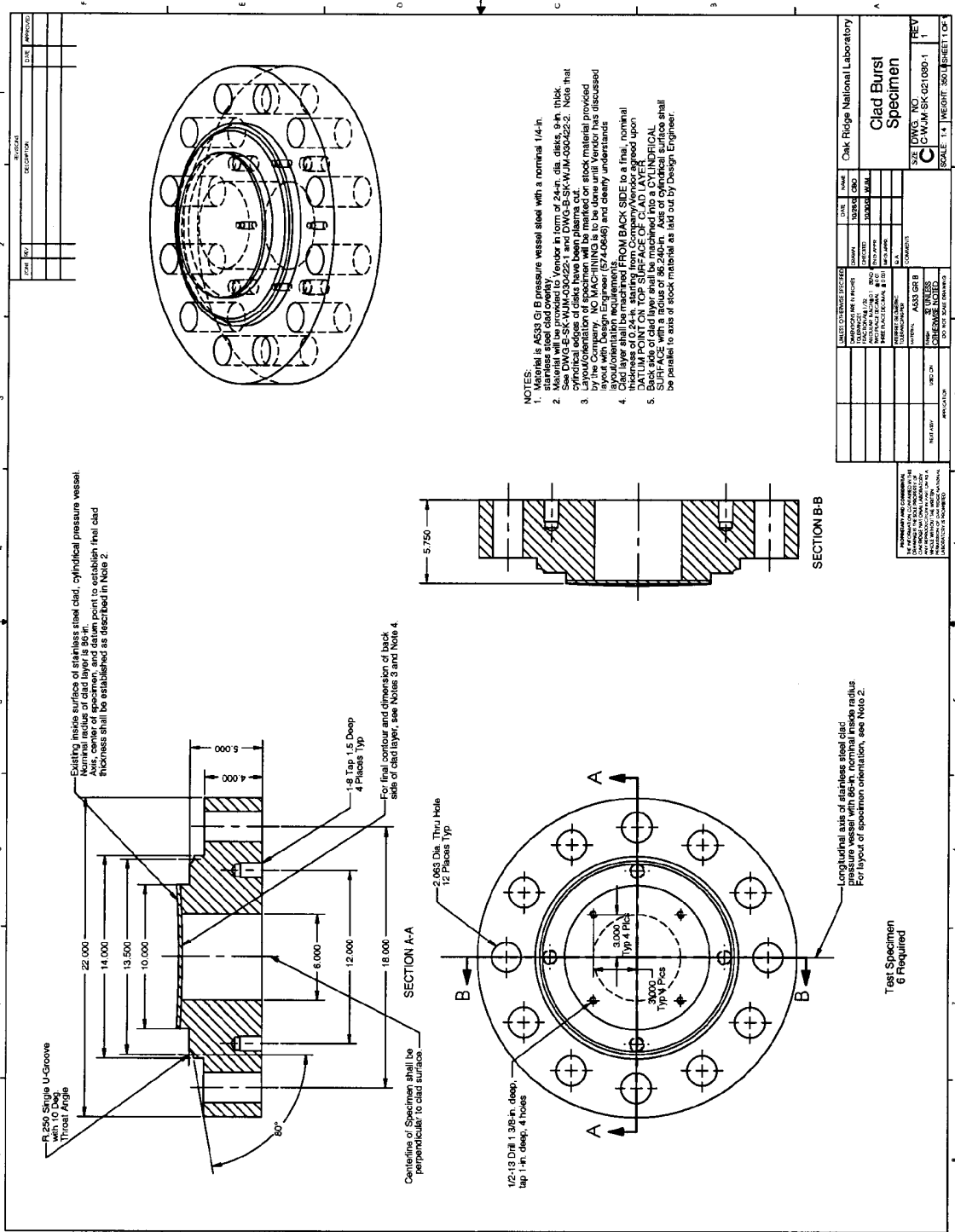


Fig. 2.1. Test specimen design utilized in the HSST clad burst testing program.

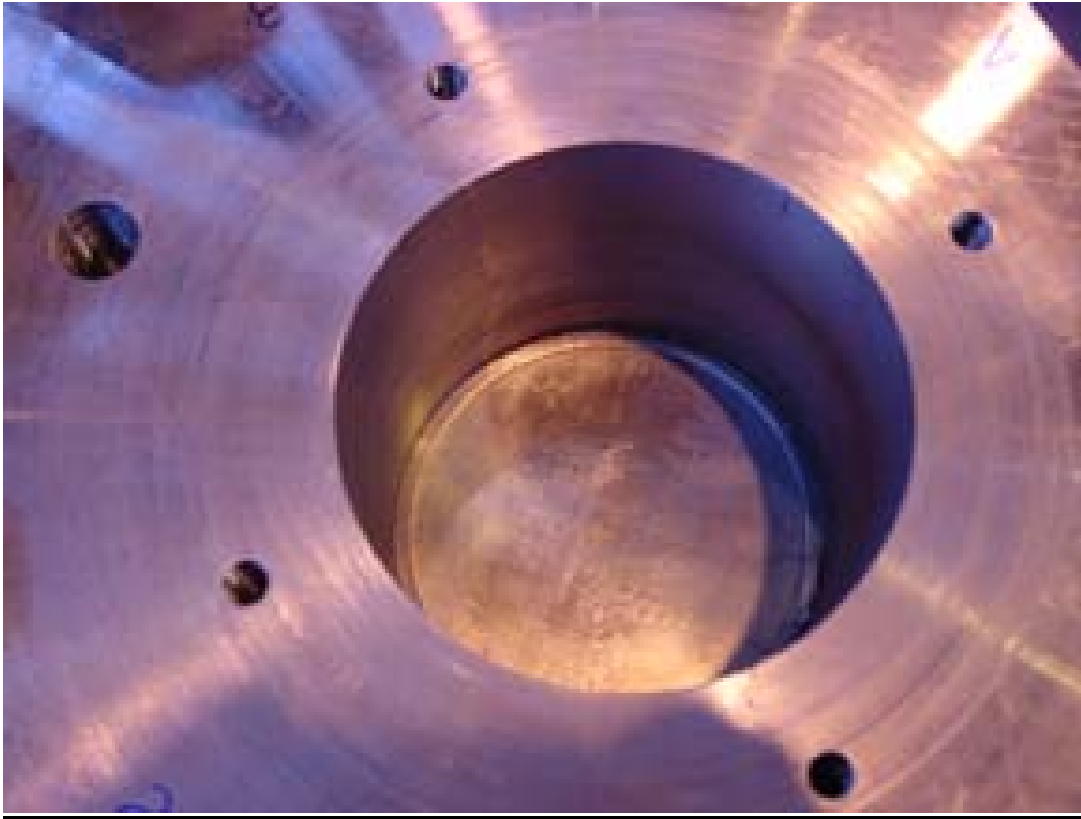
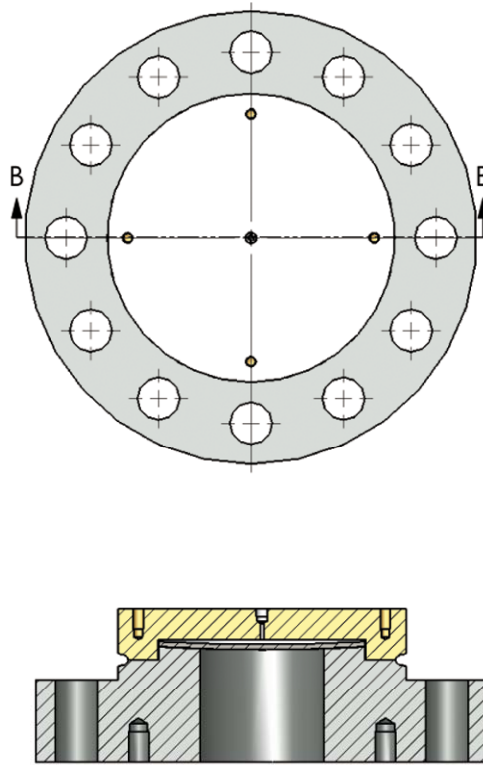


Fig. 2.2. Clad layer at the bottom of the machined cavity (6-in. diameter) of the test specimen.



(a)



(b)

Fig. 2.3. Cavity plate/clad specimen assembly prior to attachment of backing plate: (a) plan view and cross section; (b) cavity plate being welded to clad specimen. The cavity plate provides a thin, sealed cavity that is bounded on one side by the inner clad surface.

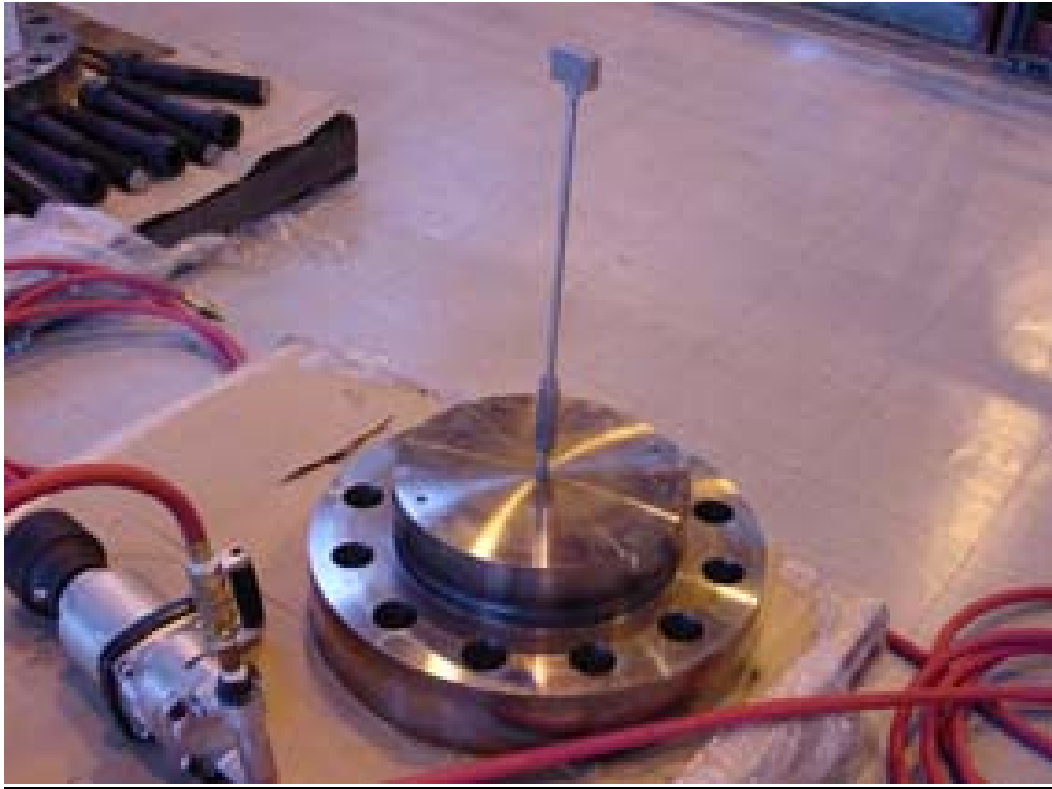


Fig. 2.4. High-pressure connection through the cavity plate of the test specimen assembly.



(a)



(b)



(c)

Fig. 2.5. Test specimen assembly: (a) test specimen and backing plate; (b) backing plate being attached to specimen/cavity-plate assembly; and (c) assembly being moved to containment facility.

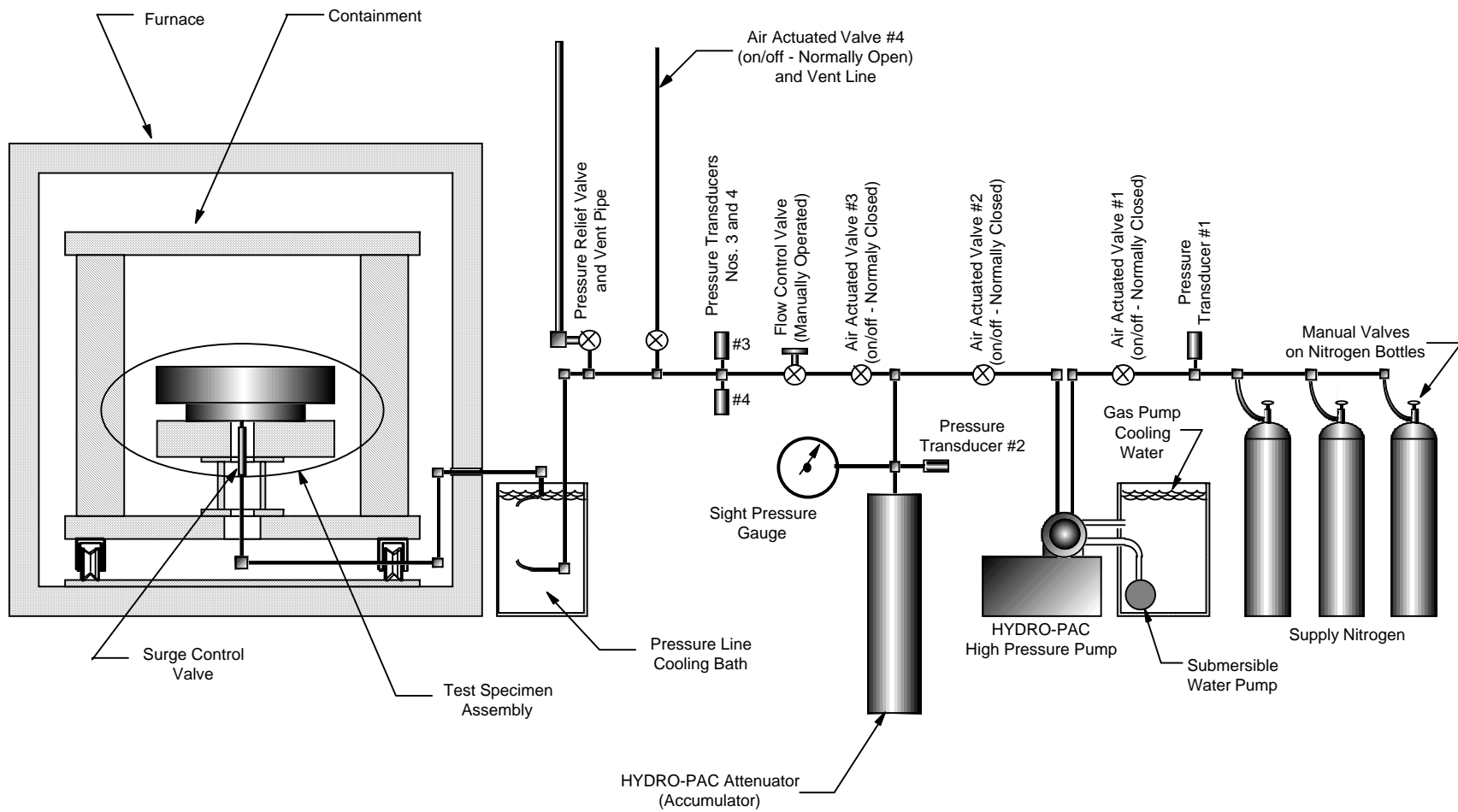
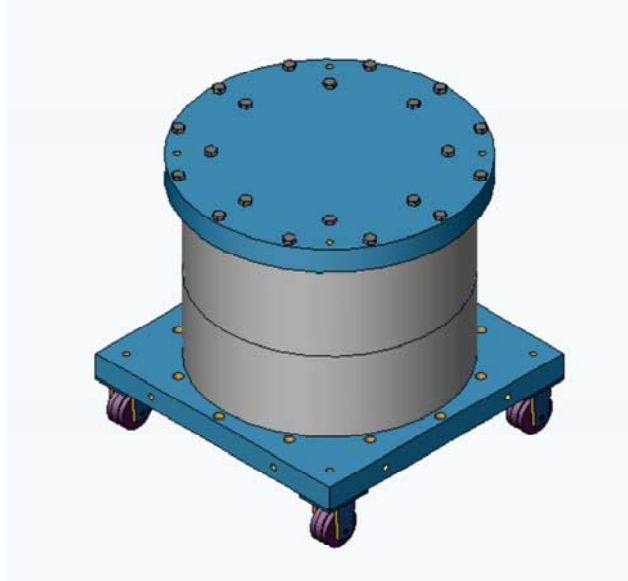
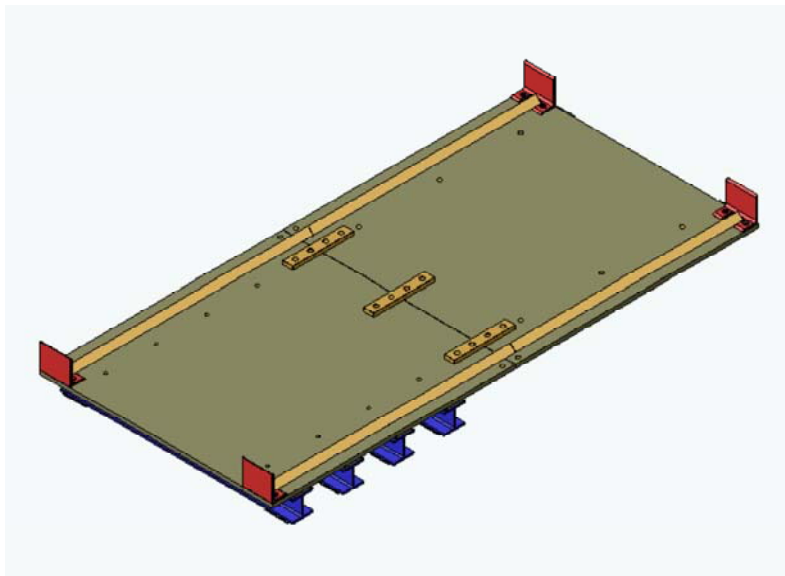


Fig. 2.6. Schematic drawing of ORNL/HSST clad burst test facility.



(a)



(b)

Fig. 2.7. Isometric drawing of containment vessel assembly: (a) containment vessel with upper and lower closure plates (tracked wheels are attached to lower closure plate); (b) support plate with mounted rails to move containment vessel in and out of thermal oven (only one-half of support plate extends into thermal oven).



Fig. 2.8. Containment vessel prior to being rolled into thermal oven.



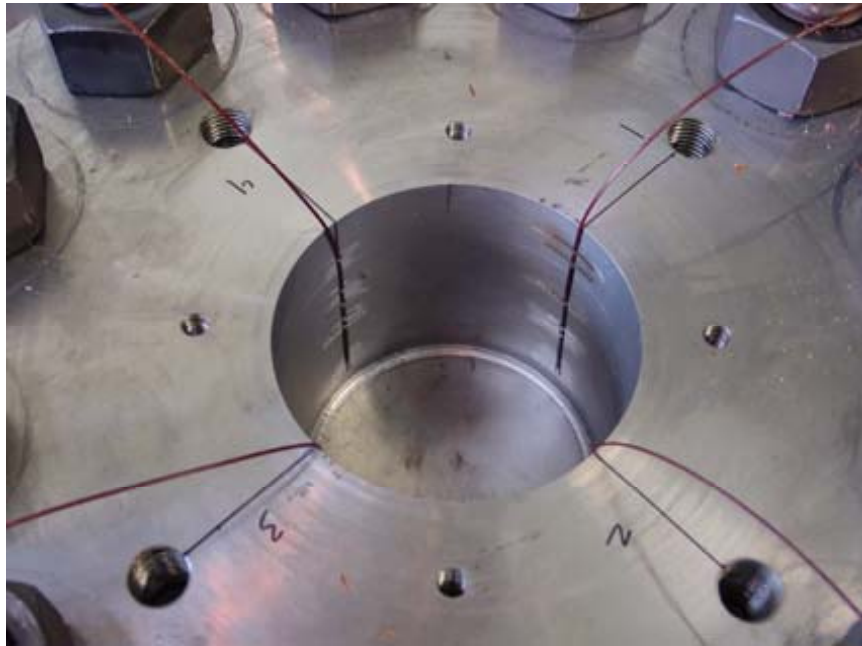
Fig. 2.9. Digital controller unit for Thermcraft heater oven.



Fig. 2.10. High-pressure system: (a) system overview; (b) intensifier unit and accumulator tank; (c) air-actuated control valves; and (d) cooling tank.



Fig. 2.11. Console of data acquisition system used to control clad-burst test facility during failure test.



(a)



(b)

Fig. 2.12. Photographs of thermocouple gages placed on test specimen: (a) gages interior to the specimen cavity; and (b) an exterior gage.

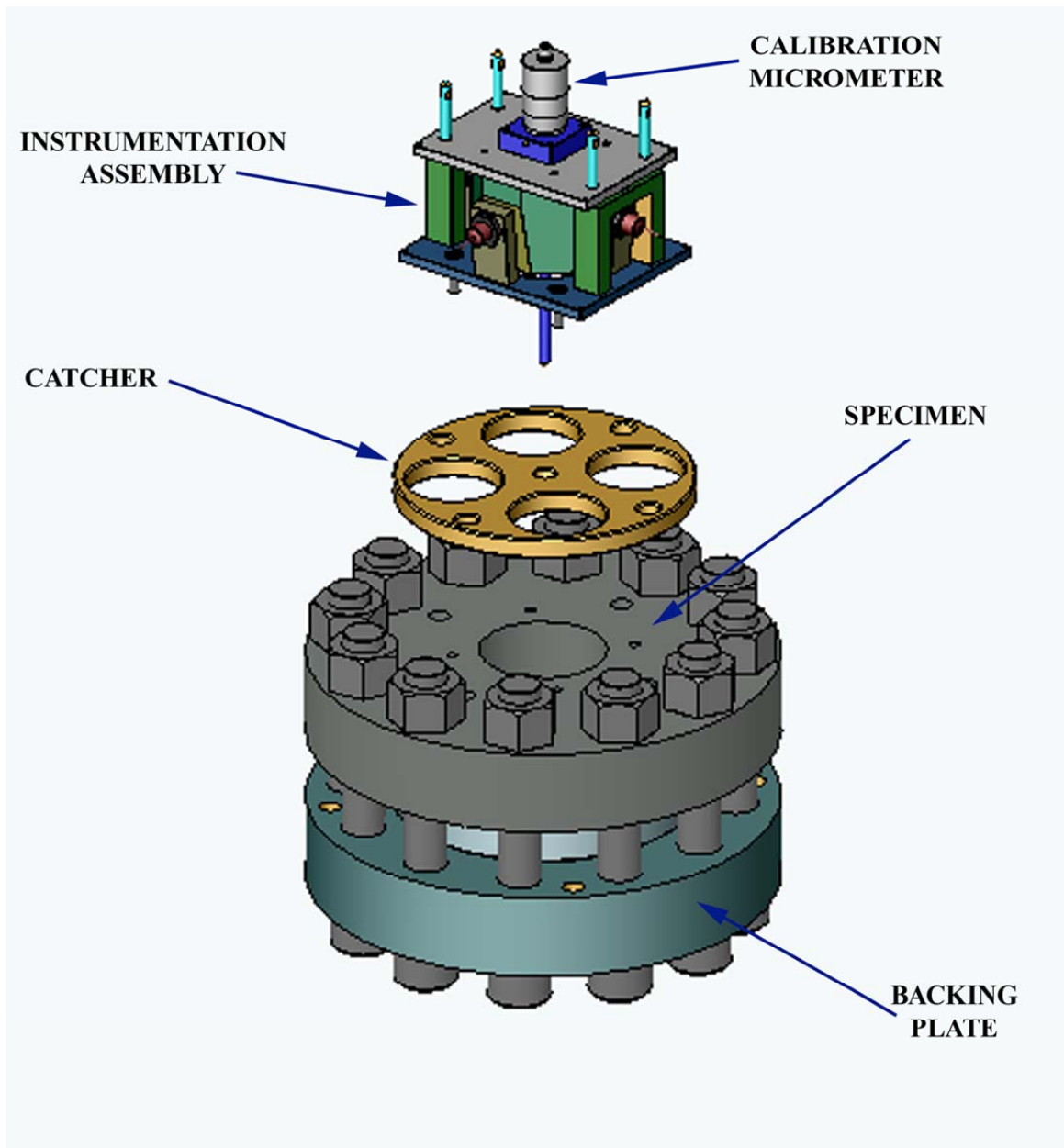


Fig. 2.13. Exploded view indicating orientation of instrumentation assembly (proximity transducer for measuring center-point clad deflection) and catcher plate relative to the test specimen assembly.



Fig. 2.14. View of proximity transducer for measuring center point deflection of the clad layer under applied pressure loading.



(a)



(b)

Fig. 2.15. CMOD gage used in Phase 2 test matrix: (a) capacitance-type gage; (b) knife-edge attachment of CMOD gage to clad burst specimen CB-11.



Fig. 2.16. Modified fixture for measuring lateral deflection of the clad disk at quarter-point locations, designed and fabricated to be compatible with simultaneous use of the capacitance-type CMOD gage.



(a)



(b)



(c)

Fig. 2.17. Final assembly of vessel containing the test specimen assembly: (a) attachment of proximity transducer; (b) closure head lowered into position; and (c) bolting down of closure head.



(a)



(b)

Fig. 3.1. Views of the deformed clad layer segment resulting from the first clad-burst test: (a) surface of clad layer corresponding to clad/base metal interface prior to machining of cavity; (b) deformation of surface due to impact with proximity gage probe used to measure center point deflection of cladding under pressure loading.

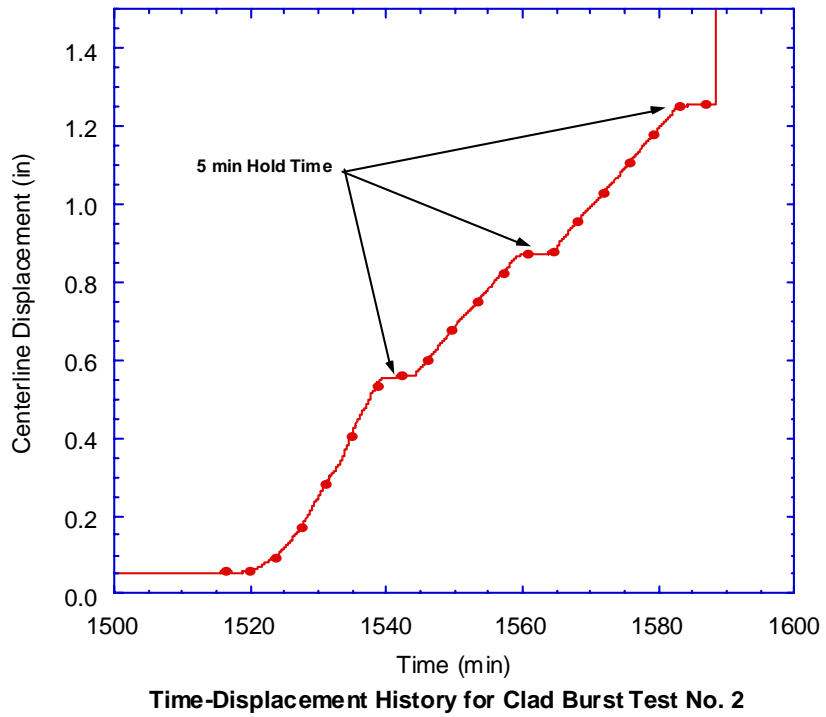
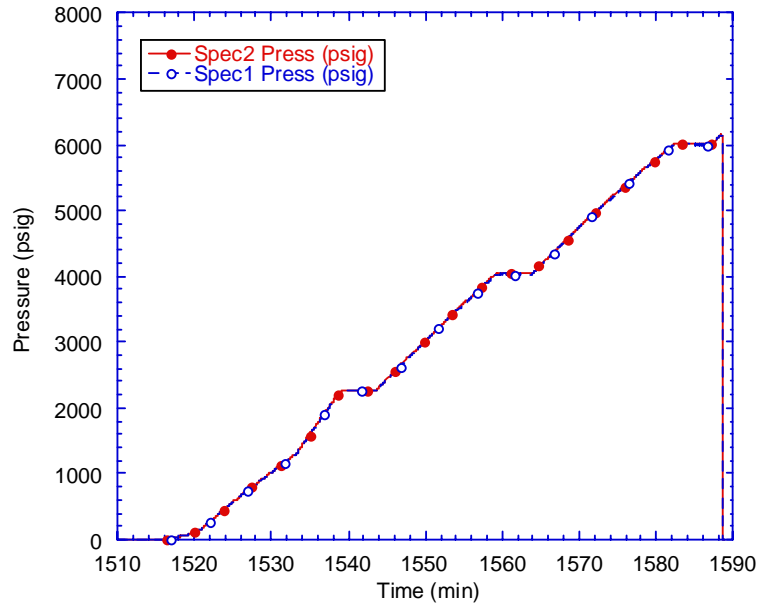
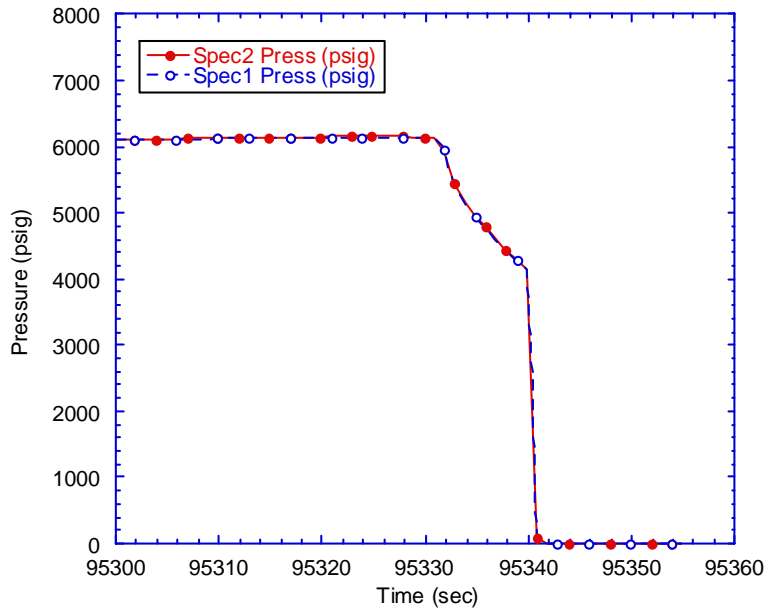


Fig. 3.2. Centerline displacement versus time as recorded during the second clad burst disk experiment, CB 2.



Pressure-Time History for Clad Burst test No. 2

(a)

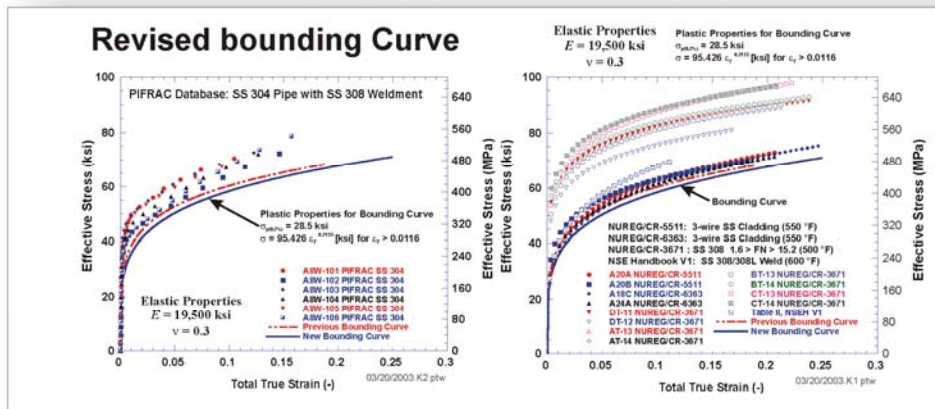
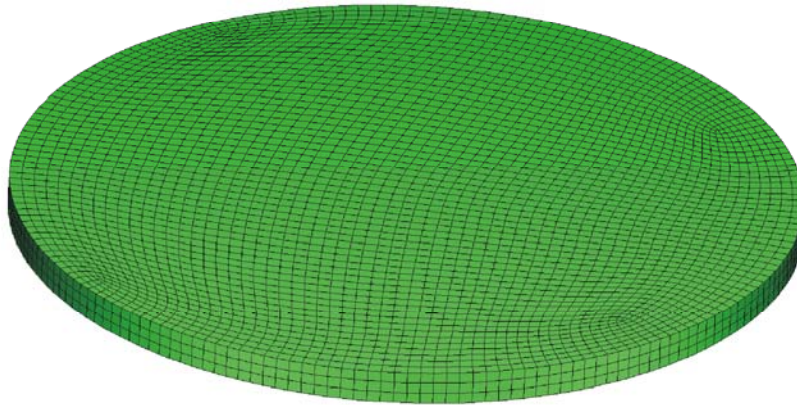


Pressure-Time History for Clad Burst test No. 2

(b)

Fig. 3.3. Applied pressure load versus time: (a) complete loading history; and (b) loading history near time of failure for specimen CB 2.

Finite-Element Model Used for Cladburst Test Analysis



13,896 nodes
10,134 C3D8R

PT Williams
4/14/2003

Fig. 3.4. Finite-element model used for ORNL analyses of clad-burst specimens (unflawed).

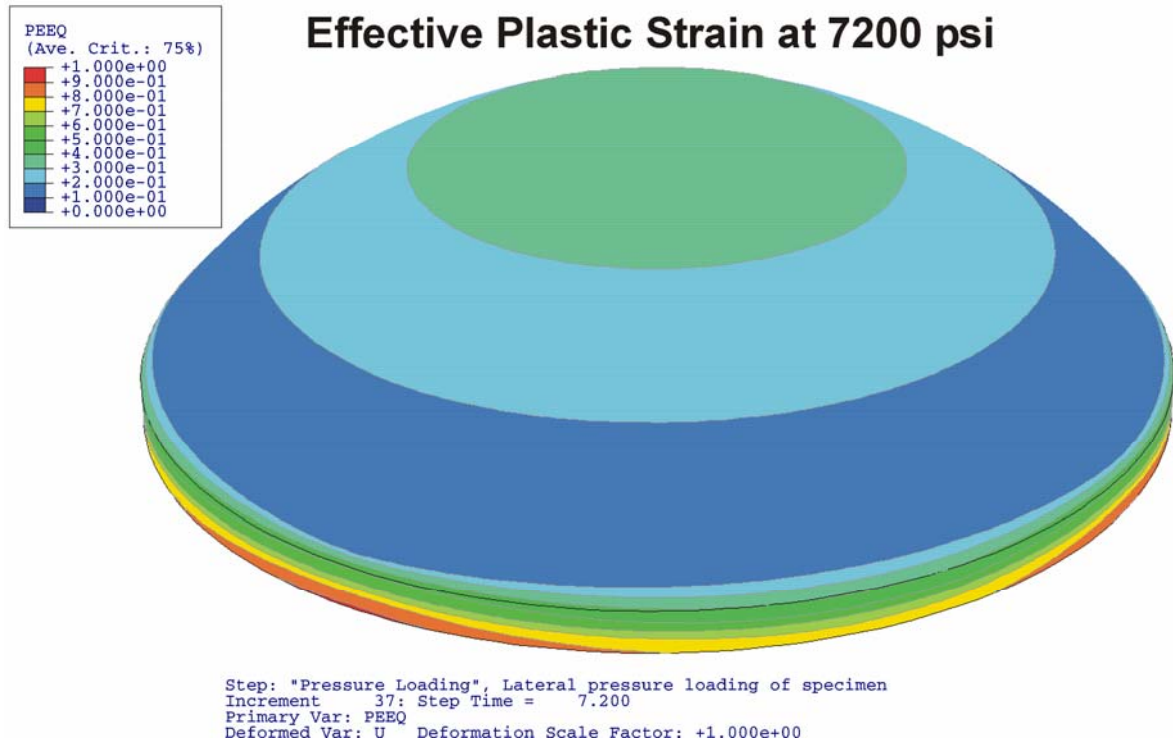


Fig. 3.5. Contours of effective plastic strain computed from finite element model of clad disk specimen.

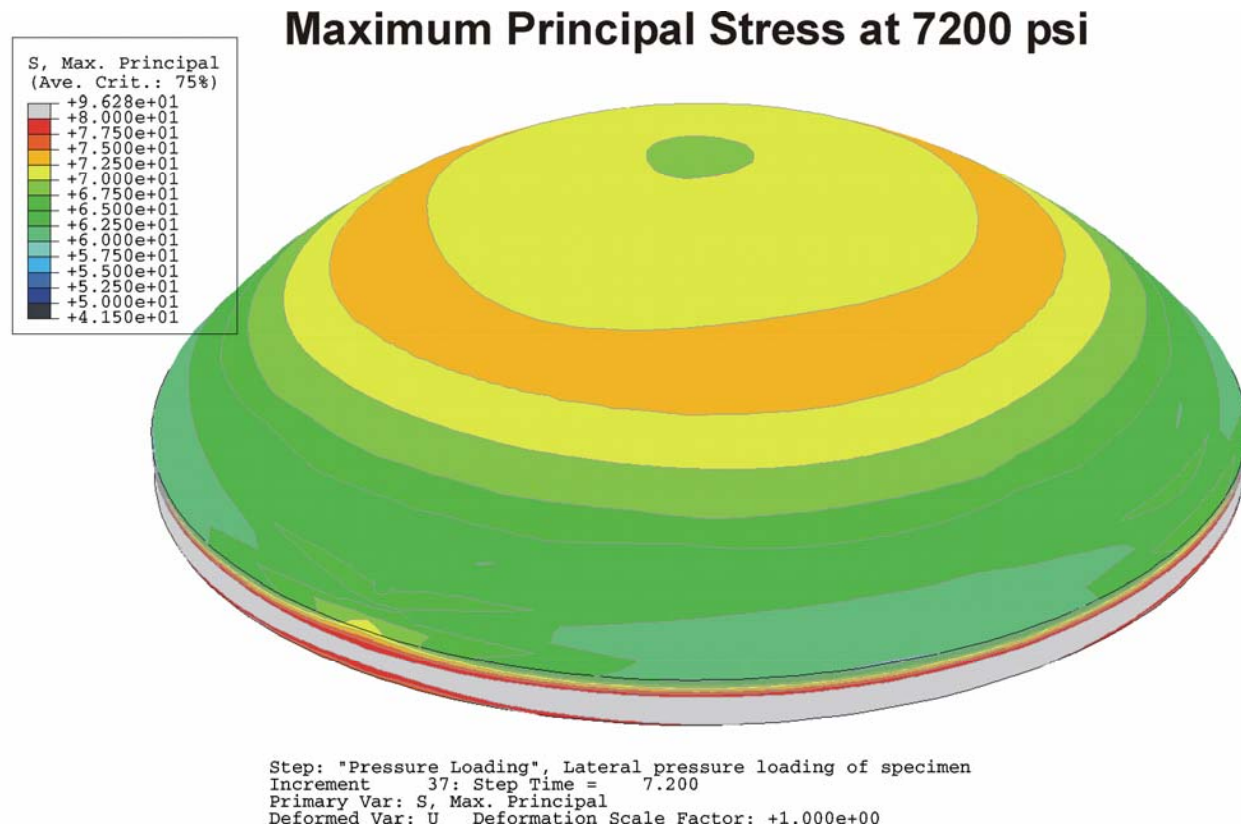


Fig. 3.6. Contours of maximum principal stress computed from finite element model of clad disk specimen.

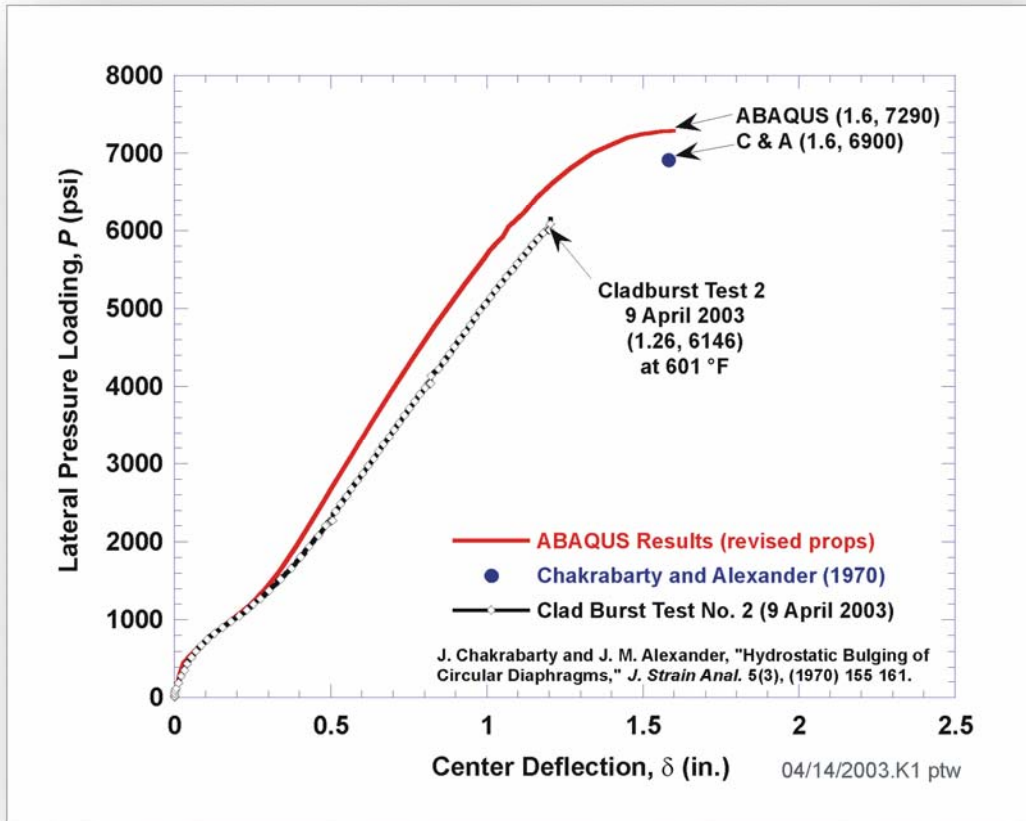


Fig. 3.7. Applied pressure versus clad center-point deflection and instability pressure for the second clad burst experiment: comparison of ABAQUS finite-element predictions with measured data.



(a)



(b)

Fig. 4.1. Clad disk removed from specimen CB 5, containing a notch of 0.050 in. initial depth; the specimen failed at a pressure of 2,641 psi.



(a)



(b)

Fig. 4.2. Clad disk removed from specimen CB 8, containing a notch of 0.025 in. initial depth (the specimen failed at a pressure of 3,139 psi): (a) flawed surface; and (b) clad surface corresponding to inner surface of vessel.

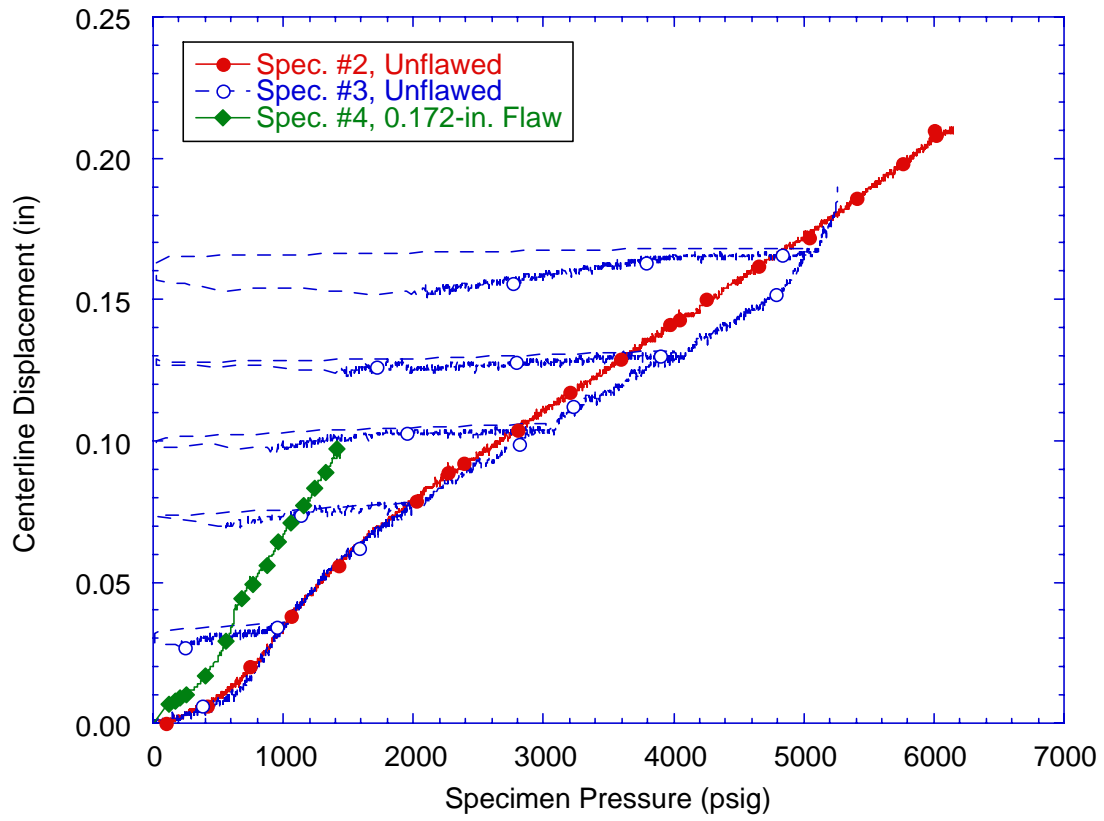


Fig. 4.3. Centerline displacements versus lateral pressure loading for clad-burst specimens CB 2, 3, and 4.

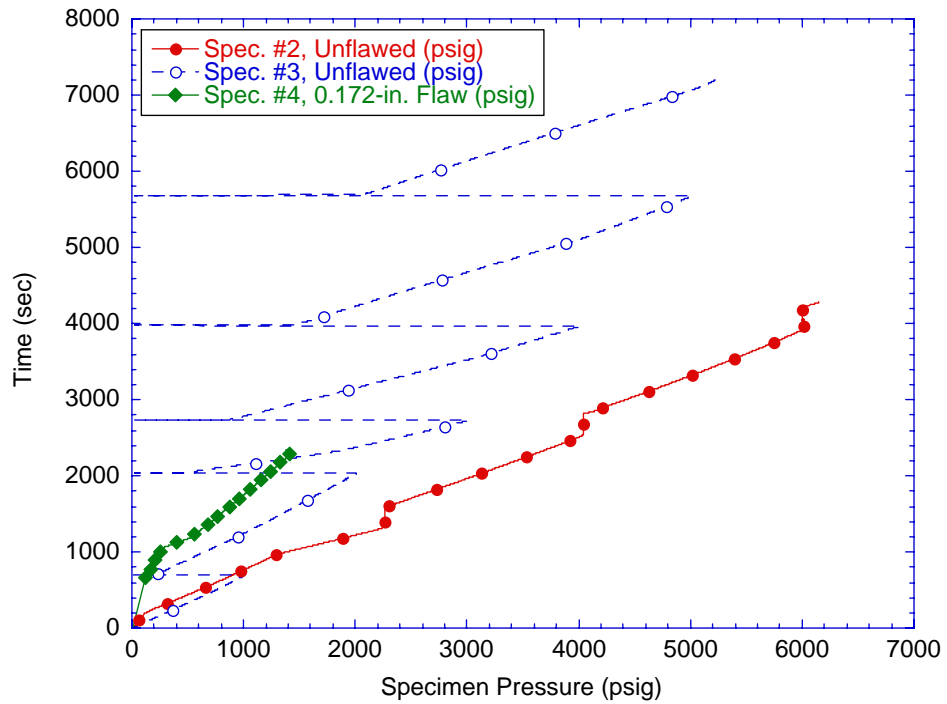


Fig. 4.4. Elapsed time versus lateral pressure loading for clad-burst specimens CB 2, 3, and 4.

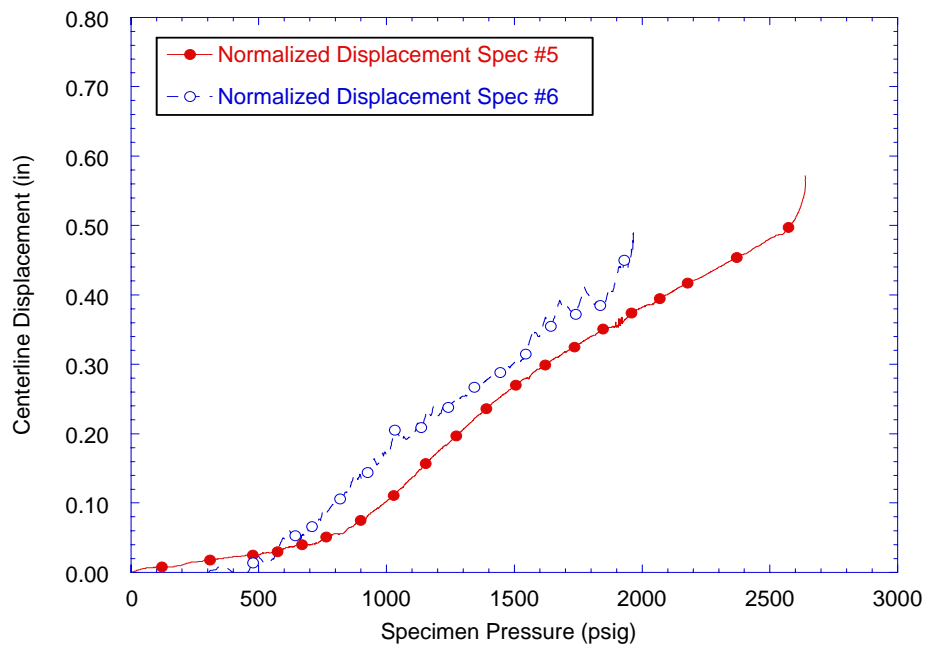


Fig. 4.5. Centerline displacements versus lateral pressure loading for clad-burst specimens CB 5 and CB 6.

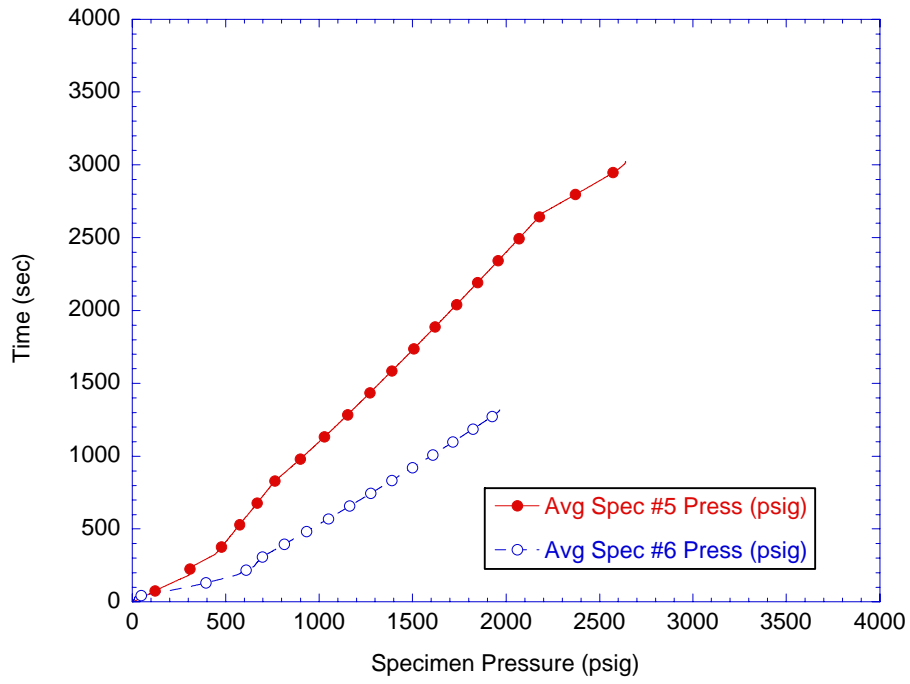
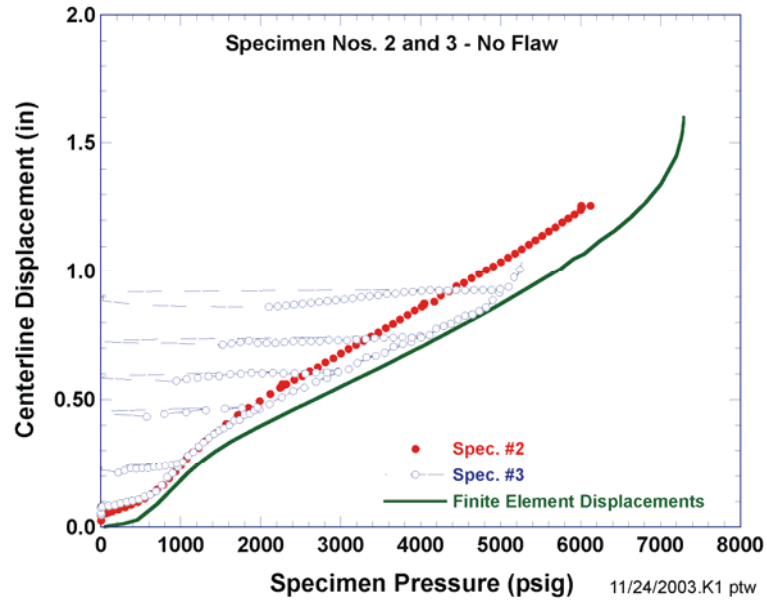
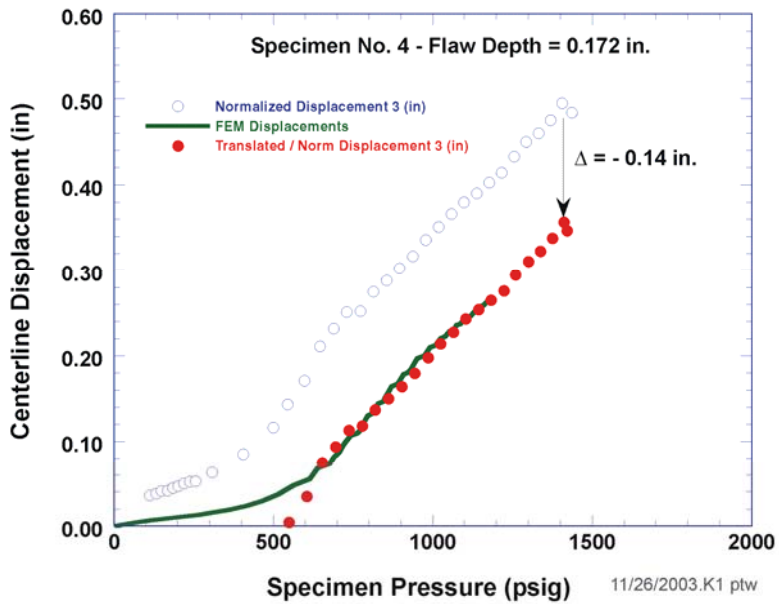


Fig. 4.6. Elapsed time versus lateral pressure loading for clad-burst specimens CB 5 and CB 6.

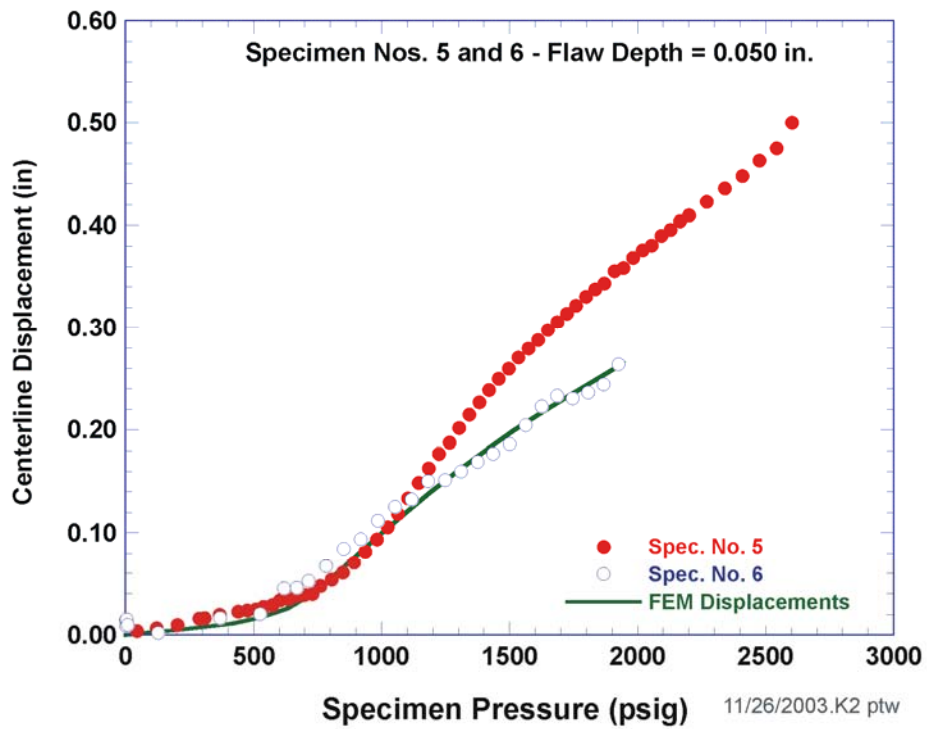


(a)



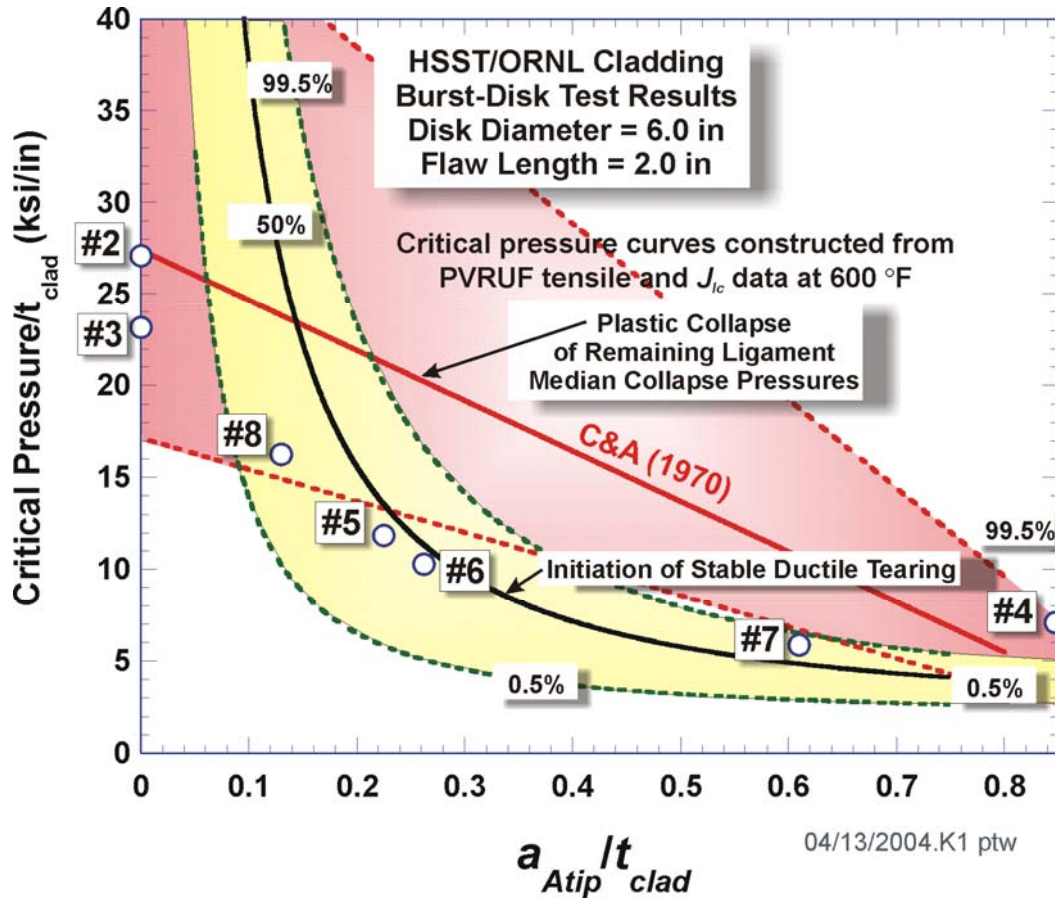
(b)

Fig. 4.7. Comparison of measured centerline displacements to finite-element model predictions for (a) specimens CB 2 and CB 3, (b) specimen CB 4.



(c)

Fig. 4.7. (continued) Comparison of measured centerline displacements to finite-element model predictions for (c) specimens CB 5 and CB 6.



(a)

Fig. 4.8. Experimentally-observed failure pressures compared to two modeled failure mechanisms: (1) plastic collapse of remaining ligament based on modified theory of Chakrabarty and Alexander (1970) for median prediction and (2) ductile tearing: (a) using J_{Ic} data from pre-cracked Charpy specimens for PVRUF cladding at 316°C (600°F). The 99% confidence interval for the plastic-collapse mode is based on combined model and material uncertainties. The 99% confidence interval on ductile tearing initiation is based on a Weibull distribution fitted to the PVRUF J_{Ic} data only (see Fig. 5.8).

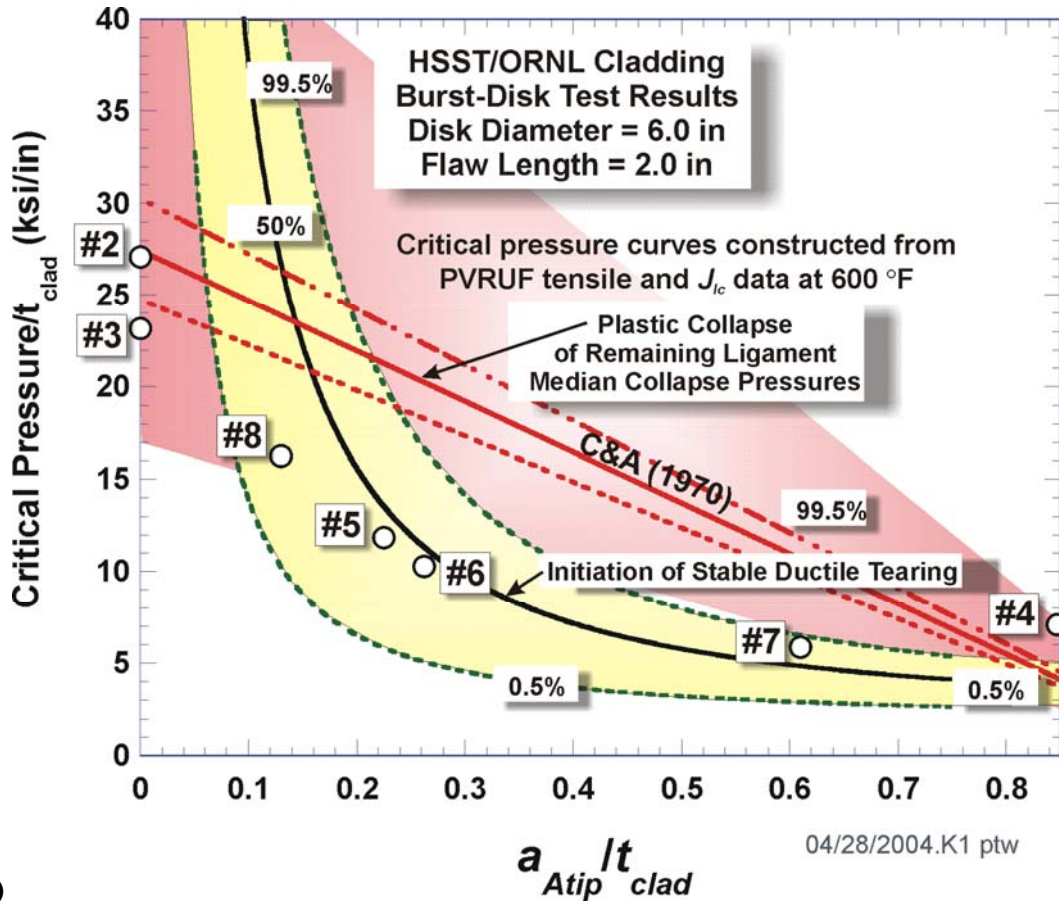


Fig. 4.8. (continued) (b) using J_{Ic} data from pre-cracked Charpy specimens for PVRUF cladding at 316°C (600°F). The 99% confidence interval for the plastic-collapse mode is based on material uncertainty only and is derived from a bivariate lognormal distribution that includes correlated uncertainties in the yield and ultimate true stresses. The 99% confidence interval on ductile tearing initiation is based on a Weibull uncertainty model fitted to the PVRUF J_{Ic} data only (see Fig. 5.8).

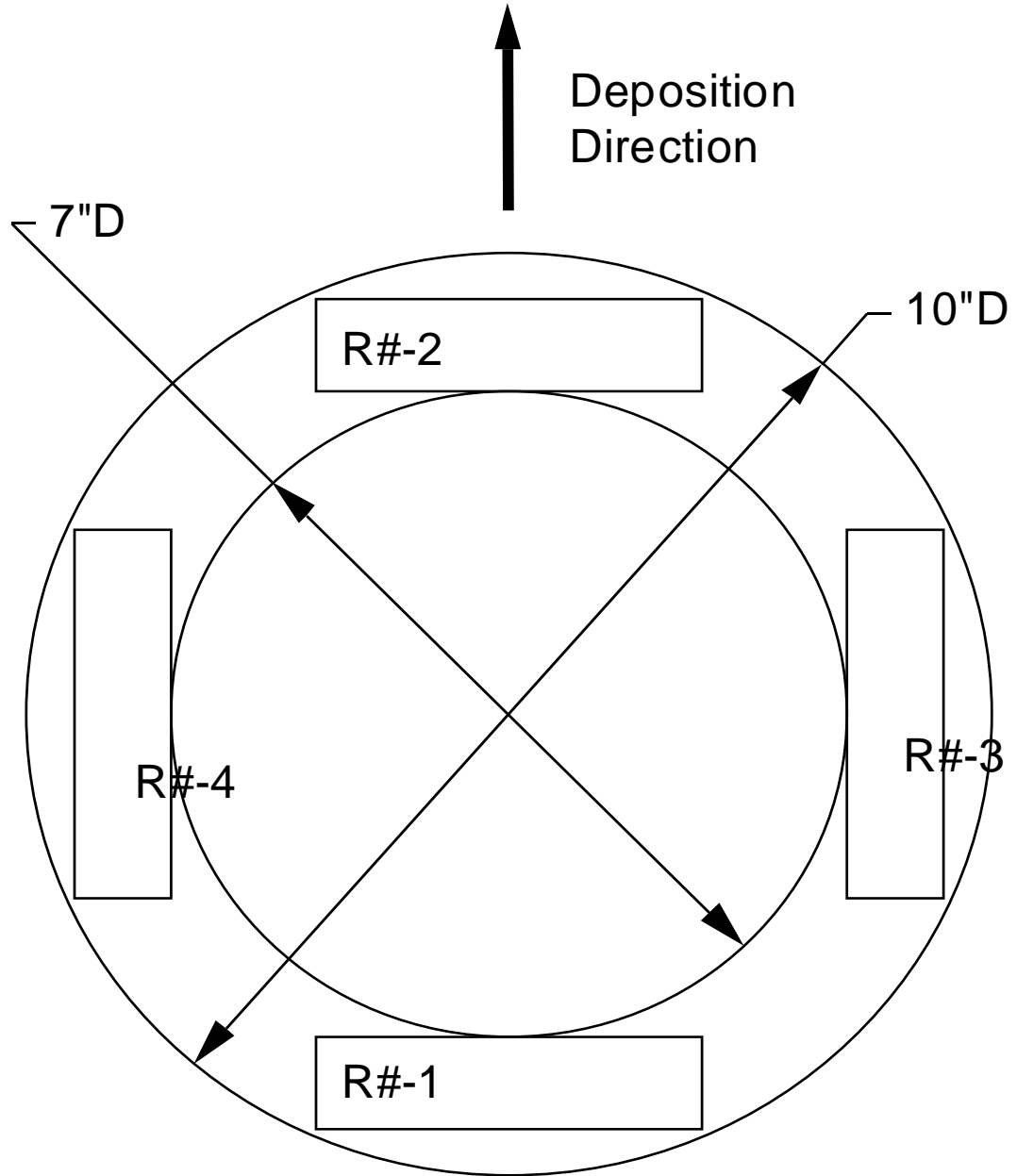
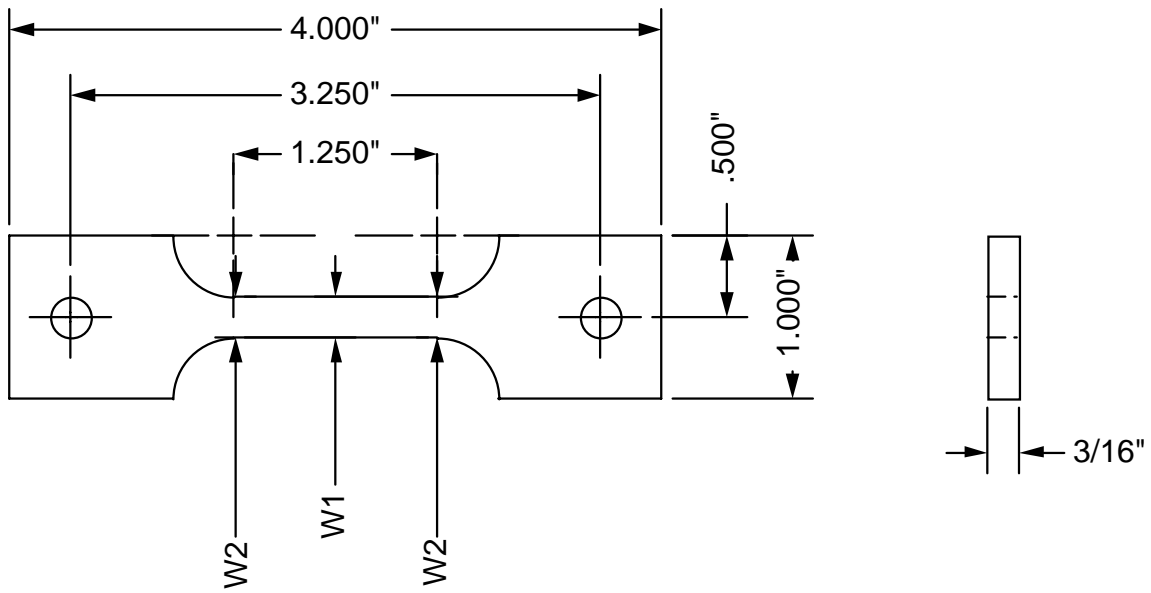
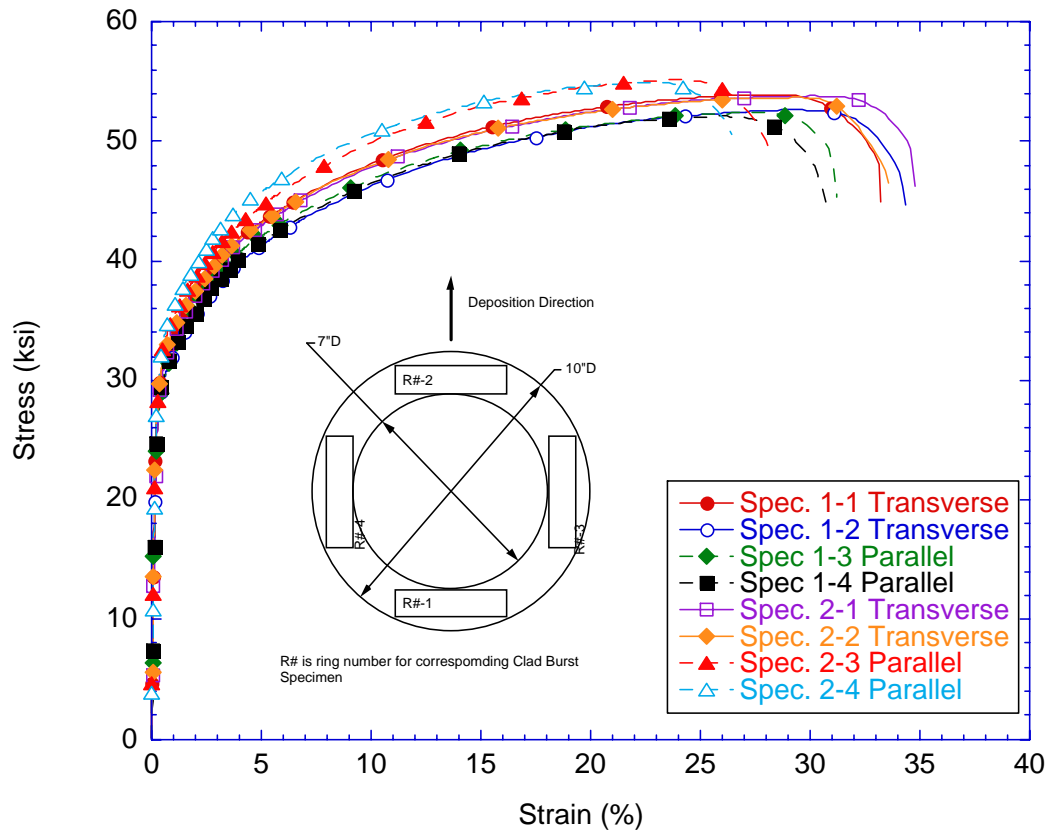


Fig. 5.1. Cutting plan for fabrication of tensile specimens. “R#” refers to the ring number R1 or R2 from which the tensile specimens were extracted; ring R1 was taken from clad burst specimen CB 4 and R2 from CB 5.



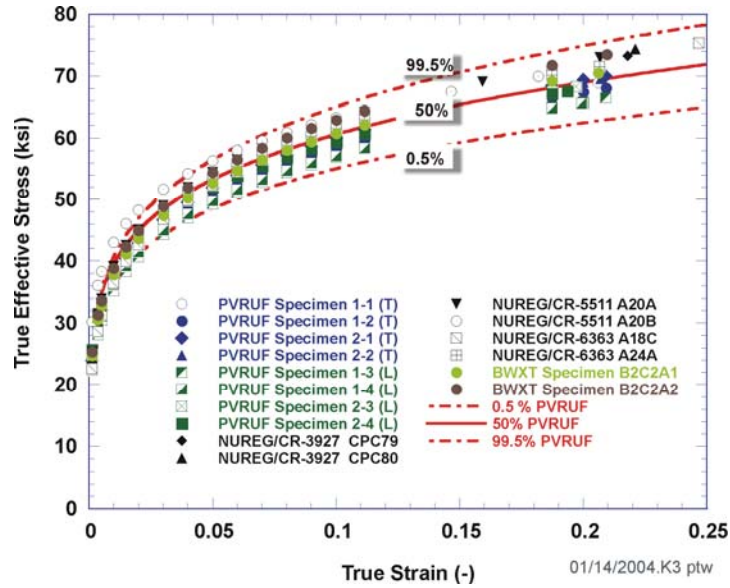
NOTE:
 $W_1 = 0.250" \pm 0.001$
 $W_2 = \text{FROM } 0.0010" \text{ TO } 0.0015"$
 GREATER THAN W_1 .

Fig. 5.2. Dimensions of clad tensile specimens.

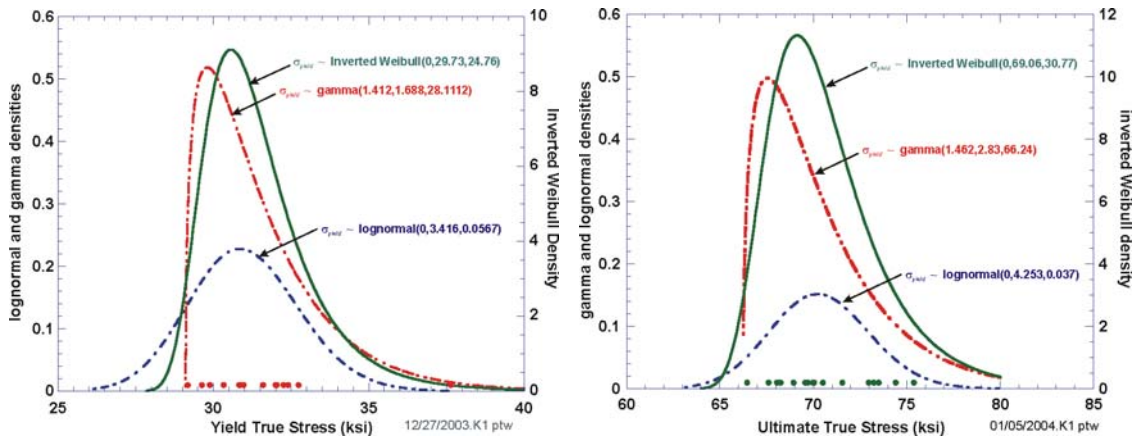


Comparison of All Tensile Data For Clad Burst Specimens

Fig. 5.3. Plots of stress versus strain (engineering) from eight clad tensile specimens.



(a)



(b)

Fig. 5.4. lots of (a) true stress versus true strain data and (b) probability density functions for fitted statistical marginal distributions based on data in Table 5.2.

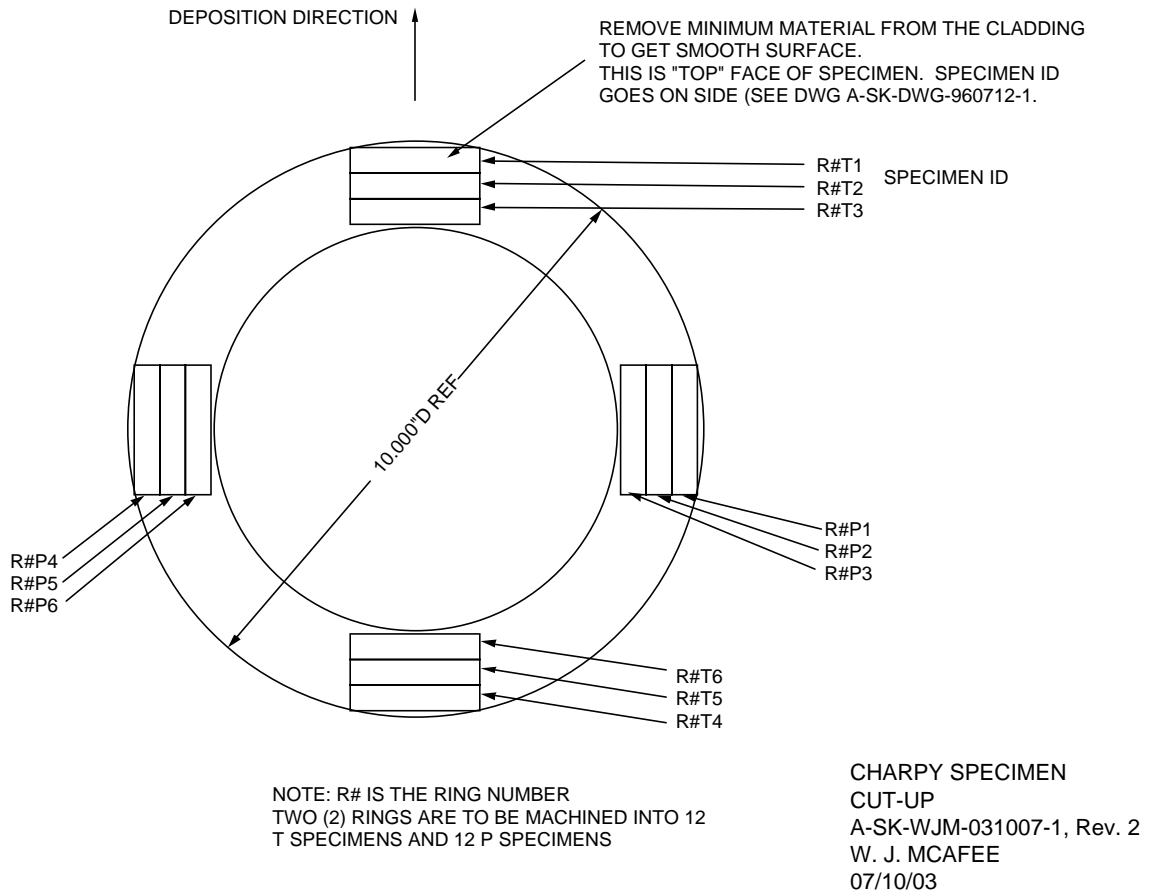


Fig. 5.5. Cutting plan for Charpy specimens taken from clad burst specimens CB 6-8 for generation of J-R curves in the T-S and L-S orientations.

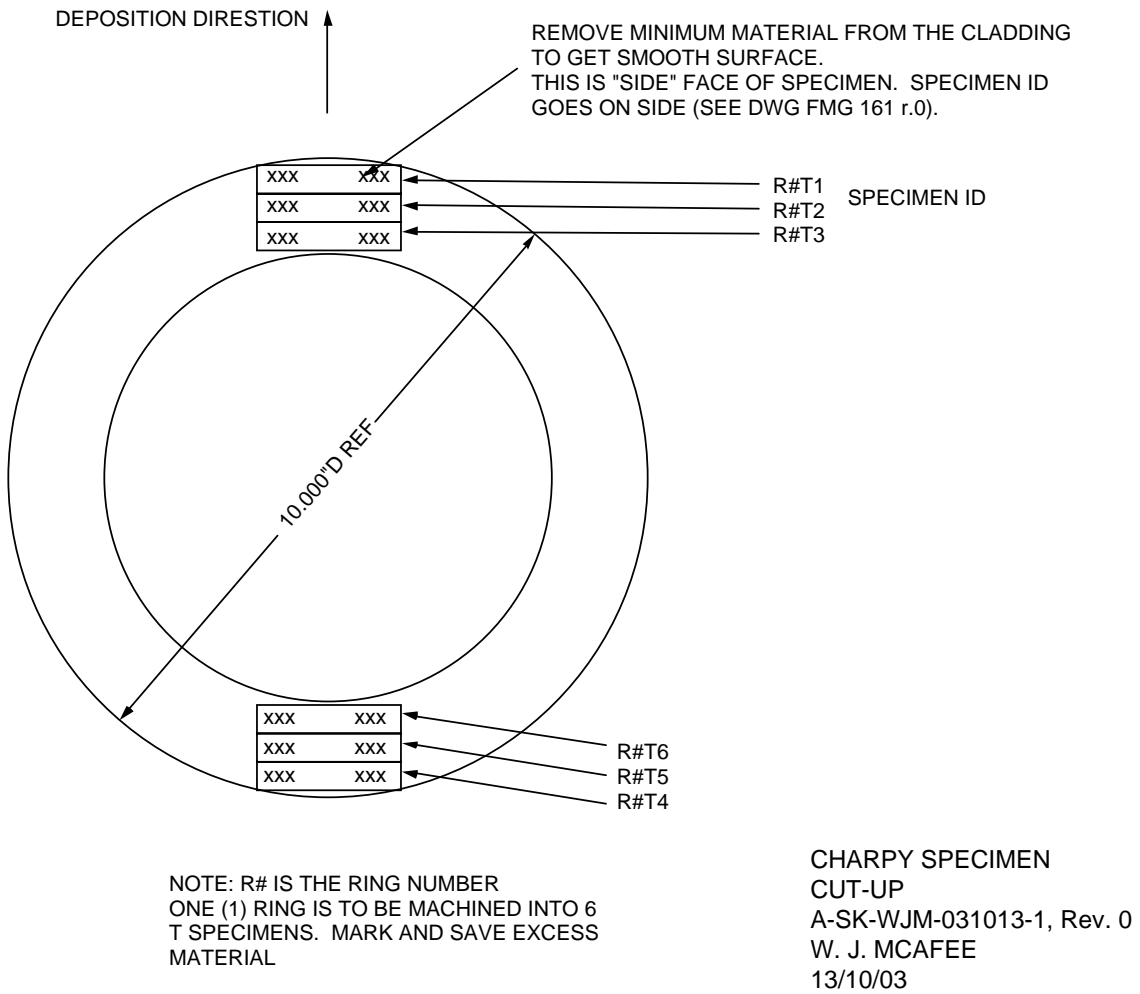


Fig. 5.6. Cutting plan for one-half thickness Charpy specimens taken from clad burst specimen CB 3 for generation of J-R curves in the T-L orientation.

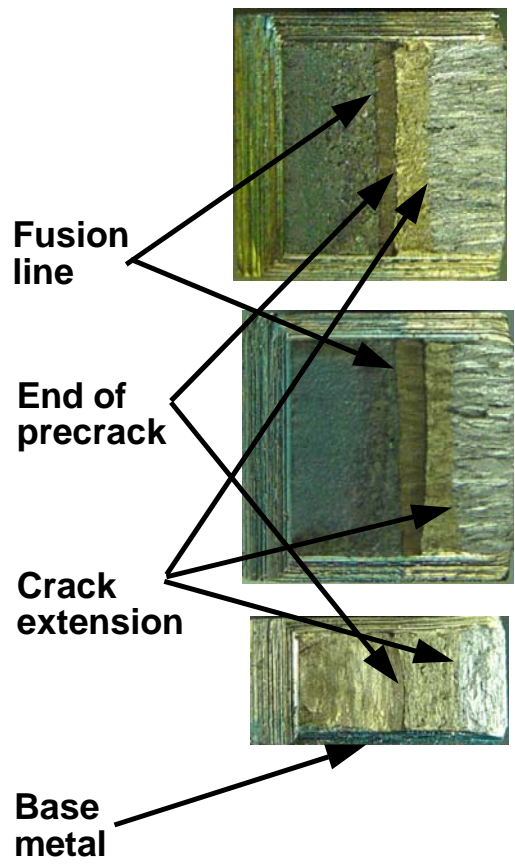
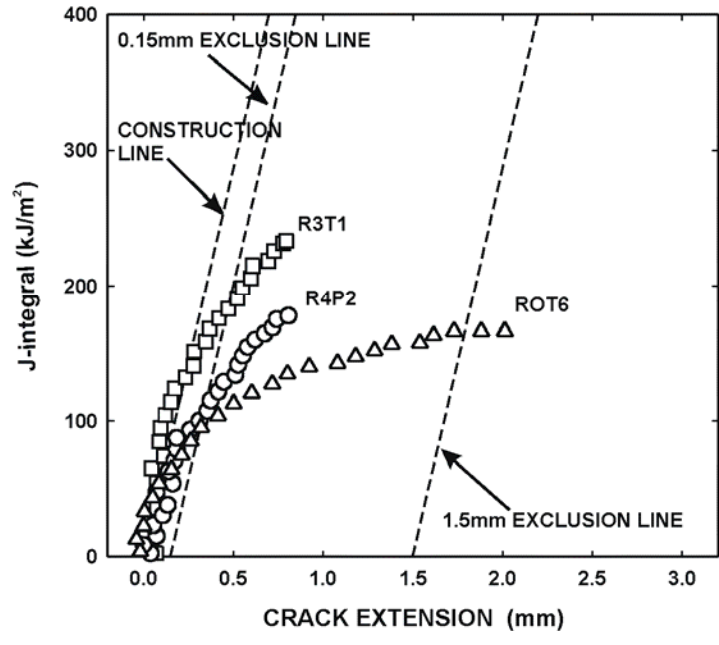


Fig. 5.7. Typical *J-R* curves obtained from the PVRUF cladding in different orientations.

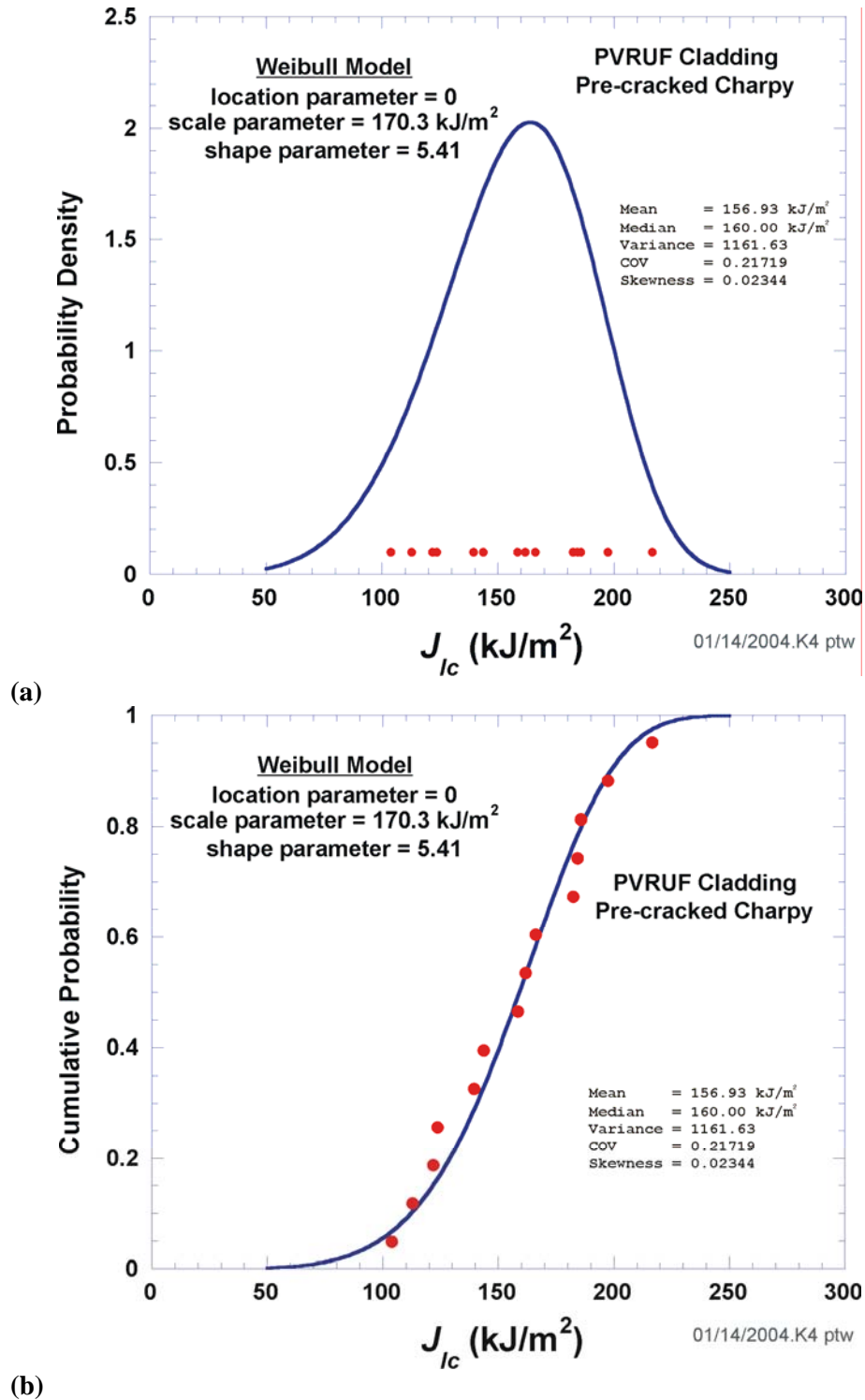
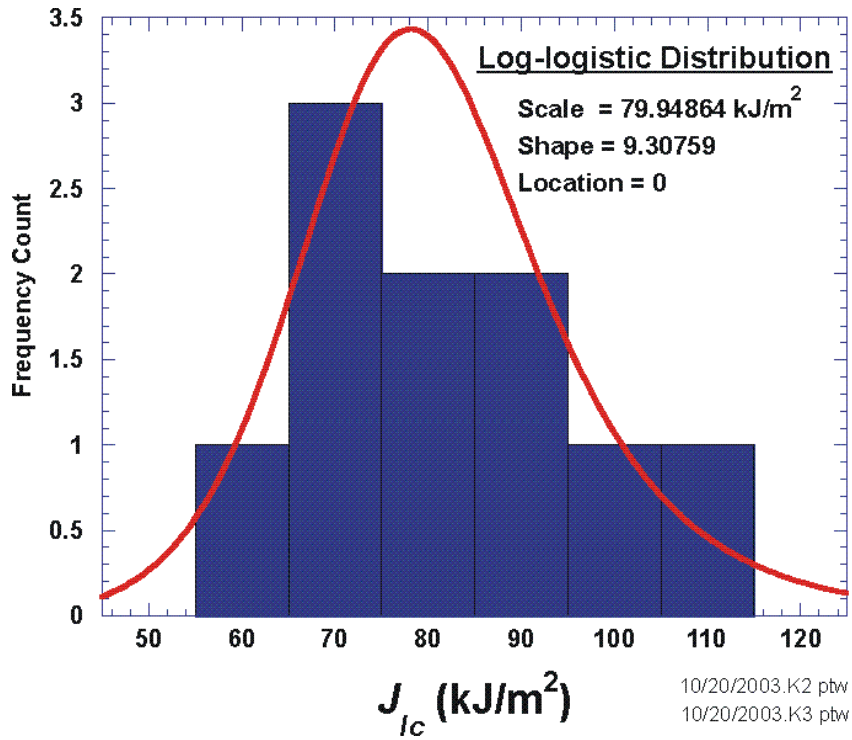
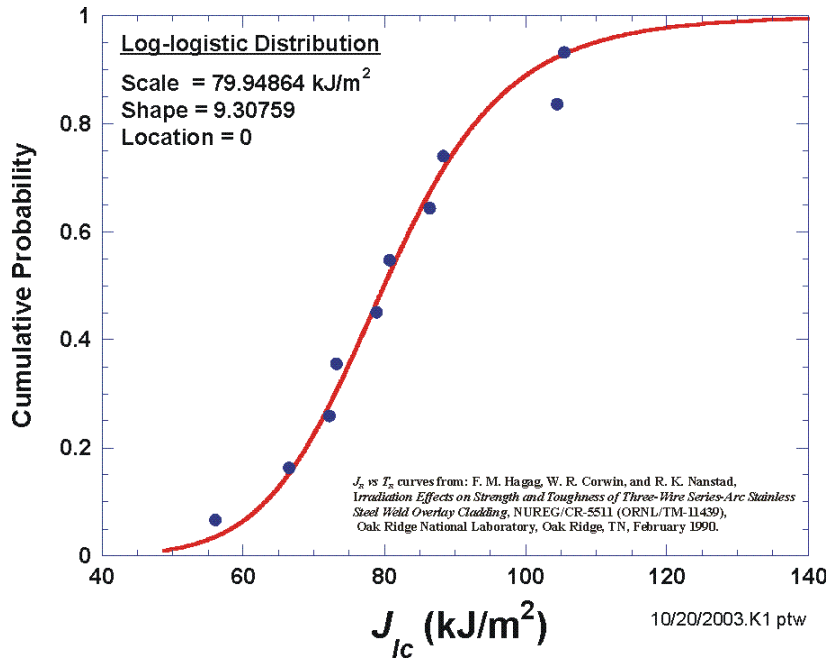


Fig. 5.8. Statistical distribution for PVRUF J_{Ic} (a) probability density with fitted Weibull density and (b) Weibull cumulative distribution function compared to cumulative probabilities of J_{Ic} data from pre-cracked Charpy specimens from PVRUF (estimated by median rank order statistic $p = (i-0.3)/(n+0.4)$).



(a)



(b)

Fig. 5.9. Statistical distribution for J_{Ic} (a) histogram of data from NUREG/CR-5511 and 6363 extrapolated to 318°C (605°F) with fitted log-logistic density overplot and (b) log-logistic cumulative distribution function compared to cumulative probabilities of J_{Ic} data from NUREG/CR-5511 and 6363 estimated by median rank order statistic $p = (i-0.3)/(n+0.4)$.

Shear region is “far” from the surface

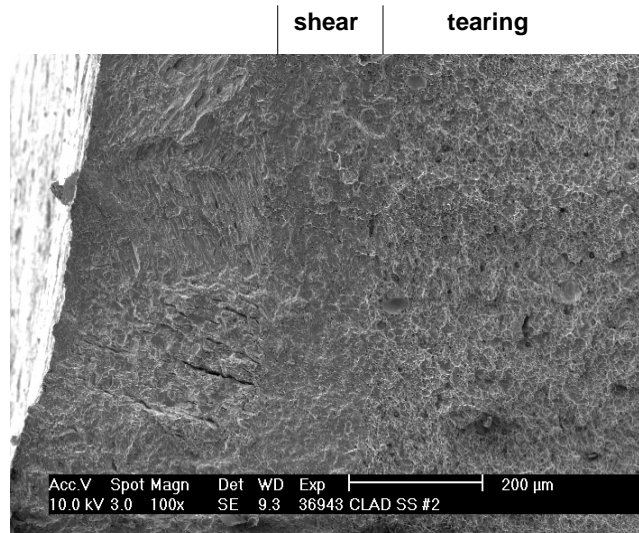


Fig. 6.1. Clad-burst specimen CB 4 containing flaw with depth 0.172 in.: shear region is far from surface.

shear band reaches the surface

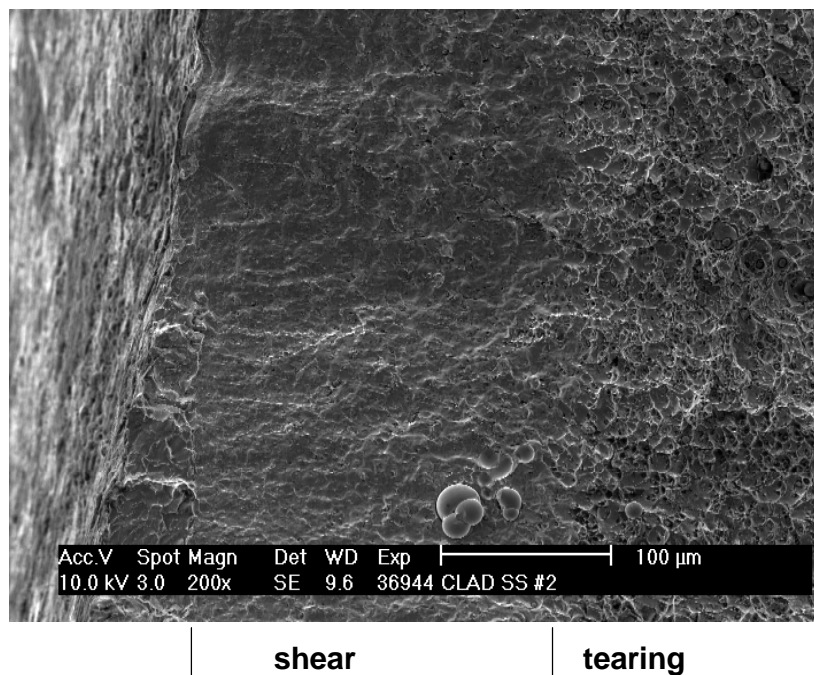


Fig. 6.2. Clad-burst specimen CB 4 containing flaw with depth 0.172 in.: shear band reaches the surface.

Transition from Tearing to Shear Mode of Fracture

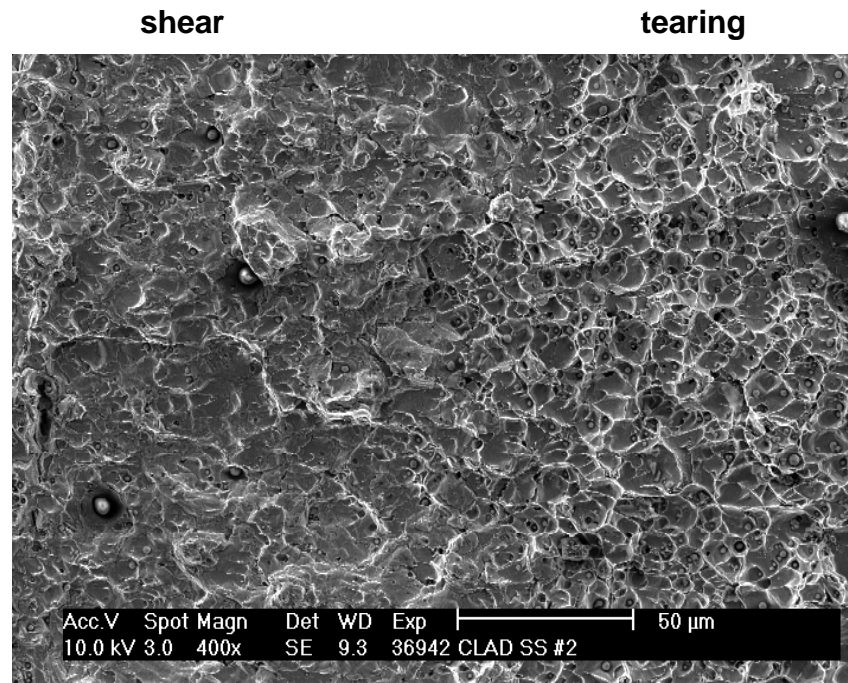


Fig. 6.3. Clad-burst specimen CB 4 containing flaw with depth 0.172 in.: transition from tearing to shear mode of fracture.

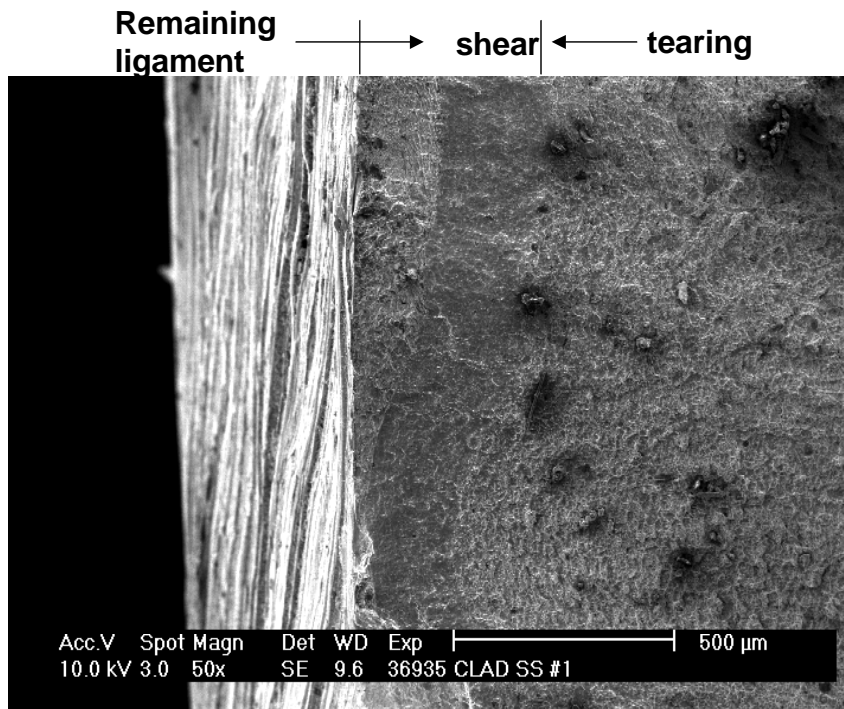


Fig. 6.4. Clad-burst specimen CB 5 containing flaw with depth 0.050 in.

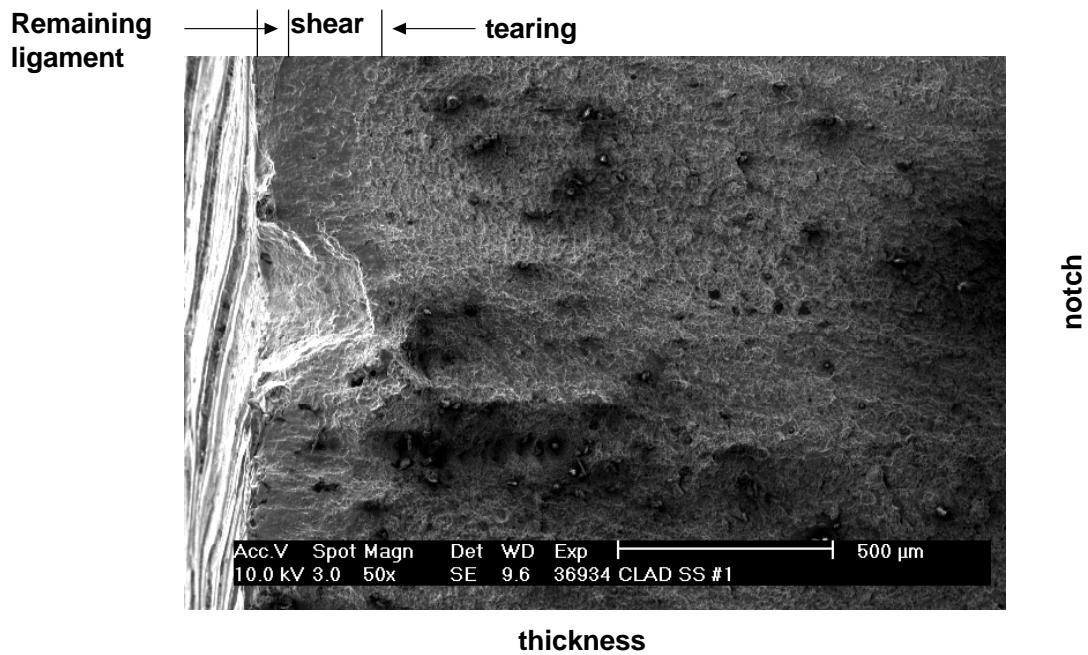


Fig. 6.5. Clad-burst specimen CB 5 containing flaw with depth 0.050 in.

Typical Fracture Surface within Tearing Region

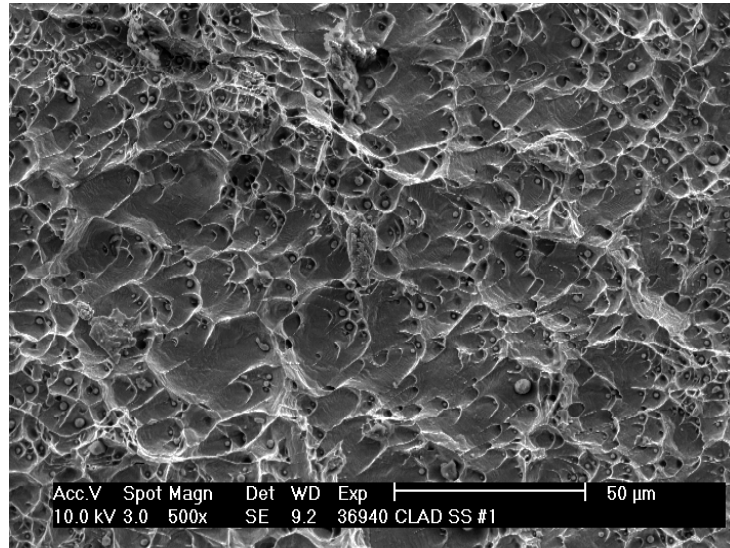


Fig. 6.6. Clad-burst specimen CB 5 containing flaw with depth 0.050 in.: typical fracture surface within tearing region.

Typical Fracture Surface within Shear Region

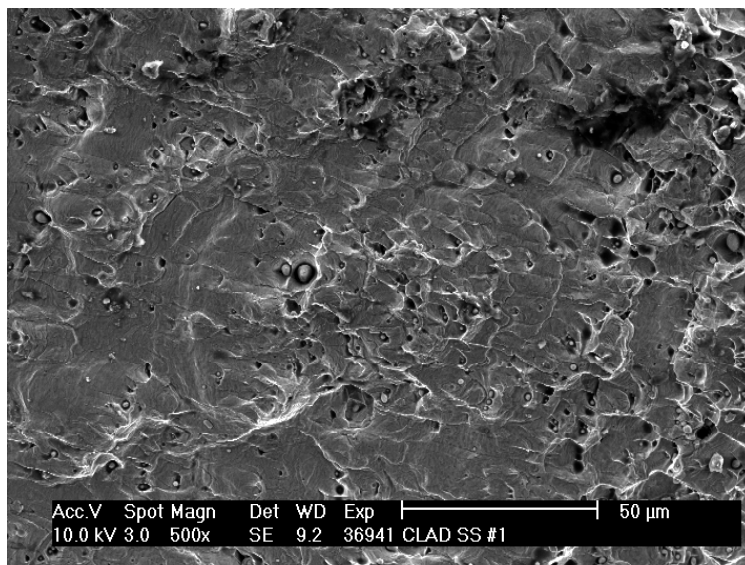


Fig. 6.7. Clad-burst specimen CB 5 containing flaw with depth 0.050 in.: typical fracture surface within shear region.



Fig. 7.1. Locations of pre-test clad thickness measurements made on Phase 2 clad burst specimens.

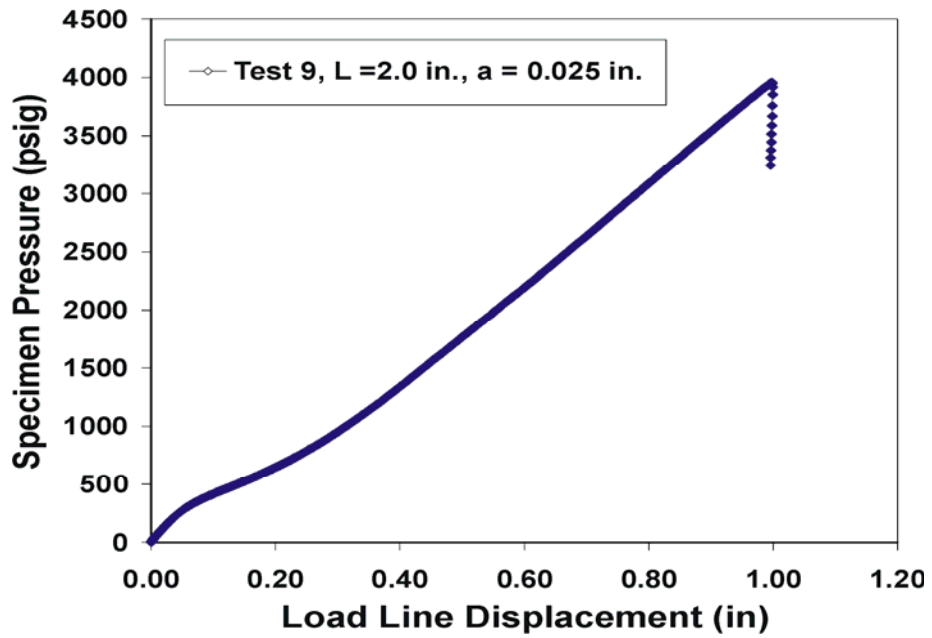


Fig. 7.2. Pressure versus load-line displacement data for clad-burst specimen CB 9. Load line displacement is the clad-layer deflection with pressure.

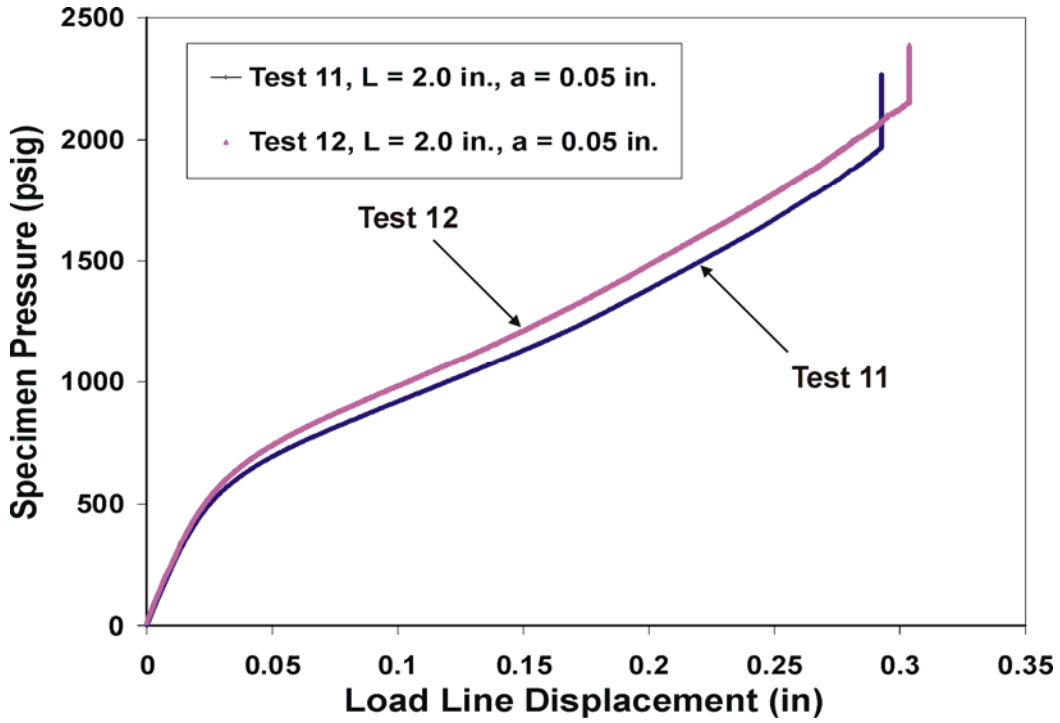


Fig. 7.3. Pressure versus load-line displacement data for clad-burst specimens CB 11 and CB 12. Load line displacement is the clad-layer deflection with pressure.

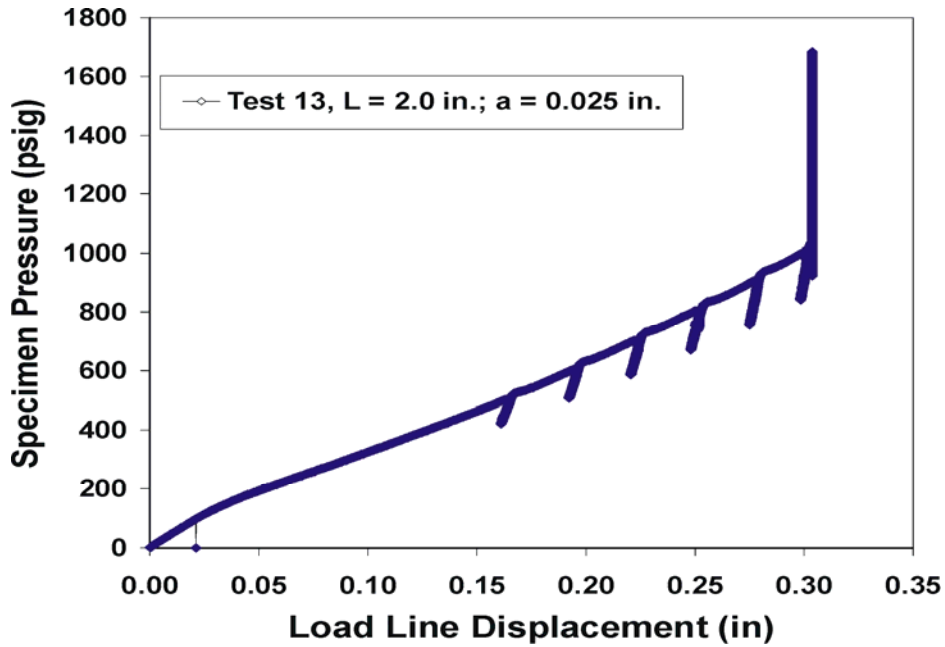


Fig. 7.4. Pressure versus load-line displacement data for clad-burst specimen CB 13. Load line displacement is the clad-layer deflection with pressure.

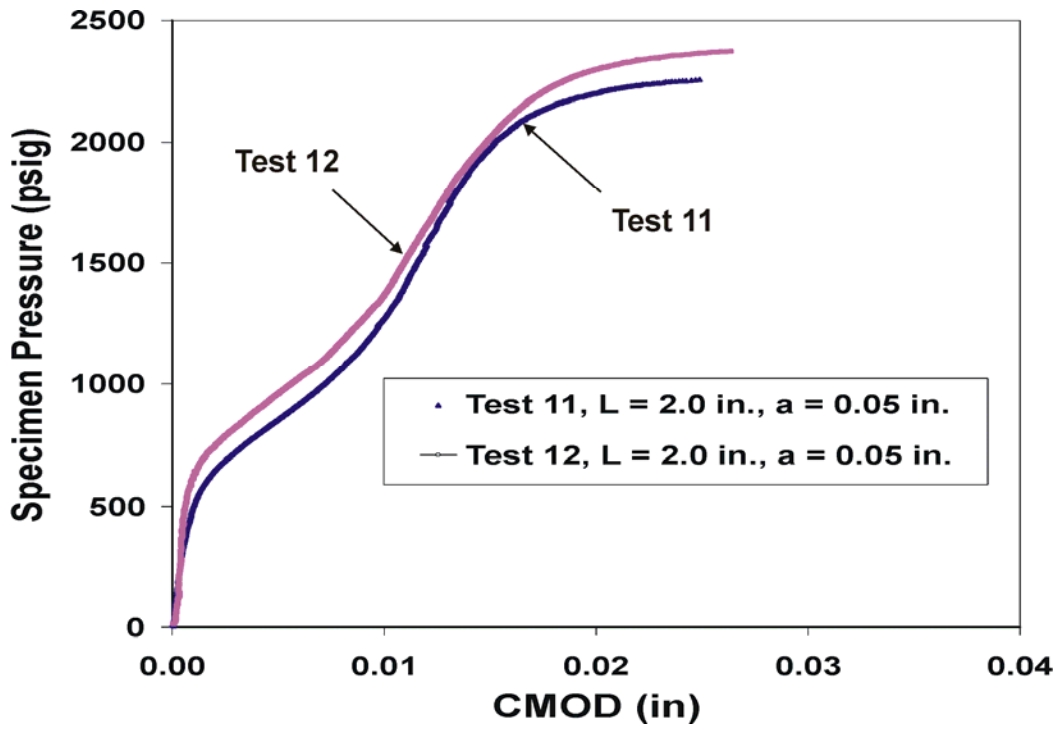


Fig. 7.5. Pressure versus CMOD data for clad-burst specimens CB 11 and CB 12.

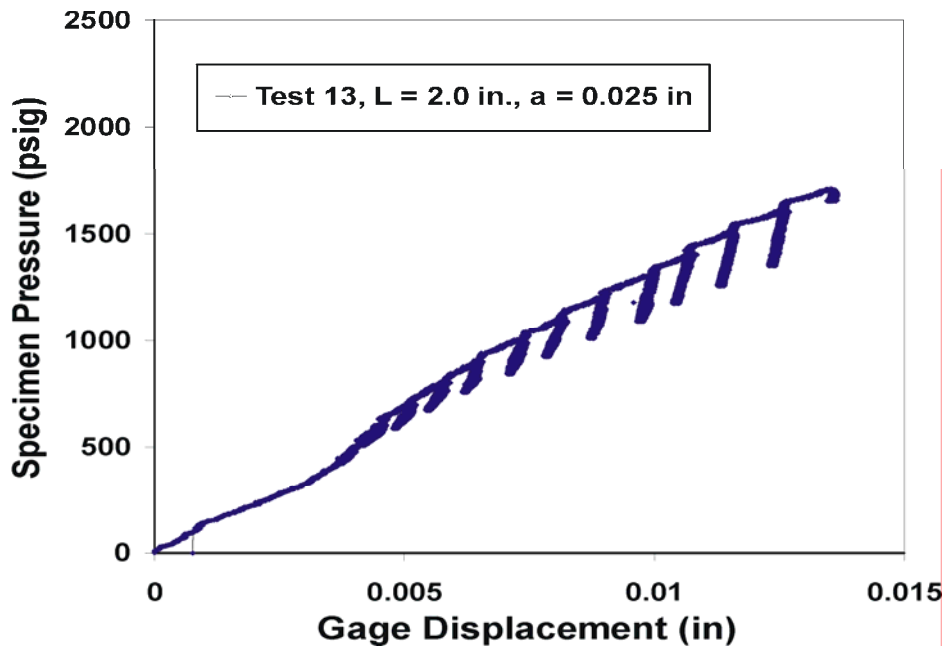


Fig. 7.6. Pressure versus gage displacement data for clad-burst specimen CB 13; no correction has been applied to data for elevation of capacitance gage above the clad surface.

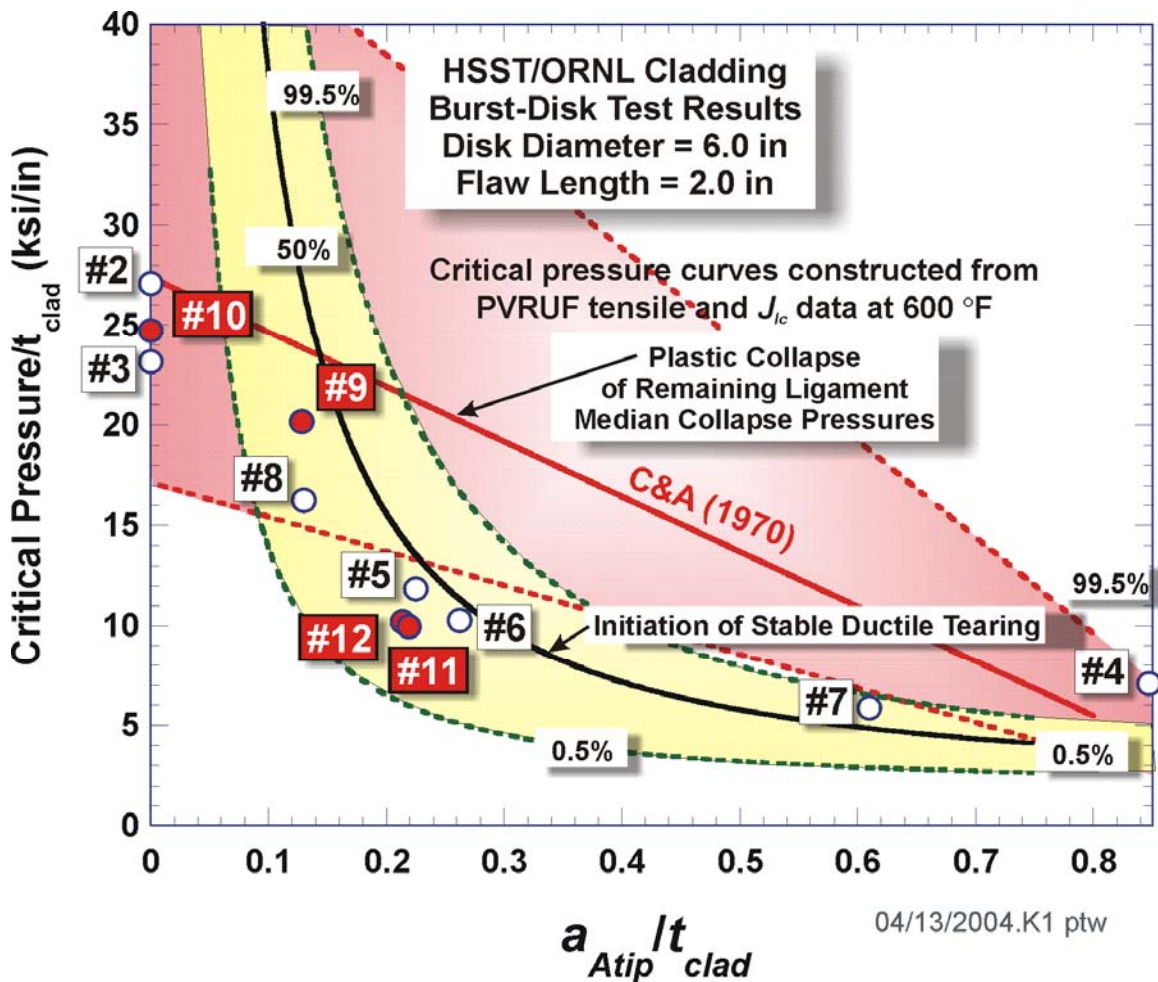


Fig. 7.7. Comparisons of failure pressure versus crack depth, both normalized by clad thickness, for the Phase 1 (open symbols) and Phase 2 (filled symbols) test series consisting of CB 9 through CB 12; test CB 13 was terminated prior to failure. The test results are compared with predictions for ductile tearing initiation (based on Weibull statistical distribution derived from PVRUF J_{Ic} PCCVN data) and predictions of plastic collapse of the remaining ligament using a statistical model of PVRUF plastic-flow tensile properties.

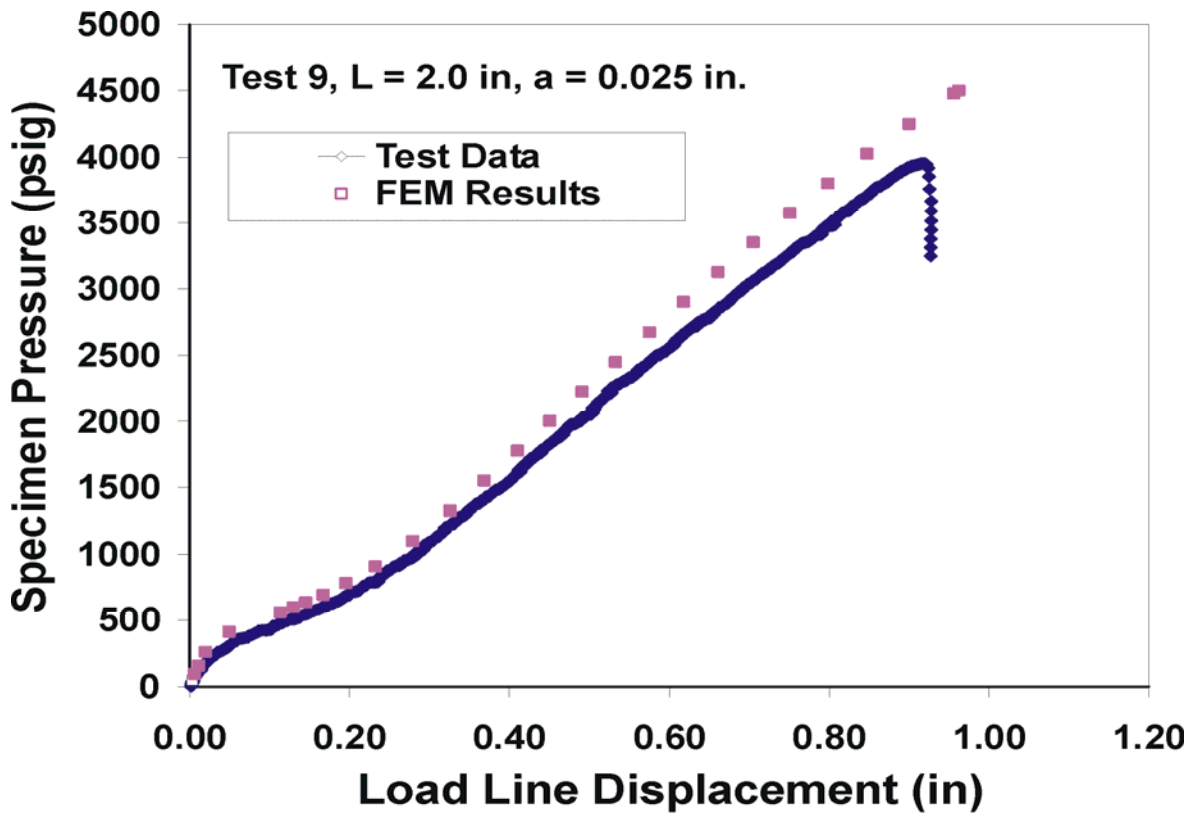


Fig. 7.8. Comparison of calculated and measured pressure versus load-line displacement for clad-burst specimen CB 9. Calculations and data represent deflections at the center of the clad disk. Initial root radius of FEM was 0.01 in.

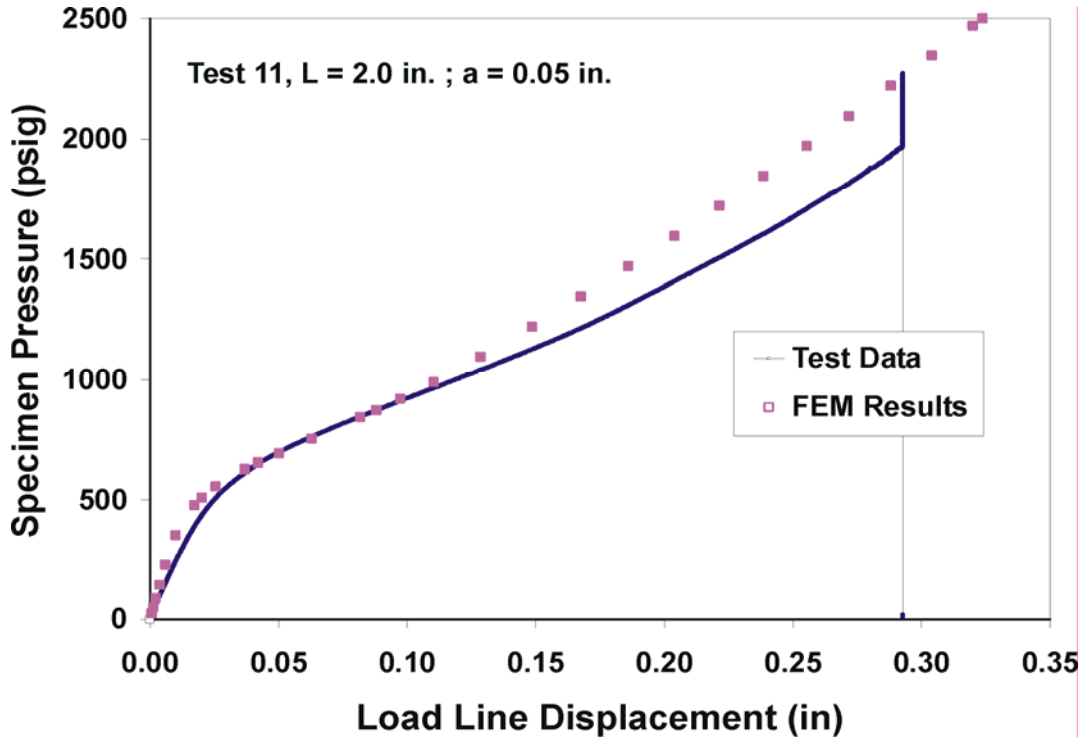


Fig. 7.9. Comparison of calculated and measured pressure versus load-line displacement for clad-burst specimen CB 11. Initial root radius of FEM was 0.01 in.

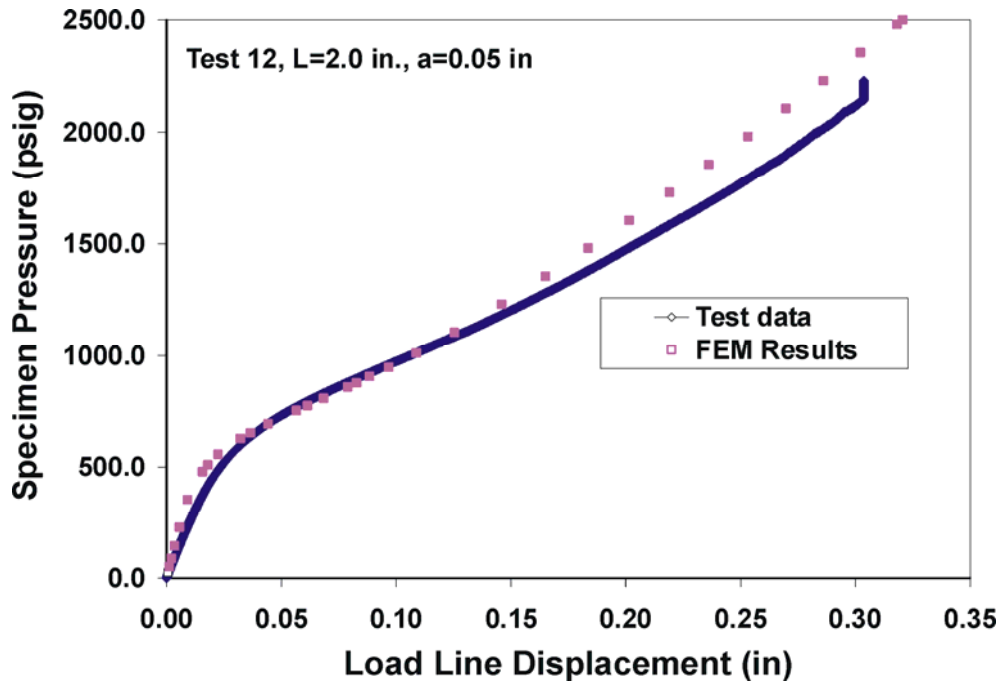


Fig. 7.10. Comparison of calculated and measured pressure versus load-line displacement for clad-burst specimen CB 12. Initial root radius of FEM was 0.001 in.

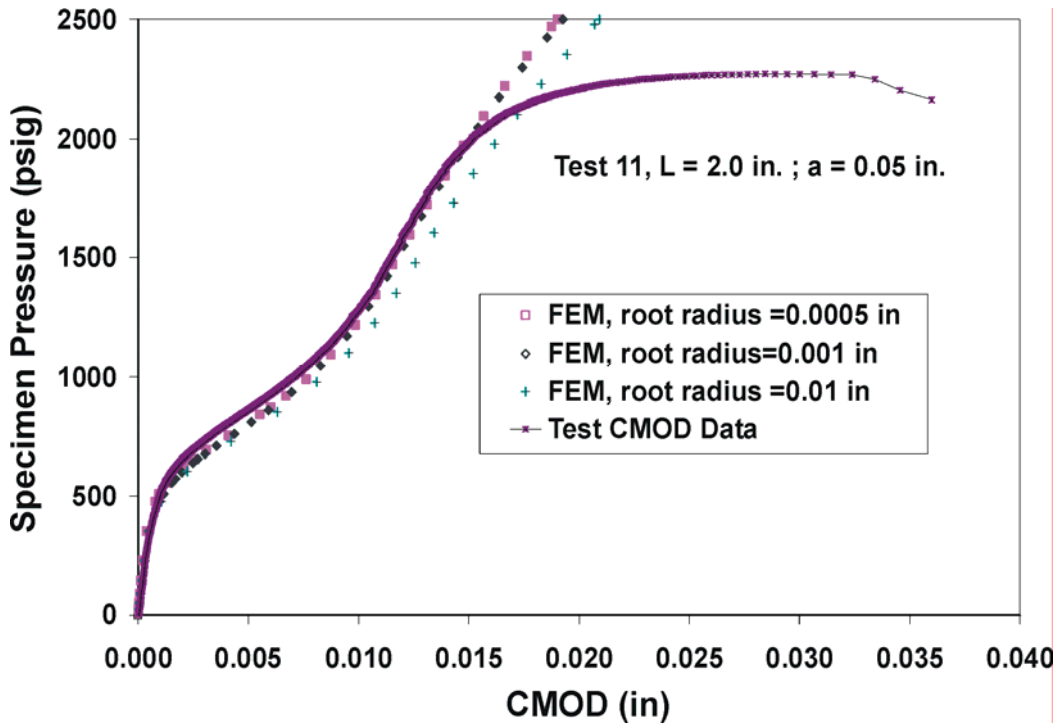


Fig. 7.11. Comparison of calculated and measured pressure versus CMOD for clad-burst specimen CB 11.

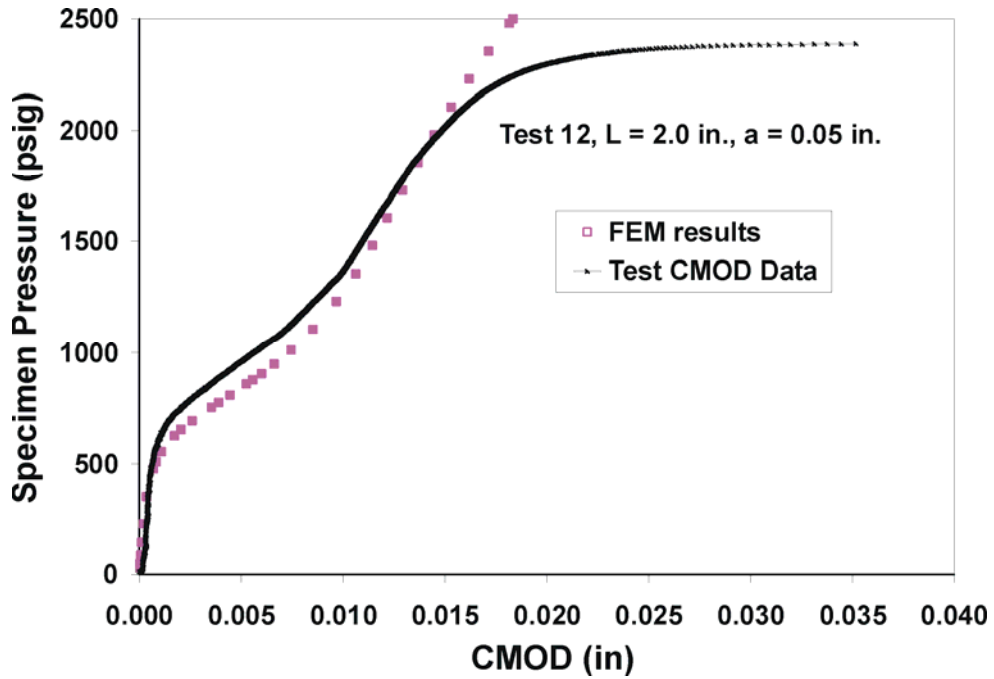


Fig. 7.12. Comparison of calculated and measured pressure versus CMOD for clad-burst specimen CB 12. Initial root radius of FEM was 0.001 in.

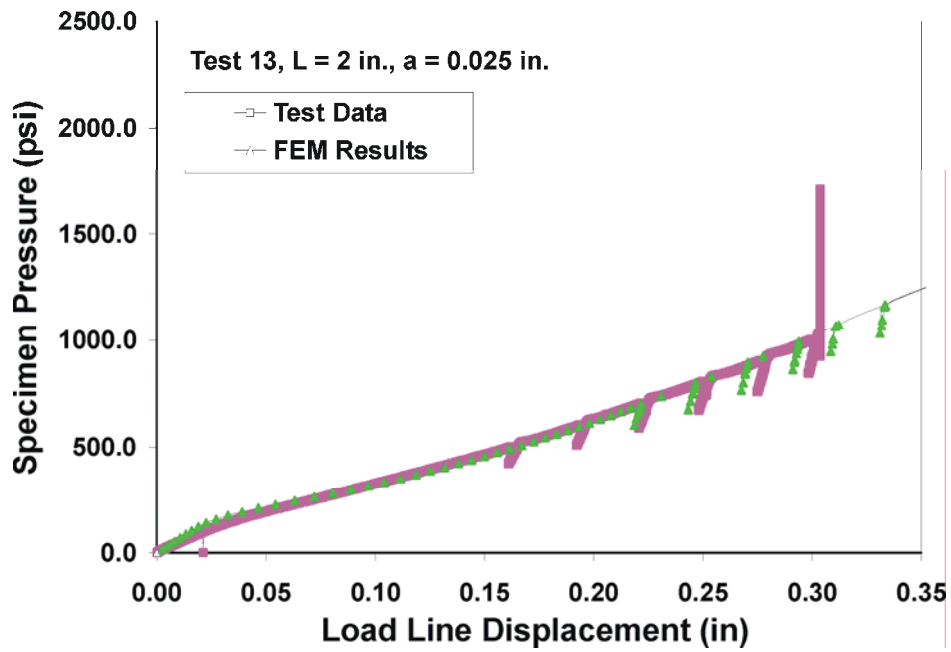


Fig. 7.13. Comparison of calculated and measured pressure versus load-line displacement for clad-burst specimen CB 13. Initial root radius of FEM was 0.01 in.

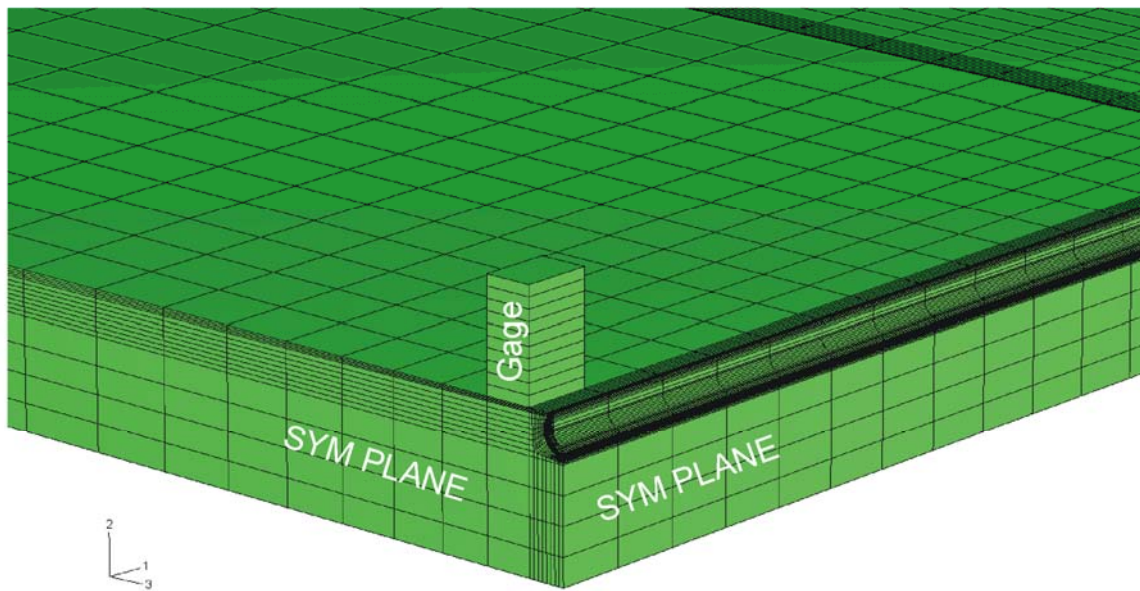


Fig. 7.14. Finite element model with simulated gage height above the clad surface used in analysis of test CB 13.

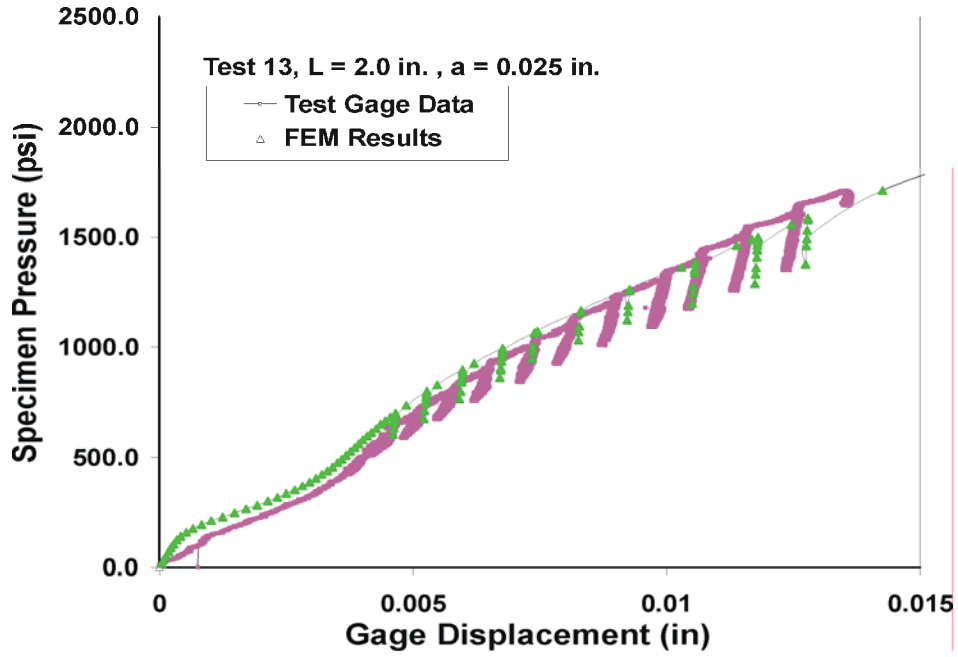


Fig. 7.15. Comparison of calculated and measured pressure versus gage displacement at 0.07 in. above the clad surface for clad-burst specimen CB 13.

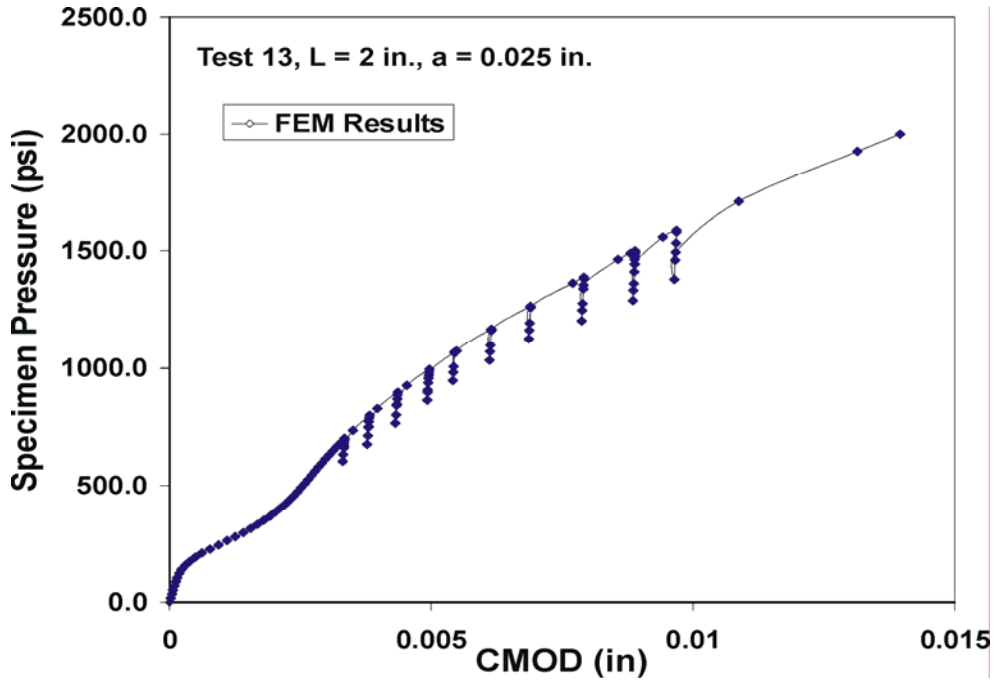
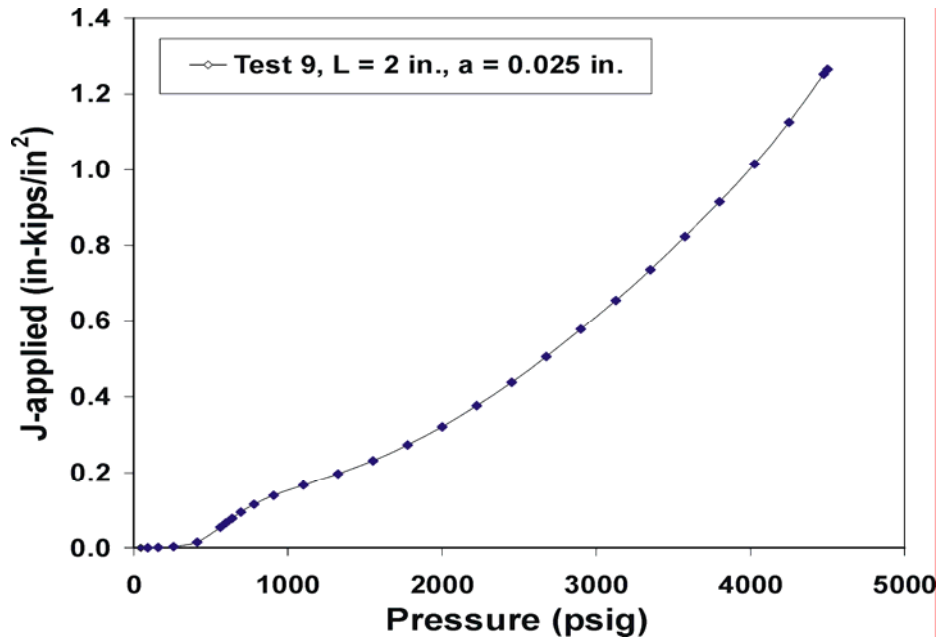
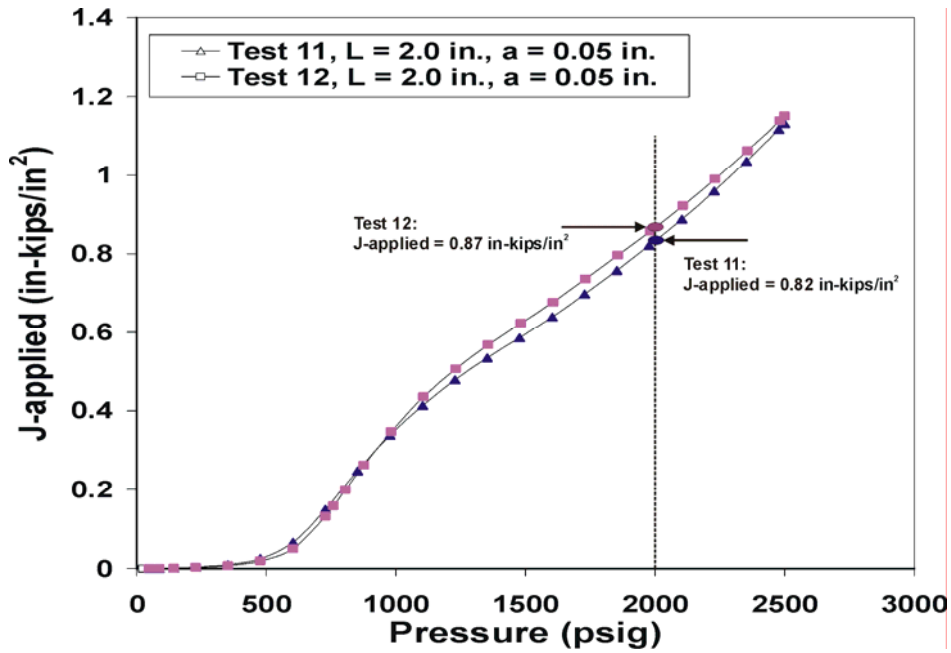


Fig. 7.16. Calculated pressure versus CMOD for clad-burst specimen CB 13.

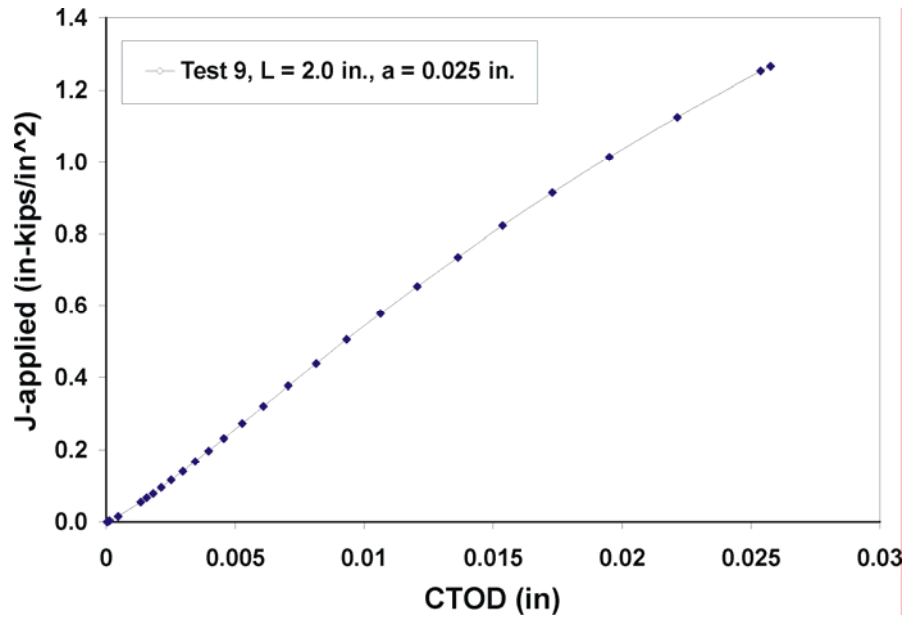


(a)

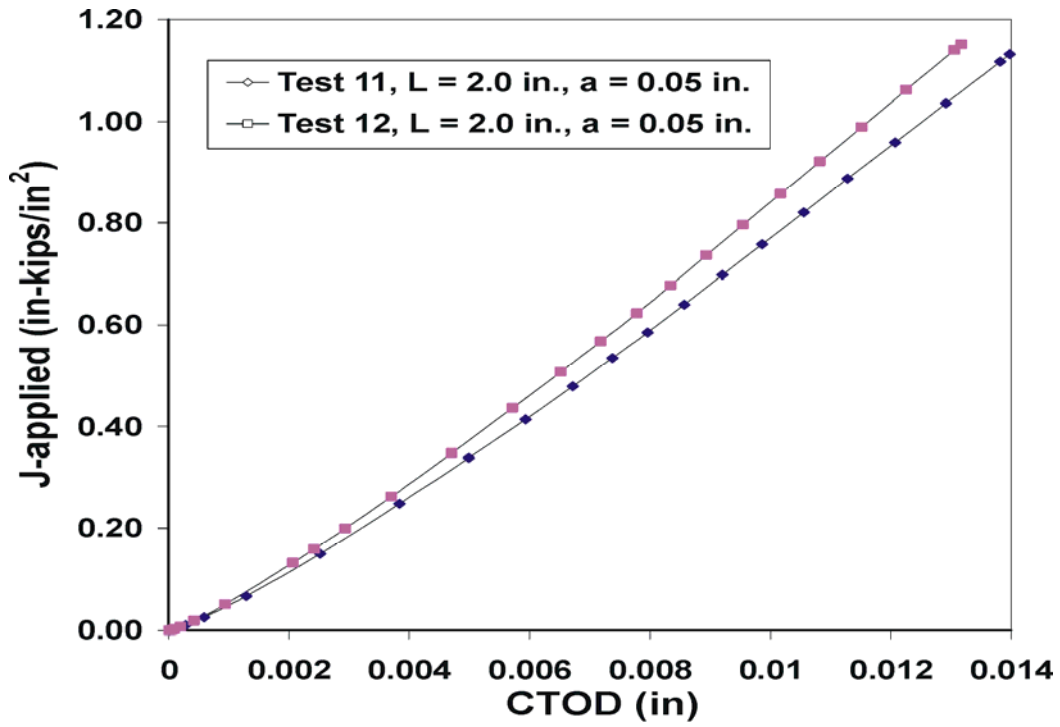


(b)

Fig. 7.17. Applied J versus measured pressure for clad-burst specimens: (a) CB 9 (failure pressure was 3,955 psi), and (b) CB 11 and CB 12. Initial root radius of FEMs was 0.01 in.

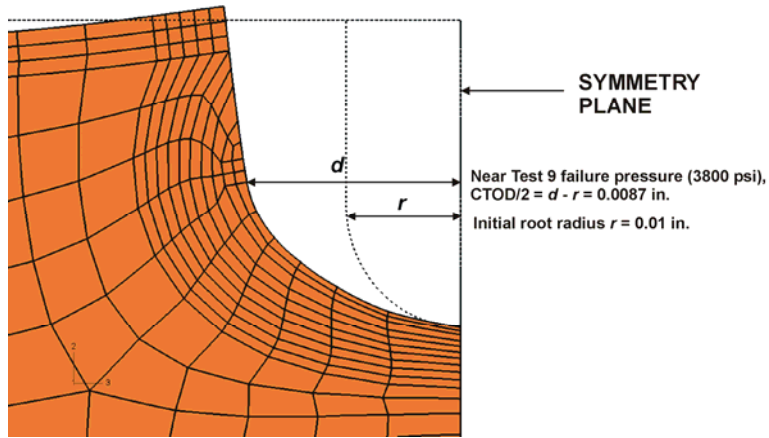


(a)

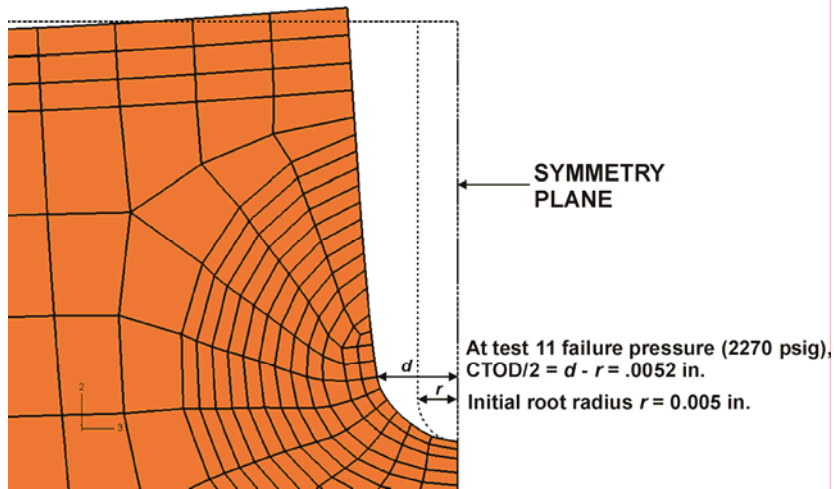


(b)

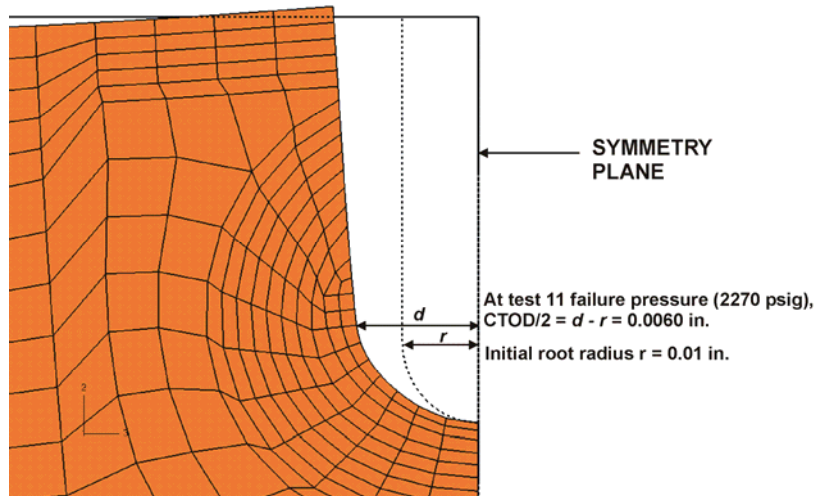
Fig. 7.18. J-applied versus CTOD: (a) CB 9, and (b) CB 11 and CB 12.



(a)

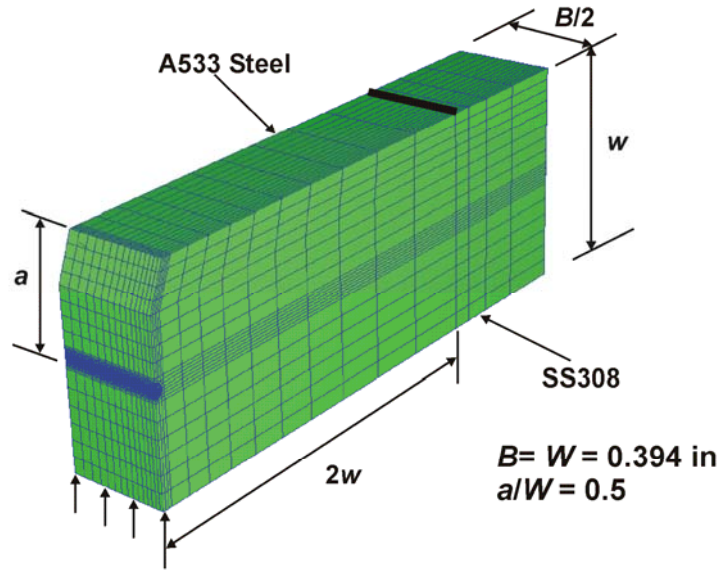


(b)

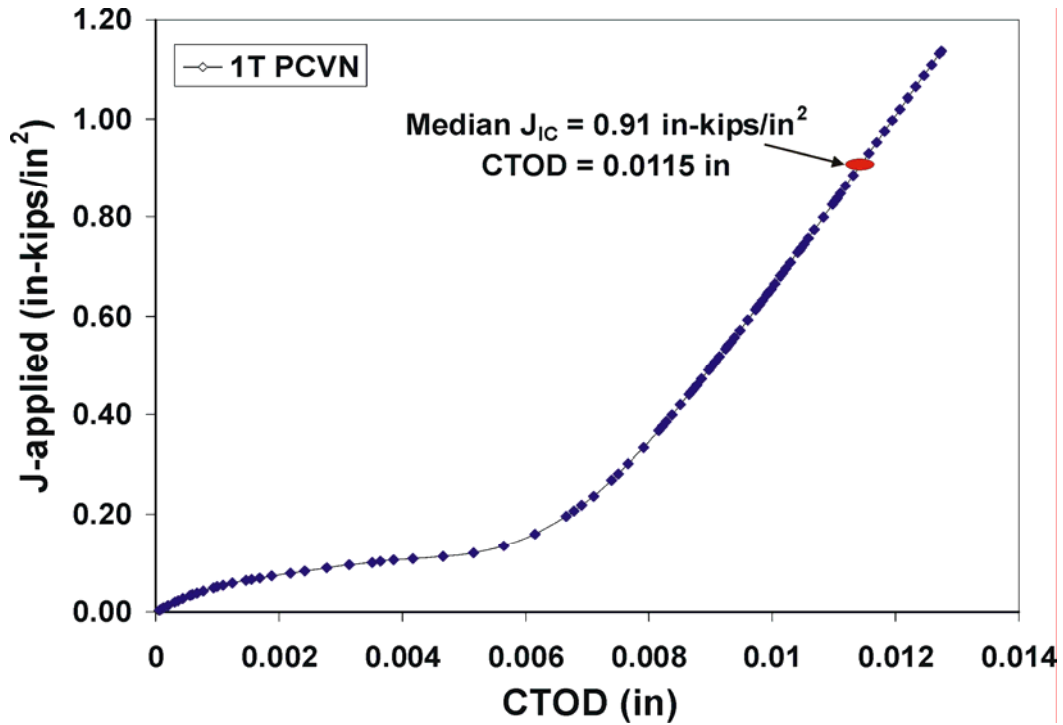


(c)

Fig. 7.19. Undeformed and deformed flaw-tip of FEM model: (a) CB 9 with root radius = 0.01 in (b) CB 11 with root radius = 0.005 in, and (c) CB 11 with root radius = 0.01 in.



(a)



(b)

Fig. 7.20. Analysis of pre-cracked Charpy specimen: (a) 3-D finite element model of PCVN specimen; (b) applied J versus CTOD curve generated from analysis

APPENDIX A

OPERATING PROCEDURE

for

HSST CLAD BURST TEST FACILITY

Specification No. **MET-EMP-SOG81 Rev 0**

January 28, 2003

Prepared by: _____ Date: _____
W. J. McAfee (Project Engineer)

Approved by: _____ Date: _____
B. R. Bass (Program manager)

Approved by: _____ Date: _____
E. Lara-Curzio (Group Leader)

Approved by: _____ Date: _____
F. K. Edwards (M&C Div. Safety Officer)

Approved by: _____ Date: _____
M. H. Carpenter (M&C Div. QA Specialist)

RPV CLAD BURST TESTS

HEAVY-SECTION STEEL TECHNOLOGY (HSST) PROGRAM OAK RIDGE NATIONAL LABORATORY (ORNL) UT-BATTELLE, LLC

DESCRIPTION OF WORK

The purpose of this procedure is to define the necessary tasks and checks to assure the safe, effective operation of the Clad Burst Test Facility located in Building 9204-1 of the Y-12 complex. This procedure does not include assembly of the components and insertion of the specimen and containment vessel into the furnace.

A Research Safety Summary (RSS) was prepared and reviewed, and responses were prepared to all reviewer questions.

The operations listed below are to be performed in the numbered sequence shown. For reference, a schematic of the test system is included as Fig. 1.

1. Perform a walk-down of the facility to check the following items:
 - a. Proper barriers are in place to prevent casual movement of unauthorized personnel into the test area.
 - b. The furnace door is securely closed and latched.
 - c. The reservoirs containing cooling water for the pressure line exiting the furnace and for the pressure pump are filled with clean water.
 - d. All instrumentation cables are connected and are clear of the passageways around the furnace.
 - e. Verify that the main power to the furnace is on. Disconnect is located behind the furnace on concrete column H-43. Power handle in the up position is "ON."
 - f. Start the furnace by pushing the toggle switch on the front console to "UP" position. The furnace should come on and go through self-diagnostics. (NOTE: The furnace should not begin to heat until Step 3a is performed.)
 - g. Verify that the initial set-point for the furnace controller is 700°F.
 - h. Verify that the over-temperature limit set-point for the furnace controller is 725°F.
 - i. Verify that manually operated valves on the nitrogen supply bottles are closed.
 - j. Set pressure pump lever in the "ON" position. NOTE: If pump starts up, immediately return lever back to "OFF" position. Check malfunction of Data Acquisition System (DAS).

- k. Check setting of Flow Control Valve on gas manifold. NOTE: Flow Control Valve has been pre-set and marked using a red pen. Do not change setting without approval of Project Engineer.
2. At the DAS inside the INSTRON lab:
NOTE: After the Labview VI software is running, do not press the “STOP” button until the test is finished.
 - a. Verify that the 24 VDC power supply is plugged in and operational by opening the door of the gray cabinet mounted on the wall behind and to the right of the DAS. The green power light should be on. Close the cabinet door.
 - b. Start the DAS and launch the test software (Labview VI) using “Cladding Burst” icon on monitor screen.
 - c. Enter data file name in Labview VI.
 - d. Start DAS Labview VI using cursor to press the arrow at the top left of the screen.
 - e. Verify nominal pressure, temperature, and displacement values displayed on screen.
 - f. Set “PLOT MODE” switch on screen to “Temperatures”.
 - g. Verify operation of the four (4) pressure control valves. To do this, one person must stand at the pressure manifold mounted on the back side of the furnace while each valve is cycled at the DAS (Open/Closed buttons). An audible sound of setting and air flow will be emitted by both the solenoid valve and air valve (the pair comprise a control valve unit) as the unit operates.
 - h. Set each valve to the closed position.
 - i. Enter an initial “LOG TIME” of 60 seconds. Press “START LOGGING” button on screen.
 3. At the furnace controller:
 - a. To start the heat process, press and hold the reset button on the high temperature limit controller located on the lower left of the furnace control panel. When this reset is complete, the small indicator light on the lower right of the high temperature limit controller will extinguish, and the relays for the heater contacts will close (Audible “Thump”)
 - b. Verify furnace operation by audible (fan starts up) and visual (indicated air temperature begins to rise).
 4. Heat-up control:
 - a. Monitor specimen temperature at DAS.
 - b. When specimen temperature reaches 580°F, reduce furnace set-point temperature to 640°F. Note: This set-point temperature is approximate based on results of thermal shake-down test and may need to be revised

as experience with test assembly is gained to achieve stable test temperature of 600°F.

5. Gas supply system pressurization:
 - a. When specimen mean temperature is stabilized at 600°F (no hold period is required), start pressurization of gas supply system.
 - b. Press “LOGGING TO DISK” button on screen to stop logging data to disk.
 - i. Set “LOG TIME” at 5 seconds.
 - ii. Press “START LOGGING” button.
 - c. At DAS, set air valves as follows:
 - i. Valve #1 and Valve #2 are opened.
 - ii. Valve #3 and Valve #4 are closed.
 - d. At gas manifold, turn on electric pump that supplies cooling water to high pressure gas pump.
 - e. Verify that the pump is operating correctly by monitoring the return fitting for water flow back into the container. (NOTE: This may take 1-2 minutes for the flow to be established.)
 - f. Slowly open manual valve on one bottle of high pressure Nitrogen gas while monitoring the sight pressure gauge for indication of pressure increase in gas manifold. Do not “slug” gas through pressure pump.
 - g. When pressure has stabilized as indicated by sight gauge, slowly open manual valves on additional two bottles of Nitrogen gas. (NOTE: Set all 3 manual valves to the full OPEN position minus 1/4 turn in the CLOSE position.)
 - h. Perform final check of test area and return to Instron Lab.
 - i. At DAS, check indicated pressure for Pressure Transducers (PTs). Outputs should be approximately:
 - i. 1,000-4,500 psig for PT #1 and #2 depending on how many times supply bottles have been used.
 - ii. 10 psig for PT #3 and #4.
 - iii. If PT #1 and #2 indicate a supply pressure less than 1,000 psig, replace bottles.
 - iv. If PT #3 and #4 show pressure to be increasing, this indicates Valve #3 has malfunctioned. Close Valves #1 and #2 and open Value #4 to vent pressure.
 - v. Let accumulator fully depressurize before checking condition of Valve #3.
 - vi. If Valve #3 can be returned to proper status, reinitiate test sequence from 5a.
 - vii. If Valve #3 cannot be restored, discontinue test.
 - j. Start Hydro-Pac pump. Monitor indicated pressure at PT #2. When pressure has reached 11,800 psig, shut pump off.
 - k. Close Valve #1 and Valve #2.

6. Perform test:
- a. Press “LOGGING TO DISK” button to stop data acquisition.
 - b. Set “PLOT MODE” switch on screen to “Displacements.”
 - c. Set log time to 0.5 seconds.
 - d. Press “START LOGGING” button.
 - e. Open Valve #3 to release high pressure gas into specimen.
 - f. Monitor test progress from parameters displayed on DAS monitor, and react as specified below.
 - i. IF CLAD DEFLECTION DOES NOT INCREASE as pressure increases, the probable cause is premature closure of the Surge Control Valve.
 - ii. Close Valve #3.
 - iii. Open Valve #4 to vent gas from specimen.
 - iv. Close Valve #4.
 - v. Reinitiate test sequence at 6c.
 - vi. If three (3) cycles of these operations does not resolve problem, terminate test (go to 7).
 - g. IF SPECIMEN FAILS, there will be a sharp pressure drop indicated by PT #3, and #4. This drop will stop when the Surge Control Valve closes isolating the specimen from the high pressure gas manifold.
 - i. Close Valve #3.
 - ii. Open Valve #4.
 - iii. Go to Step 7.
 - h. IF PRESSURE CONTINUES TO INCREASE UNTIL PT #2, #3, AND #4 ARE EQUAL, specimen has not failed.
 - i. If pressure is greater than 10,000 psig, discontinue test.
 - ii. Close Valve #3.
 - iii. Open Valve #4 to vent gas from specimen.
 - iv. If pressure is less than 10,000 psig, go to (i) below.
 - i. SPECIMEN PRESSURE MAY BE INCREASED BY USING GAS PUMP.
 - i. Open Valve #1 and #2.
 - ii. Start high pressure gas pump.
 - iii. When pressure indicated by PT #2 is 11,800 psig, stop pump.
 - iv. Close Valve #1 and #2.
 - v. Return to 6f, above.

NOTE: Steps 6e and 6f may be modified by the Project Engineer conducting the test based on an evaluation of the system instrumentation indications.

7. Shut-down sequence:
- a. Close Valve #3.
 - b. Press “LOGGING TO DISK” button to stop data acquisition.
 - c. Set “PLOT MODE” switch to “Temperatures”.

- d. Open Valve #4 to vent gas from specimen leg of manifold.
- e. When pressure indicated by PT #3 and #4 is less than 6000 psig, close manual valves on supply bottles. NOTE: Do not enter test area until indicated pressure (PT #3 and #4) has dropped below 6000 psig.
- f. Turn off power to furnace.
- g. Open Valve #2 and Valve #3.
- h. When pressure indicated by PT #1 and PT#2 are approximately equal, open Valve #1.
- i. When specimen temperature has cooled to 400°F, open furnace door approximately 2-in.
- j. When specimen temperature has cooled to 200°F, open furnace doors fully.
- k. Leave barriers in place until all temperatures are below 100°F.

APPENDIX B

**MACHINE DRAWINGS FOR FABRICATION OF CONTAINMENT VESSEL ASSEMBLY
ORNL/HSST CLAD-BURST TEST FACILITY**

